

NUMERICAL STUDY OF A
VISCOELASTIC MODEL FOR
HYDROCEPHALUS

by

Jenny H.M. Lee

A thesis
presented to the University of Waterloo
in fulfillment of the
thesis requirement for the degree of
Master of Mathematics
in
Applied Mathematics

Waterloo, Ontario, Canada, 2006

©Jenny H.M. Lee 2006

AUTHOR'S DECLARATION FOR ELECTRONIC SUBMISSION OF A THESIS

I hereby declare that I am the sole author of this thesis. This is a true copy of the thesis, including any required final revisions, as accepted by my examiners.

I understand that my thesis may be made electronically available to the public.

Abstract

Hydrocephalus is a clinical condition where the brain tissue is deformed by the expanding ventricles. In this thesis, the mechanical deformation of a hydrocephalic brain is studied using a biomechanical model, where the material properties of the tissue are described by a viscoelastic model. A set of governing equations is derived when the motion is quasi-static motion and deformation is small. Then, finite element method is used for spatial discretization, and finite difference and trapezoidal rule are used for time-stepping. Moreover, the computational meshes are generated from medical images of patient's brain using level set method and a program called DistMesh. Numerical stability of the time-stepping scheme is also studied.

Several numerical studies are conducted to investigate several aspects of the brain with hydrocephalus. The state of stress of the tissue is found to be compressive everywhere in the brain. The viscoelastic properties of the brain are investigated and found to be dominated by elastic response. Lastly, the displacement made by the ventricular wall as it expands and shrinks is found to be non-uniform.

Acknowledgements

There are many challenges in the work of this thesis. The most challenging part is to develop the numerical methods, but when the method works, it is the most satisfying feeling! There are many people who have helped me throughout this process.

I would like to thank my supervisor, Prof. Justin W.L. Wan, for his patience and support throughout this process. Your expertise in numerical methods encourage me to learn more about this subject. Thank you very much!

I would like to thank Prof. G. Tenti and Prof. M. Stastna for answering my questions regarding the solid mechanics in this thesis. In particular, thank you, Prof. G. Tenti, for helping me to develop the boundary conditions for the models. Thank you, Prof. M. Stastna, for your discussion regarding the analytical solutions of the models.

I would also like to thank, Prof. S. Sivaloganathan and Prof. N. Lanson, for reading this thesis. Your comments are much appreciated.

Thank you, Joe West, for letting me use your programs for images segmentation. Thank you, Corina Drapaca, for answering my questions in the early stage of my research. Thank you, Paul Ullrich, for your assistance in grid generation. Thank you, Lei Tang, for your discussion in finite element methods.

I would like to thank my mentor, Prof. Kevin G. Lamb, for his advice and support throughout my undergraduate studies and research assistantships. Your expertise in continuum mechanics kept my interest in mathematics and mechanics alive. Thank you very much!

Thank you, Helen Warren, for doing a great job as a graduate secretary and for helping me with my NSERC and OGS applications.

There are also many of my friends in the department who are dear to me. Thank you for your encouragement and kindness.

Lastly, I would like to thank my parents for packing many home-cooked meals for me to bring back to Waterloo. Also, I would like to thank, my fiance, Lawrence, for his understanding and support during the two past years.

Contents

1	Introduction	1
1.1	Hydrocephalus	1
1.2	Current Biomechanical Models for Hydrocephalus	3
1.3	Problem statement and Objective	5
2	Biomechanical Model	7
2.1	Governing Equations and Boundary conditions	7
2.1.1	Stress and Strain	8
2.1.2	Physical Laws	10
2.1.3	Geometry and Boundary Conditions	12
2.2	Constitutive Equations for Linear Elastic Material	14
2.3	Constitutive Equations for Linear Viscoelastic Material	16
2.3.1	1-D Differential Form	18
2.3.2	1-D Integral form	24
2.3.3	Higher Dimensional Model	26
2.4	Viscoelastic Properties of Brain Tissue	27
2.5	Model Equations for a Hydrocephalus Brain	29
2.6	Analytical Solutions	31
3	Numerical Method	35
3.1	Finite Element Method for the Elastic Problem	36
3.1.1	Step 1: Weak Formulation	36
3.1.2	Step 2: Discretizing the Weak Formulation	39

3.1.3	Step 3: Assembling the Elementary Matrix and Vector	42
3.2	Numerical Solution for the Viscoelastic Problem	45
3.2.1	Semi-Discretization	46
3.2.2	Fully Discrete Formulation	48
3.2.3	Computing Stress and Strain	52
3.3	Grid Generation from an Image	55
3.4	Compare with Analytical Solution	58
3.5	Stability Analysis	63
4	Numerical Studies	69
4.1	Background Information	69
4.1.1	Computational Mesh	69
4.1.2	Material Parameter for the Elastic and Viscoelastic Problem	70
4.1.3	Time Step	71
4.2	State of Stress of Brain Tissue	71
4.3	Material Parameter for the Viscoelastic Problem	76
4.3.1	Choice of Bulk Modulus	76
4.3.2	Choice of Shear Modulus	77
4.4	Movement of the Ventricular Wall	82
4.4.1	Movement of the Ventricular Wall	82
4.4.2	Predicting the Shape of Ventricles During Treatment	87
4.5	Assumptions of Linearity	89
5	Conclusions	93
5.1	Summary	93
5.2	Future work	94
A	Existence and Uniqueness of Solutions	97

List of Tables

3.1	Test Case 1 for the elastic problem: $P_0 = 200Pa$, $E = 600Pa$ and $\nu = 0.25$	62
3.2	Test Case 2 for the elastic problem: $P_0 = 10^6Pa$, $E = 3.07 \times 10^5Pa$, and $\nu = 0.49$	62
3.3	Test Case 1 for the viscoelastic problem: $K = 1Pa$, $p_1 = 1s$ $q_1 = 1Pa \cdot s$, $q_0 = 0.1Pa$, and $P(t) = 1Pa$.	63

List of Figures

1.1	(a) A simplified schema of the connection between the subarachnoid space and the ventricles from a top view of the brain. Features are exaggerated for illustrative purpose. (b) Side view of a human brain [1]. CSF produced in the ventricles travel through the aqueduct to the subarachnoid space and the spinal column.	2
1.2	When hydrocephalus develops, CSF accumulates within the system of ventricles, and the ventricles enlarge and compressed the brain. ©1999-2006, Cincinnati Children’s Hospital Medical Center, see [7] for details	3
2.1	Geometry of the Brain and its Boundary	12
2.2	(a) A constant strain is applied to a viscoelastic material. (b) The resulting stress. The decay in stress is known as stress relaxation.	17
2.3	Stress and Strain Relationship for Linear and Nonlinear Viscoelastic Material	17
2.4	(a) linear spring element, (b) dashpot element	18
2.5	Maxwell Model	20
2.6	Kelvin Model	21
2.7	Maxwell Solid Model	22
2.8	Domain Ω for analytical solutions.	32
3.1	$\psi_k(\mathbf{x})$ of \mathcal{V}_h at $\mathbf{x} = \mathbf{x}_j$	40
3.2	Visualization of the level set function $z = \phi(x, y, t)$ and its zero level set $\phi = 0$.	55
3.3	To segment the ventricles, start with a simple signed distance function as in (a), then evolve the function to match the ventricles as in (b).	56

3.4	(a) Segmentation of the ventricles. (b) Segmentation of the skull. (c) Combine (a) and (b).	57
3.5	The final level set function, where the region with negative distance is the region of interest.	57
3.6	A triangular mesh of a patient's brain	59
3.7	Comparison between analytical and numerical solution of the viscoelastic problem. Solid line represents numerical solution and dotted line represents analytical solution. In case (a), the mesh size is $h=5\text{mm}$; in case (b), $h=2.5\text{mm}$; in case (c), $h=1.25\text{mm}$. For all these cases, $\Delta t = 0.1\tau_R$	64
4.1	(a) The original shape of Ω_h . (b) The resulted shape of Ω_h after 8 hours of simulated time. (c) The pressure $P(t)$ at the ventricular wall which linearly increases over 8 hours.	72
4.2	Volumetric stress of the resulted Ω_h at day 14.	73
4.3	(a) The volumetric stress at one of the anterior horns. (b) The corresponding principle stress and direction, where the principle direction is represented by an arrow, and the magnitude of a principle stress is represented by the length of an arrow.	75
4.4	Pressure $P(t)$ as a function of time	79
4.5	The radial displacement at the inner boundary when the material is (a) viscoelastic, and (b) elastic.	79
4.6	The volumetric stress of (a) the viscoelastic problem at $t = 590\text{s}$, and (b) the elastic problem at $t = 590\text{s}$	80
4.7	The symbol " Δ " outlines the original boundaries of Ω_h . The symbol "*" outlines the deformed boundaries of Ω_h of the viscoelastic problem. The symbol "o" outlines the deformed boundaries of Ω_h of the elastic problem.	81
4.8	Pressure $P(t)$ as a function of time	83
4.9	Ω_h represent the brain of Patient A. The symbol "o" outlines the boundaries of Ω_h at day 14. The symbol "*" outlines the boundaries of Ω_h at day 21.	84
4.10	Ω_h represent the brain of Patient C. The symbol "o" outlines the boundaries of Ω_h at day 14. The symbol "*" outlines the boundaries of Ω_h at day 21.	85

4.11	Ω_h represents the brain of Patient H. The symbol “o” outlines the boundaries of Ω_h at day 14. The symbol “*” outlines the boundaries of Ω_h at day 21.	86
4.12	(a) The original shape of Ω_h . (b) The resulted shape of Ω_h after 14 days of simulated time. (c) The pressure $P(t)$ at the ventricular wall which linearly decreases over 14 days.	88
4.13	(a) a pre-shunt image of Patient C. (b) a post-shunt image of Patient C.	89
4.14	(a) The original shape of Ω_h . The deformed Ω_h with parameters (b) $P(t) = 10KPa$, $\max \mathbf{u} = 4.70mm$, and $\kappa = 0.13$, (c) $P(t) = 20KPa$, $\max \mathbf{u} = 9.41mm$, and $\kappa = 0.27$, (d) $P(t) = 40KPa$, $\max \mathbf{u} = 18.82mm$, and $\kappa = 0.54$. (e) $P(t) = 80KPa$, $\max \mathbf{u} = 37.64mm$, and $\kappa = 1.09$	91

Chapter 1

Introduction

1.1 Hydrocephalus

Hydrocephalus is a clinical condition of the brain, where an abnormal amount of fluid accumulates within a system of cavities inside the brain. This system of cavities called ventricles, and the fluid is called cerebrospinal fluid (CSF). This condition presents approximately in 1-3 per 1000 birth of a child and can also be diagnosed in older adults. It causes pressure inside the head to increase and brain tissue to be compressed. In the case of an infant, where the skull is not rigid, the skull is enlarged. If untreated, hydrocephalus can cause very serious neurological damages to the brain and even death. There are no known way to prevent or cure hydrocephalus. A common treatment, that do not guarantee success, is a surgical insertion of a shunt.

Cerebrospinal fluid is a watery liquid produced in the ventricles. Once produced, it circulates through the ventricular system, into the subarachnoid space and also down the spinal column. The subarachnoid space is the space between the brain and the skull, and it is where CSF is absorbed into the bloodstream. See Figure 1.1. In a healthy body, CSF is in constant circulation and has many important functions. It surrounds the brain and the spinal cord and protects them in case of mechanical shocks. It also contains nutrients and proteins necessary for the nourishment and normal function of the brain and also carries waste product away from surrounding tissue.

When the balance between production and absorption of CSF is disrupted, an excess

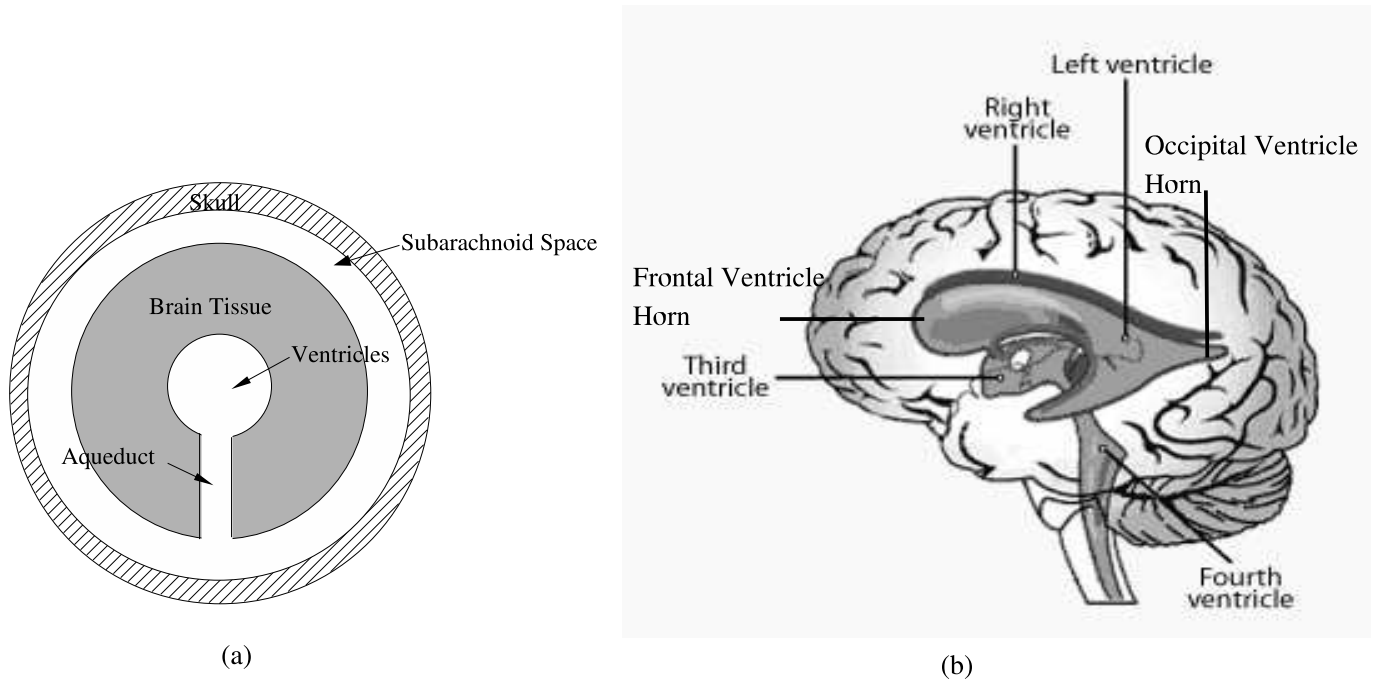


Figure 1.1: (a) A simplified schema of the connection between the subarachnoid space and the ventricles from a top view of the brain. Features are exaggerated for illustrative purpose. (b) Side view of a human brain [1]. CSF produces in the ventricles travel through the aqueduct to the subarachnoid space and the spinal column.

of CSF accumulates in the ventricles. This build up may occur either over a long time or relatively quickly, and it is usually the result of insufficient absorption of CSF. This leads to expansion of the ventricles and compression of the brain. See Figure 1.2.

A common treatment of hydrocephalus is to drain excess CSF by inserting a shunt into the ventricles surgically. A shunt is a catheter inserted through the brain into the ventricles, implanted under the skin. It diverts the excess CSF into either the heart or into the abdomen cavity. Outside the skull is a pressure-operated valve designed to regulate the shunt, which allows fluid flow out only when the CSF pressure has exceeded a threshold.

Once a shunt is implanted, it stays with the patient for life, and it may function properly for many years and the dilatation of the ventricles may be reversed. However, it is common for a shunt to malfunction. According to a clinical trial described in Drake *et al.*[11], 40%

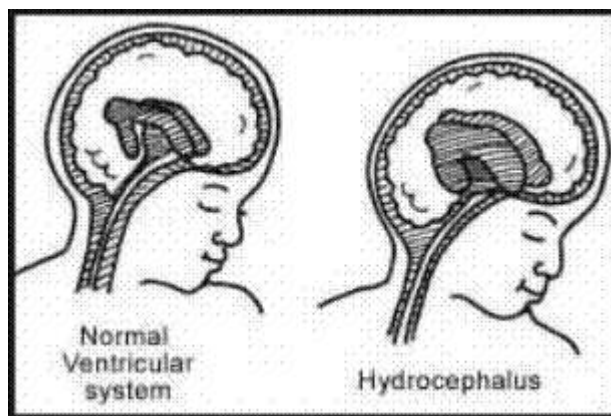


Figure 1.2: When hydrocephalus develops, CSF accumulates within the system of ventricles, and the ventricles enlarge and compressed the brain. ©1999-2006, Cincinnati Children’s Hospital Medical Center, see [7] for details .

of the shunts malfunction after they are implanted for 1 year, and 50% of them malfunction after 2 years, and the most common cause of shunt failure is obstruction. Obstruction of the catheter is a result of buildup of cells in the holes of the catheter, and it could occur when the shrinking ventricles move past the catheter tip. Thus, the shape of the ventricles often needs to be monitored using MRI or CT scans, and when the shunt fails, the patient needs to have surgery again.

Currently, there are various research activities trying to devise more effective and safer treatments of hydrocephalus. One approach is to study the biomechanics of the underlying biological process using mathematical models.

1.2 Current Biomechanical Models for Hydrocephalus

In a biomechanical model, the brain is assumed to be undergoing mechanical deformation as the ventricles enlarge or shrink. This model focuses on the macroscopic and physical process and omits the microscopic and cellular process during the deformation. Such a model requires knowledge about the mechanical properties of brain tissue.

Depending on the application, in order to study the mechanical properties of brain

tissue, the tissue has been modeled either as a viscoelastic or poroelastic, or even as a purely elastic material. For hydrocephalus, the brain tissue was first modeled as a poroelastic material. A poroelastic material is like a sponge saturated with fluid. When the sponge deforms, fluid flows through the sponge. It is inhomogeneous since it is composed of an elastic solid and a fluid. “A major step in the development of brain biomechanics was taken by Nagashima *et al.* [27]. [46]” They formulated a set of governing equations to model the brain as a poroelastic material and used the finite element method to solve these equations numerically with an anatomically realistic geometry of the brain.

Since then, Tenti *et al.*, [46, 40, 44], extended the governing equations to include transient effects and variable permeability and found analytical solutions for a cylindrical geometry. Kaczmarek *et al.* [21] studied large deformation by superposition of responses from small deformation. Recently, Smillie *et al.* [39] combined the set of governing equations with a compartmental model, which allows them to model the flow of CSF in the ventricular system.

In addition to Nagashima *et al.*, other researchers who have performed numerical simulation of hydrocephalus with realistic geometry includes [29, 45]. Peña *et al.*, [29], predicted that the dilatation of the brain tissue would occur near the anterior and posterior horn of the ventricles, sites of the ventricular wall with convex geometry. Both [27] and [29] focus on simulating edema, which is a feature of acute stages of hydrocephalus where fluid accumulates in the brain tissue.

On the other hand, brain tissue has also been modeled as a viscoelastic material. A porous medium, such as brain tissue, behaves like a poroelastic material when the Reynolds number is small, but behaves like a viscoelastic material when the Reynolds number is large [12]. If one is interested in studying the interaction between the CSF and the brain tissue, such as edema, modeling the brain as a poroelastic medium would likely give good results. If, however, one is interested in studying the response of the brain to applied forces and the resulted deformation, viscoelastic material is more appropriate. Although treating the brain as viscoelastic material is a new approach in modeling hydrocephalus, it is common in modeling traumatic brain injury.

In [41, 42], Sivaloganathan *et. al.* modeled the brain as viscoelastic solid and used the elastic-viscoelastic analogy to obtain analytical solutions for a cylindrical geometry. They

also extended their model to include pulsatile effect of the intracranial pressure (ICP), pressure of the CSF. A nonlinear viscoelastic model is chosen in [12] to account for the observed large deformation in a brain with hydrocephalus, and the speed of the ventricular wall during a deformation is investigated.

A very different approach in modeling hydrocephalus is employed in West's thesis, [48], where a level set method is used to model the movement of the ventricular wall. Although this is not a biomechanical model, it is worth mentioning because of its simplicity and usefulness. This method describes the ventricular wall of a 2D image with a level set function, and this function is evolved according to a hyperbolic equation that moves the ventricles wall inward or outward.

1.3 Problem statement and Objective

This thesis is a numerical study of hydrocephalus where the brain tissue is considered to be a viscoelastic material, and a realistic brain geometry is used. A common perspective about numerical modeling of viscoelastic materials is that it is computationally expensive to evaluate an integral term that arises in the governing equations. However, it is little known that the relaxation modulus of the viscoelastic model of brain tissue has a special form, so that the evaluation of the integral can be simple and efficient. Specifically, the computational time and memory required can be linearly proportional to the number of time steps. Without this special form, the computational time and memory would increase quadratically.

Currently, there are a few numerical studies of hydrocephalus that consider the brain tissue to be a poroelastic solid filled with fluid. In these studies, the focus is on studying edema, because the distribution of fluid and the type of stress of the poroelastic solid indicates where edema may occur and so where the tissue may be damaged. Since the brain tissue is also known to behave like a viscoelastic material, how would tissue damage be presented if a viscoelastic description of the tissue is used? This is investigated in this thesis by studying the state of stress of the viscoelastic material.

Brain tissue is commonly considered to be viscoelastic in the study traumatic brain injury, and so many experiments conducted to determine its viscoelastic property were

designed to mimic the conditions leading to brain injury. So, if brain matter is described as a viscoelastic material in the study of hydrocephalus, how would these viscoelastic properties play a role in the evolution of hydrocephalus? Both the bulk modulus and the shear modulus of the viscoelastic tissue are investigated in this thesis.

Recall that the shunting procedure has a high failure rate, and the major cause of failure is obstruction. It would be beneficial if the position of the ventricles as it shrinks could be numerically simulated so that an optimal position for the shunt can be found before surgery. Several people have addressed this goal, including [12, 48]. The use of the level set method in [48] is simple, however it requires more information about how the ventricular wall moves since it is not based on any mechanical or biological model. Numerical studies using a viscoelastic model can provide some understanding of how the ventricular wall moves and can also address the challenges of predicting the geometry of the ventricles.

Therefore, the first of the objectives of this thesis is to develop a numerical method for solving the viscoelastic model using a realistic geometry of the brain. Then, three numerical studies related to hydrocephalus are conducted. One of them is to study the state of stress of the brain with hydrocephalus. Then, the role of the viscoelastic property of the brain in modeling hydrocephalus is investigated. Lastly, the movement of the ventricular wall after a shunting procedure is observed.

This thesis is divided into 3 major parts. First, the mathematical and physical background of biomechanical model are discussed in Chapter 2. In addition to the viscoelastic model, an elastic model of the brain is discussed throughout this thesis, since it helps to develop an analytical and numerical solution for the viscoelastic model. In Chapter 3, numerical methods for solving the biomechanical models and for generating grid are introduced. Finally, several numerical studies are described in Chapter 4.

Chapter 2

Biomechanical Model

A biomechanical model of the brain is formulated using mechanics to describe how the brain deforms under an applied force. The mechanical deformation greatly depends on the material property of the brain, and thus an important part of the model is to have a constitutive equation that describes the mechanical property of the brain accurately.

In this chapter, concepts of mechanical deformation are introduced. In Section 2.1, stress and strain, physical laws and boundary conditions concerning the biomechanical model of the brain are introduced. Then, to develop a biomechanical model with viscoelastic material, a simpler elastic material and its constitutive equations are first studied in Section 2.2. Then, viscoelastic materials and their constitutive equations are discussed in greater detail in Section 2.3. In Section 2.4, the particular viscoelastic properties of brain tissue are described. Lastly, Section 2.5 summarizes the set of governing equations for the biomechanical models of the brain as an elastic and a viscoelastic material, and then the corresponding analytical solution is found in Section 2.6 for a simple geometry.

2.1 Governing Equations and Boundary conditions

A mathematical model for a hydrocephalic brain is developed by considering the deformation of brain tissue when the ventricles enlarge or shrink. First let's introduce some notation to describe a deformation. Consider the brain as a continuous body $\Omega \subset \mathfrak{R}^3$ made of a certain material, then when hydrocephalus develops, the brain Ω , deforms from an

initial configuration C_0 defined at time t_0 to a new configuration C_t defined at a later time t . C_0 is taken as the reference configuration, and C_t is taken as the current configuration. Then, the resulting motion is a mapping between C_0 and C_t , for $t \in I$ where $I = [0, T]$. When the motion is small, both C_0 and C_t can be described using the same Cartesian coordinate system. Let a material point in C_0 be $\mathbf{x} = (x_i)$ for $i = 1..3$. After a continuous deformation, the same material point is located at the new position $\mathbf{X} = \mathbf{x} + \mathbf{u}(\mathbf{x}, t)$ in C_t , where $\mathbf{u}(\mathbf{x}, t) = (u_i(\mathbf{x}, t))$, $i = 1..3$, is the displacement.

In this section, the mechanics of deformation is introduced in three parts. First, the state of stress and strain at a material point is defined. Then, physical laws governing a deformation are established. Lastly, boundary conditions imposed on the brain are described. For more information about mechanical deformation, one can refer to [16], [4] and [14].

2.1.1 Stress and Strain

Consider a unit cube around \mathbf{x} in C_t . When Ω undergoes deformation, this small cube is also deformed. This deformation at \mathbf{x} and t is described by a strain tensor. The Green's strain tensor is defined as

$$E_{ij} = \frac{1}{2} \left[\frac{\partial u_i}{\partial x_j} + \frac{\partial u_j}{\partial x_i} + \frac{\partial u_\alpha}{\partial x_i} \frac{\partial u_\alpha}{\partial x_j} \right], \quad (2.1)$$

and it is sometimes called the Lagrangian strain tensor. Note that Einstein summation convention is used here, *i.e.*, $\frac{\partial u_\alpha}{\partial x_i} \frac{\partial u_\alpha}{\partial x_j} = \sum_{\alpha=1}^3 \frac{\partial u_\alpha}{\partial x_i} \frac{\partial u_\alpha}{\partial x_j}$.

When the motion is small, the displacements are small so that the last term $\frac{\partial u_\alpha}{\partial x_i} \frac{\partial u_\alpha}{\partial x_j}$ of (2.1) are negligible compared to the first two terms. This assumption is called infinitesimal deformation. Under this assumption, the Green's Strain tensor reduces to the Cauchy's infinitesimal strain tensor

$$\varepsilon_{ij} = \frac{1}{2} \left(\frac{\partial u_i}{\partial x_j} + \frac{\partial u_j}{\partial x_i} \right).$$

Cauchy's infinitesimal strain tensor is symmetric by definition.

There are two kinds of strain represented in this strain tensor, and they are longitudinal strain and shear strain. Longitudinal strain describes the change of length of a line element and is the diagonal terms of the strain tensor. Tensorial shear strain is the half of the change

of angle between two mutually perpendicular line, and it is represented in the off-diagonal terms of the strain tensor.

The strain tensor may be divided into a volumetric strain, ε_v and a deviatoric strain, ε'_{ij} as follows

$$\begin{aligned}\varepsilon_{ij} &= \begin{bmatrix} \varepsilon_v & 0 & 0 \\ 0 & \varepsilon_v & 0 \\ 0 & 0 & \varepsilon_v \end{bmatrix} + \begin{bmatrix} \varepsilon'_{11} & \varepsilon_{12} & \varepsilon_{13} \\ \varepsilon_{12} & \varepsilon'_{22} & \varepsilon_{23} \\ \varepsilon_{13} & \varepsilon_{23} & \varepsilon'_{33} \end{bmatrix} \\ &= \varepsilon_v \delta_{ij} + \varepsilon'_{ij}\end{aligned}\tag{2.2}$$

where

$$\varepsilon_v = \frac{1}{3}(\varepsilon_{11} + \varepsilon_{22} + \varepsilon_{33}) = \frac{1}{3}\varepsilon_{kk},\tag{2.3}$$

and ε'_{11} , ε'_{22} and ε'_{33} are the deviations from ε_v . Physically, the volumetric strain ε_v describes a pure dilatation, that is expansion or contraction of a material body without changing its shape. The deviatoric strain ε'_{ij} describes pure distortion at constant volume, that is a change of the material shape without changing its volume.

One way to deform the unit cube around \mathbf{x} in C_t is to have forces acting on its surface. Such forces are called surface forces, and examples are friction and pressure. Stress describes surface forces, which is defined as the ratio between a force acting on a given area and that area. A stress tensor σ_{ij} has nine components, and each of them describes a force per unit area on a surface of the unit cube. Because of the conservation of moment, the stress tensor is symmetric. So only six out of nine components are needed to completely describe the state of stress at \mathbf{x} and t .

The stress vector or traction \mathbf{g} is defined as the force per unit area acting on a surface with an outward unit normal \mathbf{n} . An outward unit normal means that if the surface is a side of the unit cube, \mathbf{n} points away from the center of a cube. The stress vector \mathbf{g} is related to stress tensor σ_{ij} by $\mathbf{g}_i = \sigma_{ij}\mathbf{n}_j$ according to Cauchy's Theorem. Stress vector \mathbf{g} can be projected onto a unit normal or a unit tangent of the surface. The vector projection of \mathbf{g} onto a unit normal is called the normal stress vector \mathbf{g}_n , and it describes the tensile stress on that surface. The vector projection of \mathbf{g} onto a unit tangent is called the shear stress vector \mathbf{g}_t , and it describes shear stress on that surface.

Principle stress and direction is found when the unit cube is rotated for a constant state of stress. A particular rotation can be found such that all the stress vectors on the cube are perpendicular to its surface. Then, the shear stress vanishes and only normal stresses exist. For such a configuration, the unit normals on the rotated cube are called principle directions \mathbf{n}_p , and the normal stresses are called principle stresses $\sigma_I > \sigma_{II} > \sigma_{III}$ where one of them is a maximum, and another is a minimum. So, the stress tensor of the rotated configuration becomes

$$\begin{bmatrix} \sigma_I & 0 & 0 \\ 0 & \sigma_{II} & 0 \\ 0 & 0 & \sigma_{III} \end{bmatrix}.$$

When a particular principle direction \mathbf{n}_p gives a principle stress σ_p , Cauchy's Theorem gives

$$\sigma_{ij}\mathbf{n}_p = \sigma_p\mathbf{n}_p. \quad (2.4)$$

This equation implies that the principle directions are the eigenvectors of the stress tensor and the principle stresses are the associated eigenvalues.

Similar to the strain tensor, the stress tensor can also be divided into volumetric stress σ_v and deviatoric stress σ'_{ij} :

$$\begin{aligned} \sigma_{ij} &= \begin{bmatrix} \sigma_v & 0 & 0 \\ 0 & \sigma_v & 0 \\ 0 & 0 & \sigma_v \end{bmatrix} + \begin{bmatrix} \sigma'_{11} & \sigma_{12} & \sigma_{13} \\ \sigma_{12} & \sigma'_{22} & \sigma_{23} \\ \sigma_{13} & \sigma_{23} & \sigma'_{33} \end{bmatrix} \\ &= \sigma_v\delta_{ij} + \sigma'_{ij} \end{aligned} \quad (2.5)$$

where σ_v is

$$\sigma_v = \frac{1}{3}(\sigma_{11} + \sigma_{22} + \sigma_{33}) = \frac{1}{3}\sigma_{kk}, \quad (2.6)$$

and σ'_{11} , σ'_{22} and σ'_{33} are the deviations from σ_v . Volumetric stress describes tensile or compressive force, and deviatoric stress describes shearing force.

2.1.2 Physical Laws

The mechanical behaviour of any material is governed by certain physical laws, which relates stress and strain together. In any solid body subject to external forces and dis-

placement, the state of stress and strain at every points including points on the boundary must satisfy three basic equations which are Cauchy's equations of motion, kinematics equations and constitutive equations.

The first equations, the Cauchy's equations of motion, state that linear momentum is conserved. That is the total force acting upon a body equals the rate of change of the total momentum. The equations of motions in tensor notation are

$$\rho \frac{\partial^2 u_j}{\partial t^2} = F_j + \frac{\partial \sigma_{ij}}{\partial x_i}.$$

The term on the left hand side describes the rate of change of total momentum. The two terms on the right hand side describe the two types of force involved: body forces, F_j , and surface forces, σ_{ij} . In modeling hydrocephalus, body force is neglected. This means that the gravitational field is considered constant, and traumatic brain injury is not considered. Also, the motion is assumed to be quasi-static. This implies the motion is slow enough for the mass-acceleration term to be negligible. Physically, this quasi-static approximation describes a motion where a change in the boundary conditions causes a change in static deformation in a period of time. In this period of time, the faster wave motion damps out completely and is not detectable. So, the body is assumed to be in static equilibrium with the boundary conditions for all time. Examples of quasi-static process in neurosurgery are neurosurgical retraction, brain shift during surgery, hematomas and hydrocephalus [22]. Thus, the equations of motion for modeling hydrocephalus with the quasi-static approximation and the absence of external body forces are

$$\frac{\partial \sigma_{ij}}{\partial x_i} = 0.$$

The second equations are the kinematic equations which describe the motion of a deformation, whereas the previous equations describe the forces involved. Kinematic equations relate strain to displacement and are given in the definition of strain tensor. Assuming infinitesimal deformation, the kinematics equations are

$$\varepsilon_{ij} = \frac{1}{2} \left(\frac{\partial u_i}{\partial x_j} + \frac{\partial u_j}{\partial x_i} \right).$$

The last set of equations are the constitutive equations, and they describe the intrinsic characteristics of the material. Material bodies of same mass and same shape respond to the

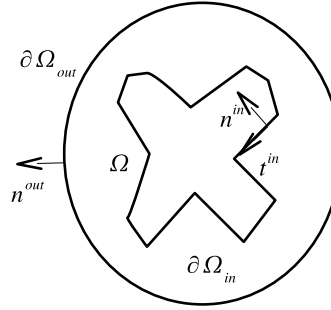


Figure 2.1: Geometry of the Brain and its Boundary

same external forces or displacement in different ways. This difference in response is due to the difference in the intrinsic characteristics of the material. Equations characterizing the individual material and its reaction to external factors are called constitutive equations [14]. The behaviour of real material is very complex, especially when it depends on temperature.

Thus, an idealized material is considered where the constitutive equations is a relationship between stress and strain. In Section 2.2 and Section 2.3, the constitutive equations for a linear elastic and viscoelastic material are discussed respectively in detail. For now, the constitutive equations have the following form

$$\sigma_{ij} = F(\varepsilon_{ij}).$$

2.1.3 Geometry and Boundary Conditions

For the purpose of developing a simple yet descriptive model, let the geometry of Ω be a horizontal cross section of the brain, so that Ω is a 2-D geometry with an empty cavity to represent the ventricles. The boundary of Ω are two curves, and let them be $\partial\Omega_{in}$ and $\partial\Omega_{out}$. Let \mathbf{n}^{in} and \mathbf{n}^{out} be the outward unit normal on $\partial\Omega_{in}$ and $\partial\Omega_{out}$ respectively, and let \mathbf{t}^{in} be the unit tangent on $\partial\Omega_{in}$. The inner boundary $\partial\Omega_{in}$ represents the ventricular wall and the outer boundary $\partial\Omega_{out}$ represents the outer surface of the brain which is in contact with the skull. See Figure 2.1.

This two dimensional problem is assumed to be in plane strain; that is, Ω is considered as a horizontal cross section of a very long cylinder extending in z direction. Assume all external forces are perpendicular to z axis and do not vary along z axis, all cross sections

are subject to the same boundary conditions; also, the end sections of the cylinder are assumed to be confined. Then, the horizontal displacements, u_1 and u_2 , are independent of z , and the vertical displacement u_3 is zero. Consequently, ε_{23} , ε_{13} and ε_{33} vanish, and so some components of stress tensor may also vanish depending on the constitutive equations.

In this thesis, Ω represents the brain of an adult, so that the skull is assumed to be a rigid medium. The rigid skull prevents the points on $\partial\Omega_{out}$ from moving, and so the boundary conditions on $\partial\Omega_{out}$ becomes

$$\mathbf{u}(\mathbf{x}, t) = \vec{0},$$

for $\mathbf{x} \in \partial\Omega_{out}$, $t \in \mathcal{I}$.

The boundary conditions on $\partial\Omega_{in}$ are specified by a stress vector $\mathbf{g}(\mathbf{x}, t)$ at a point \mathbf{x} on $\partial\Omega_{in}$. Let the vector projection of $\mathbf{g}(\mathbf{x}, t)$ onto $\mathbf{n}^{in}(\mathbf{x})$ be $\mathbf{g}_n(\mathbf{x}, t)$, and let the vector projection of $\mathbf{g}(\mathbf{x}, t)$ onto $\mathbf{t}^{in}(\mathbf{x})$ be $\mathbf{g}_t(\mathbf{x}, t)$. When CSF accumulates inside the ventricles, the CSF pressure inside the ventricles increases and exerts a surface force onto the ventricular wall $\partial\Omega_{in}$ in normal direction. This surface force is related to the normal stress vector $\mathbf{g}_n(\mathbf{x}, t)$ in an opposite direction

$$\mathbf{g}_n(\mathbf{x}, t) = -P(t)\mathbf{n}^{in}(\mathbf{x}), \quad (2.7)$$

where $P(t)$ is a scalar function of time representing the CSF pressure inside $\partial\Omega_{in}$ relative to the pressure outside $\partial\Omega_{out}$. That is, $P(t)$ represents the pressure difference across the two boundaries, which compresses Ω when it is positive and stretches Ω when it is negative. Assuming there is no shear stress on the ventricles, set

$$\mathbf{g}_t(\mathbf{x}, t) = \vec{0}. \quad (2.8)$$

Using (2.7) and (2.8), an explicit expression for $\mathbf{g}(\mathbf{x}, t)$ can be found. Let $\mathbf{t}^{in}(\mathbf{x}) = (t_1, t_2)^T$, assuming $\mathbf{t}^{in}(\mathbf{x})$ points clockwise around $\partial\Omega_{in}$, the normal $\mathbf{n}^{in}(\mathbf{x})$ is found by rotating $\mathbf{t}^{in}(\mathbf{x})$ by -90 degrees, which is $\mathbf{n}^{in} = (t_2, -t_1)^T$. Then the vector projection of $\mathbf{g}(\mathbf{x}, t)$ at \mathbf{x} are

$$\begin{aligned} \mathbf{g}_t(\mathbf{x}, t) &= (\mathbf{t}^{in} \cdot \mathbf{g}(\mathbf{x}, t))\mathbf{t}^{in} = \vec{0} \\ \mathbf{g}_n(\mathbf{x}, t) &= (\mathbf{n}^{in} \cdot \mathbf{g}(\mathbf{x}, t))\mathbf{n}^{in} = -P(t)\mathbf{n}^{in} \end{aligned}$$

or

$$\begin{bmatrix} t_1 & t_2 \\ t_2 & -t_1 \end{bmatrix} \begin{bmatrix} g_1(\mathbf{x}, t) \\ g_2(\mathbf{x}, t) \end{bmatrix} = \begin{bmatrix} 0 \\ -P(t) \end{bmatrix}$$

Solving this system of equations gives an expression for $\mathbf{g}(\mathbf{x}, t)$

$$\begin{bmatrix} g_1(\mathbf{x}, t) \\ g_2(\mathbf{x}, t) \end{bmatrix} = \frac{-1}{t_1^2 + t_2^2} \begin{bmatrix} -t_1 & -t_2 \\ -t_2 & t_1 \end{bmatrix} \begin{bmatrix} 0 \\ -P(t) \end{bmatrix}. \quad (2.9)$$

Thus the boundary conditions on $\partial\Omega_{in}$ are

$$\sigma_{ij}(\mathbf{x}, t)\mathbf{n}_j^{in} = g_i(\mathbf{x}, t), \quad \text{for } \mathbf{x} \in \partial\Omega_{in}$$

where $\mathbf{g}(\mathbf{x}, t)$ is given in (2.9).

2.2 Constitutive Equations for Linear Elastic Material

A linear elastic solid behaves like the familiar elastic spring or rubber band. When stress is applied on an elastic solid, strain responds instantaneously. When, the applied stress is removed, strain restores to its original state. This type of solid is said to have a perfect memory of its original shape.

Recall constitutive equations are a set of relationships between stress and strain; in this section, the constitutive equations for a linear elastic solid is studied. Hooke's law for an elastic solid states that the stress tensor is linearly proportional to the strain tensor, so the general constitutive equations are

$$\sigma_{ij} = C_{ijkl}\varepsilon_{kl},$$

where C_{ijkl} is a 4th order tensor describing the elastic moduli of a material and is independent of stress and strain.

When a material is homogeneous, the components of C_{ijkl} are constants. C_{ijkl} is made up of 81 constants in general; but due to the symmetry of the stress and strain tensor, the number of independent constants reduces to 36. In addition, when a material is isotropic, only two independent constants remains. A material is isotropic when it responds in every directions the same way. Consequently, the constitutive equations have the following form

$$\sigma_{ij} = \lambda\varepsilon_{kk}\delta_{ij} + \mu\varepsilon_{ij}, \quad (2.10)$$

where λ and μ are called the Lamé constants of a material.

Instead of λ and μ , the bulk modulus K and the shear modulus G are frequently used to describe the experimental response of a material. λ and μ are related to K and G by $\lambda = K - \frac{2G}{3}$ and $\mu = 2G$. The bulk modulus K relates the volumetric stress σ_v to bulk strain ε_{kk} , and the shear modulus G relates the deviatoric stress to deviatoric strain in

$$\sigma_v = K\varepsilon_{kk} \quad (2.11)$$

$$\sigma'_{ij} = 2G\varepsilon'_{ij}. \quad (2.12)$$

(2.11) means that the dilatation is proportional to the tensile stress acting on a volume's surface, and the bulk modulus K is a constant of this proportionality. When a material has a large bulk modulus K , greater tensile stress is required to expand the material; hence the greater K , the more incompressible the material becomes. The shear modulus G in (2.12) is the constant of proportionality between shear deformation and shear force. Note that when one uses a value for the shear modulus from the literature, one needs to check if the factor of 2 is included in the value. Or when one uses a commercial program to solve a linear elasticity problem, one needs to check if the program takes G or μ as input, since $\mu = 2G$.

Another common way to describe a homogeneous isotropic material is with the Young's modulus E and the Poisson's ratio ν . The λ and μ are related E and ν by $\mu = \frac{E}{(1+\nu)}$ and $\lambda = \frac{E\nu}{(1+\nu)(1-2\nu)}$. Poisson's ratio ν is also used to measure incompressibility of a material, and it is related to K by $K = \frac{E}{3(1-2\nu)}$. When its bulk modulus approaches infinity, the Poisson's ratio approaches 0.5. In terms of E and ν , the constitutive equations are

$$\sigma_{ij} = \frac{E\nu}{(1+\nu)(1-2\nu)}\varepsilon_{kk}\delta_{ij} + \frac{E}{(1+\nu)}\varepsilon_{ij} \quad (2.13)$$

which will be used in next chapter to formulate an elastic model for the brain.

Inverting (2.13) to solve for the strain tensor yields

$$\varepsilon_{ij} = \frac{1+\nu}{E}\sigma_{ij} - \frac{\nu}{E}\sigma_{kk}\delta_{ij}. \quad (2.14)$$

Recall $\varepsilon_{13} = \varepsilon_{23} = \varepsilon_{33} = 0$ in plane strain. Thus using (2.13), two components of the stress tensor become

$$\sigma_{13} = \sigma_{23} = 0,$$

and σ_{33} depends on ε_{11} and ε_{22} . Using (2.14), σ_{33} is found to be

$$\sigma_{33} = \nu(\sigma_{11} + \sigma_{22}).$$

So only stress tensor components σ_{11} , σ_{22} and σ_{12} are required to be solved in the plane strain problem for linear elasticity.

2.3 Constitutive Equations for Linear Viscoelastic Material

The general characteristic of a viscoelastic material can be compared with the characteristic of an elastic solid and a viscous fluid. A perfectly elastic solid has a perfect memory of its original shape; however, a fluid has no memory of its original shape. Upon the release of a load, a fluid deforms continuously and eventually takes the shape of its container. A viscoelastic material has the characteristics of both an elastic solid and a viscous fluid, so it is said to have a partial memory of its original shape. This partial memory means the current behaviour of a viscoelastic material depends on its recent history. Examples of viscoelastic material are plastics, wood, natural and synthetic fibers, concrete and metals at elevated temperatures [14].

The behaviour of a viscoelastic material can be precisely characterized by one of two functions called the creep compliance and the relaxation modulus. The creep compliance of a material is obtained by applying a constant stress to the material, and the compliance is deduced from the strain response. On the other hand, the relaxation modulus is obtained by applying a constant strain to the material and is deduced from the stress response. For the purpose of developing a numerical model, only the relaxation modulus is considered, because it relates stress and strain in the form $\sigma_{ij} = f(\varepsilon_{ij})$. However, a creep compliance relates stress and strain in the form $\varepsilon_{ij} = f(\sigma_{ij})$. See Figure 2.2, which illustrates stress relaxation.

A viscoelastic material is said to be linear if stress is a linear function of strain at a given time. Most material are nearly linear over a small ranges of stress, strain, time and temperature; but they are nonlinear over larger ranges of the same variables. See Figure 2.3.

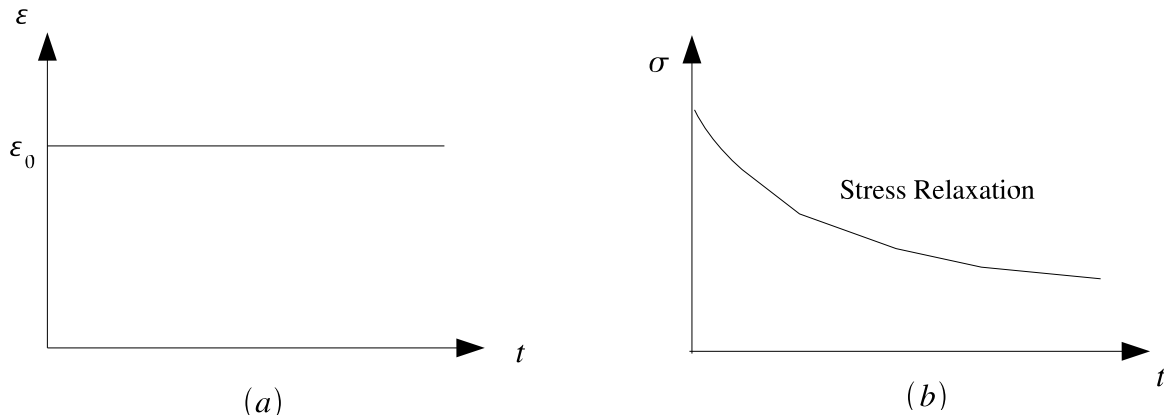


Figure 2.2: (a) A constant strain is applied to a viscoelastic material. (b) The resulting stress. The decay in stress is known as stress relaxation.

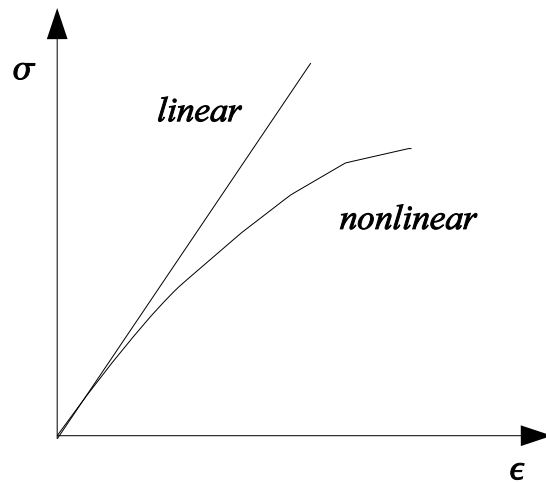


Figure 2.3: Stress and Strain Relationship for Linear and Nonlinear Viscoelastic Material

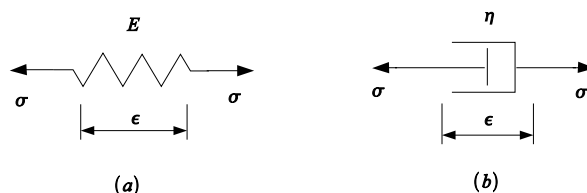


Figure 2.4: (a) linear spring element, (b) dashpot element

In this section, the constitutive equations of a linear viscoelastic material are studied in greater detail. The constitutive equations can be represented in two different ways: the differential form and the integral form. First, the differential form is derived in 1-D by considering the stress and strain relationship in an assembly of elastic springs and viscous dashpots. When the relaxation modulus of a material is found, the integral constitutive equation is derived in 1-D using Boltzmann's Superposition Principle. Lastly, both forms are generalized to higher dimensions.

2.3.1 1-D Differential Form

The differential constitutive equation of a linear viscoelastic material is derived by considering an assembly elastic and viscous elements in series or in parallel like an electric circuit. The elongation of an element refers to strain, $\epsilon = \epsilon(t)$, and the force applied to elongate an element refers to stress, $\sigma = \sigma(t)$.

When elements are connected in parallel, the strains of each element are identical, and the total stress is the sum of stresses from each element. When elements are connected in series, the stresses of each element are identical, and the total strain is the sum of strains from each element. Using these two rules, a differential constitutive equation in 1-D is derived. Like the elastic model, the linear viscoelastic material is assumed to be homogeneous, and the model parameters do not depend on space. Thus, spatial variable is omitted for convenience.

An elastic element is represented by a linear spring, see Figure 2.4(a). Its stress and strain are related by

$$\sigma = E\epsilon, \quad (2.15)$$

where E is the Young's modulus for the spring.

A viscous element is represented by a linear dashpot, see Figure 2.4(b). Its stress depends on its strain rate by

$$\sigma = \eta \frac{d\varepsilon}{dt}, \quad (2.16)$$

where η is a coefficient of viscosity.

Maxwell Model

A Maxwell model is a simple viscoelastic model represented by an elastic spring and a viscous dashpot in series, as shown in Figure 2.5. Since the elements are connected in series, their strains are different, and their stresses are identical. Let the strain of the spring and dashpot be ε_1 and ε_2 respectively, and let the stress of the two elements be σ . ε_1 and σ are related by (2.15), and ε_2 and σ are related by (2.16). Since the two elements are connected in series, the total strain is summed

$$\varepsilon = \varepsilon_1 + \varepsilon_2. \quad (2.17)$$

Differentiating (2.15) and (2.17) with respect to time gives

$$\frac{d\sigma}{dt} = E \frac{d\varepsilon_1}{dt} \quad (2.18)$$

$$\frac{d\varepsilon}{dt} = \frac{d\varepsilon_1}{dt} + \frac{d\varepsilon_2}{dt} \quad (2.19)$$

respectively. Combine (2.16) and (2.18) into (2.19) to obtain

$$E \frac{d\varepsilon}{dt} = \frac{d\sigma}{dt} + \frac{E}{\eta} \sigma. \quad (2.20)$$

This differential equation is the constitutive equation of a linear viscoelastic material represented by the Maxwell model.

To find the relaxation modulus of the Maxwell model, (2.20) is solved when a constant strain is applied, that is $\varepsilon(t) = \varepsilon_0 H(t)$, where $H(t)$ is the Heaviside step function. To solve (2.20), an initial condition is required. The sudden application of strain at $t = 0$ implies $\frac{d\varepsilon}{dt}$ is singular at this point. To deal with it, [15] suggested integrating (2.20) across this point, from a point immediately to the left of $t = 0$ to a point immediately to the right of

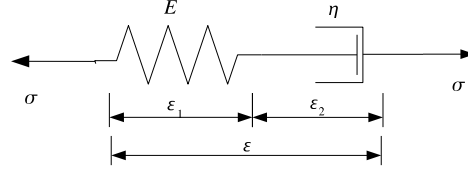


Figure 2.5: Maxwell Model

$t = 0$, which gives

$$E(\varepsilon(s^+) - \varepsilon(s^-)) = \sigma(s^+) - \sigma(s^-) + \frac{E}{\eta} \int_{s^-}^{s^+} \sigma(s) ds.$$

When s approaches zero, the last term on the right hand side goes to zero, and

$$E\varepsilon_0 = \sigma_0,$$

where $\varepsilon_0 = \varepsilon(0^+)$ and $\sigma_0 = \sigma(0^+)$ are the value of ε and σ immediately to the right of $t = 0$ respectively. Thus, the initial condition of the Maxwell model is the instantaneous elastic response of its spring element, and the initial strain of the dashpot is zero.

When the Maxwell model is subject to a constant strain $\varepsilon(t) = \varepsilon_0 H(t)$, (2.20) becomes

$$E\varepsilon_0 \delta(t) = \frac{d\sigma}{dt} + \frac{1}{\tau_R} \sigma,$$

where $\delta(t)$ is the Dirac Delta function, and $\tau_R = \frac{\eta}{E}$. Using the method of integrating factors, where the integrating factor is $e^{\frac{t}{\tau_R}}$, together with the initial condition $\sigma_0 = E\varepsilon_0$, the stress response is

$$\sigma(t) = \varepsilon_0 E e^{-\frac{t}{\tau_R}}$$

for $t > 0$. The stress response is described by a function of decay, and the rate of decay is determined by $\frac{1}{\tau_R}$. τ_R is called the relaxation time, and it is a characteristic time of the viscoelastic material when most of the stress vanishes at $t = \tau_R$. For example, at $t = \tau_R$, $\sigma(t) = \frac{\sigma_0}{e} = 0.37\sigma_0$, which means 37% of the initial stress remains at $t = \tau_R$. The relaxation modulus, $G(t)$, is obtained from the stress response, which is

$$G(t) = \frac{\sigma(t)}{\varepsilon_0} = E e^{-\frac{t}{\tau_R}}.$$

In general, the relaxation modulus is always a monotonically decreasing function of time.

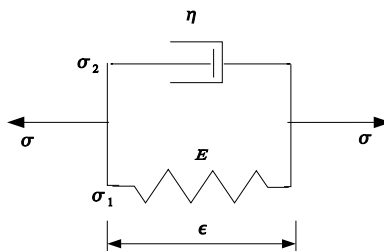


Figure 2.6: Kelvin Model

Kelvin Model

Another linear viscoelastic model is the Kelvin model. It is given by a spring and a dashpot connected in parallel, see Figure 2.6. Since the elements are connected in parallel, their stresses are different, and their strains are identical. Let the stress of the spring and dashpot be σ_1 and σ_2 respectively, and let the strain of the two elements be ε . σ_1 and ε are governed by (2.15), and σ_2 and ε are governed by (2.16). Since the two elements are connected in parallel, the total stress is additive

$$\sigma = \sigma_1 + \sigma_2. \quad (2.21)$$

Substitute (2.15) and (2.16) into (2.21), and obtain

$$\eta \frac{d\varepsilon}{dt} + E\varepsilon = \sigma. \quad (2.22)$$

This differential equation is the constitutive equation of a linear viscoelastic material described by a Kelvin model.

Unlike the Maxwell model, the Kelvin model does not have relaxation modulus. When substitute a constant strain, $\varepsilon(t) = \varepsilon_0 H(t)$, into (2.22), it becomes

$$\varepsilon_0 \delta(t) + \frac{\varepsilon_0}{\tau} H(t) = \frac{\sigma(t)}{\eta},$$

where the first term describes an infinite stress at $t = 0$, which is physically unattainable. However, the Kelvin model can be combined with a spring to obtain a more realistic model, as described next.

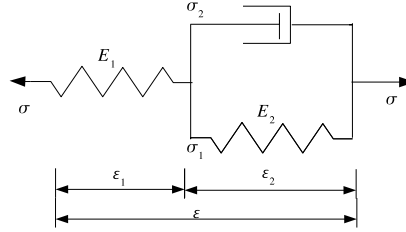


Figure 2.7: Maxwell Solid Model

Maxwell Solid

Both the Maxwell and Kelvin model are not sufficient to represent the behaviour of most viscoelastic material accurately[14]. A more realistic model, called a Maxwell Solid model, is based on connecting a Kelvin model with a spring in series, as shown in Figure 2.7.

Since the Kelvin model is connected with a spring in series, their strains are different, and their stresses are identical. Let the strain of the spring E_1 be ε_1 , and let the strain of the Kelvin model be ε_2 . Their strains are summed

$$\varepsilon = \varepsilon_1 + \varepsilon_2. \quad (2.23)$$

Let the stress of both the spring E_1 and the Kelvin model be σ . Among the elements of the Kelvin model, the stress and strain relationship is

$$\sigma = \eta \frac{d\varepsilon_2}{dt} + E_2 \varepsilon_2. \quad (2.24)$$

Use the fact $\varepsilon_2 = \varepsilon - \varepsilon_1$ in this equation to obtain

$$\sigma = E_2(\varepsilon - \varepsilon_1) + \eta \frac{d}{dt}(\varepsilon - \varepsilon_1).$$

Since the stress σ and strain ε_1 of the spring is related by $\varepsilon_1 = \frac{\sigma}{E_1}$, substitute this into the above equation to obtain

$$\sigma + p_1 \frac{d\sigma}{dt} = q_0 \varepsilon + q_1 \frac{d\varepsilon}{dt}. \quad (2.25)$$

where $p_1 = \frac{\eta}{E_1 + E_2}$, $q_0 = \frac{E_1 E_2}{E_1 + E_2}$ and $q_1 = \frac{\eta E_1}{E_1 + E_2}$. This is the differential constitutive equation of the Maxwell Solid model.

To find the relaxation modulus of this model, let strain be $\varepsilon(t) = \varepsilon_0 H(t)$, and substitute it into (2.25) to obtain

$$\sigma + p_1 \frac{d\sigma}{dt} = q_0 \varepsilon_0 H(t) + q_1 \varepsilon_0 \delta(t).$$

Multiply both sides by $\frac{1}{p_1}$ and an integration factor $e^{\frac{t}{p_1}}$, and rearrange to give

$$\frac{d}{dt}(\sigma e^{\frac{t}{p_1}}) = \varepsilon_0 \left(\frac{q_0}{p_1} e^{\frac{t}{p_1}} H(t) + \frac{q_1}{p_1} e^{\frac{t}{p_1}} \delta(t) \right).$$

Integrate from $s = 0^+$ to $s = t$

$$\begin{aligned} \left[\sigma(s) e^{\frac{s}{p_1}} \right]_{0^+}^t &= \varepsilon_0 \int_{0^+}^t \frac{q_0}{p_1} e^{\frac{s}{p_1}} H(s) + \frac{q_1}{p_1} e^{\frac{s}{p_1}} \delta(s) ds \\ \sigma(t) e^{\frac{t}{p_1}} - \sigma(0^+) &= \varepsilon_0 \left(q_0 e^{\frac{t}{p_1}} - \frac{q_1}{p_1} \right) \end{aligned} \quad (2.26)$$

where assuming $e^{0^+} = 1$. The initial condition of a Maxwell Solid model comes from the elastic spring E_1 only, since $\varepsilon_2(0) = 0$ for the Kelvin element. That is, $\sigma_0 = E\varepsilon_0 = \frac{q_1}{p_1}\varepsilon_0$. Rearranging (2.26) using this information to obtain

$$\sigma(t) = \varepsilon_0 q_0 \left(1 - e^{-\frac{t}{p_1}} \right) + \varepsilon_0 \frac{q_1}{p_1} e^{-\frac{t}{p_1}}$$

for $t > 0$. Thus, the relaxation modulus for a Maxwell Solid model is

$$G(t) = \frac{\sigma(t)}{\varepsilon_0} = q_0 \left(1 - e^{-\frac{t}{\tau_R}} \right) + \frac{q_1}{p_1} e^{-\frac{t}{\tau_R}},$$

where the relaxation time is $\tau_R = p_1$.

Generalized Maxwell Solid

A generalized Maxwell Solid is assembled by adding more Kelvin elements in series to the above Maxwell Solid, and it has a constitutive equation of the form

$$\sigma(x, t) + p_1 \frac{d\sigma(x, t)}{dt} + p_2 \frac{d^2\sigma(x, t)}{dt^2} + \dots = q_0 \varepsilon(x, t) + q_1 \frac{d\varepsilon(x, t)}{dt} + q_2 \frac{d^2\varepsilon(x, t)}{dt^2} + \dots \quad (2.27)$$

Its stress relaxation modulus has multiple relaxation times and has the form of a Prony series

$$G(t) = g_0 + \sum_{i=1}^N g_i e^{-\frac{t}{\tau_i}}. \quad (2.28)$$

In this thesis, the viscoelastic behaviour of brain tissue is represented by a generalized Maxwell solid. Note the spatial dependence is included back here for clarity. (2.27) can be written as

$$\mathbf{P}\sigma(x, t) = \mathbf{Q}\varepsilon(x, t)$$

where \mathbf{P} and \mathbf{Q} are time operators

$$\mathbf{P} = \sum_{k=0}^n p_k \frac{d^k}{dt^k}, \quad \mathbf{Q} = \sum_{k=0}^m q_k \frac{d^k}{dt^k},$$

where n and m depend on the number of terms in (2.27).

2.3.2 1-D Integral form

Another way to describe a constitutive equation is through a hereditary integral. An integral constitutive equation can describe all the characteristics contained in a differential equation and has greater flexibility when it comes to rendering the measured properties of an actual material [15]. For the differential form, the stress response can only be obtained when the strain input is a constant function. However, for the integral constitutive equation, the stress response can be found for any arbitrary strain function.

The hereditary integral is derived as follows for a non-aging homogeneous material. This integral involves two time variables, t which describes the current time, and s which describes the previous time, $s \leq t$. Then, the relaxation modulus is a function of t and s , $G(t, s)$. A non-aging material implies the material does not change with time, and so its relaxation modulus remains unchanged under time translation. That is, $G(t, s) = G(t - s)$, $s \leq t$, depends on the elapsed time, $t - s$. A homogeneous material implies the relaxation modulus does not depend on position. Note that the generalized Maxwell Solid describes a material that is non-aging and homogeneous.

If an arbitrary strain function becomes nonzero at t_0 , $\varepsilon(t_0) = \varepsilon_0$, then the stress starts to relax at $t = t_0$, and has the form $\sigma(t) = \varepsilon_0 G(t - t_0)$ for $t \geq t_0$. If the strain remains unchanged, the stress will be described by this equation for all $t \geq t_0$. However, if at $t = t_1$, an incremental strain of $\Delta\varepsilon_1$ is added, then for $t \geq t_1$, an additional stress of $\Delta\varepsilon_1 G(t - t_1)$ is produced according to the same relaxation modulus but at starting time $t = t_1$. Thus,

the total stress for $t \geq t_0$ is

$$\sigma(t) = \varepsilon_0 G(t - t_0) + \Delta \varepsilon_1 G(t - t_1).$$

This is one step of a very general case. Assuming that the strain is a general function $\varepsilon(t)$ that is nonzero for $t \geq t_0$, an incremental change in strain is $d\varepsilon = \frac{d\varepsilon}{ds} ds$, where ds is a change in time. According to Boltzmann's Principle, the total stress at time t is the sum of the stress resulted from each incremental change in strain at times $t < s$, that is

$$\sigma(x, t) = G(t - t_0)\varepsilon(x, t_0) + \int_{t_0}^t G(t - s) \frac{d\varepsilon(x, s)}{ds} ds \quad (2.29)$$

for $t \geq t_0$. The integral in (2.29) is called a hereditary integral, and it shows how stress at any time depends on all that has happened before, on the entire strain history of $\frac{d\varepsilon(s)}{ds}$, $s < t$. Through integration by parts, (2.29) can be rewritten in another way

$$\sigma(x, t) = G(0)\varepsilon(x, t) - \int_{t_0}^t \frac{dG(t - s)}{ds} \varepsilon(x, s) ds \quad (2.30)$$

for $t \geq t_0$. Consequently, the stress response for an arbitrary strain function can be either (2.29) or (2.30), and they are also the integral constitutive equations for a material with stress relaxation modulus $G(t - s)$. However, only the form appearing in (2.29) is used in the rest of this thesis.

In general, the relaxation modulus $G(x, t, s)$ can be a general function that depend on position x , current time t and previous time s , $s < t$. In this case, the material is aging and inhomogeneous. Then, the constitutive equations can be written as follows:

$$\sigma(x, t) = G(x, t, t_0)\varepsilon(x, t_0) + \int_{t_0}^t G(x, t, s) \frac{d\varepsilon(x, s)}{ds} ds$$

or as

$$\sigma(x, t) = G(x, t, t)\varepsilon(x, t) - \int_{t_0}^t \frac{dG(s, t, s)}{ds} \varepsilon(x, s) ds$$

for $t \geq t_0$.

2.3.3 Higher Dimensional Model

The differential or integral constitutive equation considered so far is one-dimensional, thus it can only describes uni-axial deformation. The constitutive equation of a viscoelastic material can be generalized to higher dimensions by considering elastic constitutive equation (2.10), and (2.11) and (2.12), which are restated here for convenience

$$\sigma_{ij} = \lambda \varepsilon_{kk} \delta_{ij} + \mu \varepsilon_{ij}(\mathbf{x}, t). \quad (2.31)$$

and

$$\begin{aligned} \sigma'_{ij}(\mathbf{x}, t) &= 2G\varepsilon'_{ij}(\mathbf{x}, t) \\ \sigma_{kk}(\mathbf{x}, t) &= 3K\varepsilon_{kk}(\mathbf{x}, t) \end{aligned} \quad (2.32)$$

The constant G and K in (2.32) can be replaced with bulk relaxation modulus $K(t-s)$ and shear relaxation modulus $G(t-s)$, using hereditary integrals, such that the following integral constitutive equations are formed

$$\sigma'_{ij}(\mathbf{x}, t) = 2G(t-t_0)\varepsilon'_{ij}(\mathbf{x}, t_0) + \int_{t_0}^t 2G(t-s) \frac{d\varepsilon'_{ij}(\mathbf{x}, s)}{ds} ds \quad (2.33)$$

$$\sigma_{kk}(\mathbf{x}, t) = 3K(t-t_0)\sigma_{kk}(\mathbf{x}, t_0) + \int_{t_0}^t 3K(t-s) \frac{d\sigma_{kk}(\mathbf{x}, s)}{ds} ds \quad (2.34)$$

for $t \geq t_0$.

Another form of the integral constitutive equations is found by replacing the Lamé constants in (2.31) with their viscoelastic counterparts, $\lambda(t-s)$ and $\mu(t-s)$, using hereditary integrals

$$\begin{aligned} \sigma_{ij}(\mathbf{x}, t) &= \lambda(t-t_0)\varepsilon_{kk}(\mathbf{x}, t_0)\delta_{ij} + \mu(t-t_0)\varepsilon_{ij}(\mathbf{x}, t_0) \\ &+ \int_{t_0}^t \lambda(t-s) \frac{d\varepsilon_{kk}(\mathbf{x}, s)}{ds} \delta_{ij} + \mu(t-s) \frac{d\varepsilon_{ij}(\mathbf{x}, s)}{ds} ds, \end{aligned} \quad (2.35)$$

where $\lambda(t-s)$ and $\mu(t-s)$, $s < t$, are also called relaxation functions.

To derive a 3 dimensions constitutive equations in differential form, consider (2.32) where the dilatation and deviatoric part are separated, and replace the constant G and K with differential operators to obtain

$$\begin{aligned} \mathbf{P}_1 \sigma'_{ij}(\mathbf{x}, t) &= \mathbf{Q}_1 \varepsilon'_{ij}(\mathbf{x}, t) \\ \mathbf{P}_2 \sigma_{kk}(\mathbf{x}, t) &= \mathbf{Q}_2 \varepsilon_{kk}(\mathbf{x}, t) \end{aligned} \quad (2.36)$$

The two pairs, \mathbf{P}_1 and \mathbf{Q}_1 , and \mathbf{P}_2 and \mathbf{Q}_2 are differential operators defined as

$$\begin{aligned}\mathbf{P}_1 &= \sum_{k=0}^{n_1} (p_1)_k \frac{d^k}{dt^k}, \\ \mathbf{Q}_1 &= 2 \sum_{k=0}^{m_1} (q_1)_k \frac{d^k}{dt^k}, \\ \mathbf{P}_2 &= \sum_{k=0}^{n_2} (p_2)_k \frac{d^k}{dt^k}, \\ \mathbf{Q}_2 &= 3 \sum_{k=0}^{m_2} (q_2)_k \frac{d^k}{dt^k},\end{aligned}$$

where $(p_1)_k$ and $(q_1)_k$ are the parameters that describe the viscoelastic dilatation, and $(p_2)_k$ and $(q_2)_k$ are the parameters that describe the viscoelastic shear. The two pairs of operators are independent of each other, and each pair can be modeled by an assembly of springs and dashpots element as discussed previously.

Recall that the two dimensional problem of this thesis is assumed to be in plane strain, which implies $\varepsilon_{13}(\mathbf{x}, t) = \varepsilon_{23}(\mathbf{x}, t) = \varepsilon_{33}(\mathbf{x}, t) = 0$. Thus, when substituting these strain components into one of the above 3D viscoelastic constitutive equations, $\sigma_{13}(\mathbf{x}, t) = \sigma_{23}(\mathbf{x}, t) = 0$ and $\sigma_{33}(\mathbf{x}, t)$ depends on $\varepsilon_{11}(\mathbf{x}, t)$ and $\varepsilon_{22}(\mathbf{x}, t)$. Thus, similar to the plane strain problem for linear elasticity, only three components of strain and stress, ε_{11} , ε_{12} , ε_{22} and σ_{11} , σ_{12} , σ_{22} , are needed to be solved.

2.4 Viscoelastic Properties of Brain Tissue

Brain tissue is a complex material; it is described as a soft yielding structure that is not as stiff as gel or as plastic as paste [22]. It is composed of gray matter, which contains neuronal cell, and white matter, which contains interconnecting fibers between areas of grey matter.

Since the late 1960s, a number of studies were conducted to understand the viscoelastic properties of brain tissue, and most of them were conducted for the purpose of understanding its mechanical response in a traumatic head impact. The types of experiments include compression, tension, shear and oscillatory loading of brain tissue in vitro. Its properties are

found to be dependent on location of the brain, age of the patient, whether it is white or grey matter and is anisotropic. Since these dependencies are not fully understood, brain tissue is generally modeled as a homogeneous, non-aging and isotropic material. Also, it is found to be relatively incompressible, nonlinear and viscoelastic [17, 13, 37, 38, 10, 26, 18, 25], and its properties have been described with both the differential and integral constitutive equations.

To fully characterize the tissue's mechanical behaviour over a large range of strain and strain rates for all types of application, would require an extensive testing regime of great cost and effort. Consequently, researchers have tended to conduct tests within a regime that is relevant to an application in which they are interested. For a summary for different test regimes and proposed constitutive equations, see [9]. Also, in [9], several of the proposed viscoelastic constitutive equations of different forms have been rewritten into a shear modulus $G(t)$ of the generalized Maxwell model. Although it is unclear how they are rewritten, [9] provides a good summary for shear modulus for different test regimes.

Since the interest to many researchers is traumatic head injury, the test regimes are usually short in time, and the relaxation time of the observed shear modulus is usually in seconds. The longest observed relaxation time is 80s in [12] which used experimental data from [13, 17]. It is uncertain whether the viscoelastic parameters derived from such experiments are suitable to model a brain with hydrocephalus, which is a very slow and quasi-static process. Typical time scales may be weeks or months. However, due to a lack of information about the behaviour of brain tissue on a long time scale, a linear viscoelastic model with two relaxation times, 29.8 s and 1.82 s, taken from [18], is selected for this thesis.

In particular, the shear relaxation modulus $G(t)$ is derived from the relaxation response of indentation test on a porcine brain in vivo at $1mm/s$ with $4mm$ indentation, and the number of terms in the prony series of $G(t)$ is $N = 2$. The authors of [18] have also performed tests in situ, and they found that the long-term shear relaxation time of $G(t)$ derived in vivo is longer than the one derived in situ. In vivo refers to experimentation done in or on the living tissue of a whole, living animal, while in situ refers to experimentation done on the tissue that is in the place of a sacrificed animal.

2.5 Model Equations for a Hydrocephalus Brain

To summarize, the domain Ω , shown in Figure 2.1, represents the brain undergoing physical deformation in plane strain, and it is a 2-D geometry with two boundary curves $\partial\Omega_{in}$ and $\partial\Omega_{out}$. For $t \in I$, the displacement vector $\mathbf{u}(\mathbf{x}, t) = (u_1(\mathbf{x}, t), u_2(\mathbf{x}, t))$ is measured from position $\mathbf{x} = (x_1, x_2) \in \Omega \cup \partial\Omega$, which is the original configuration, and the displacement vector is governed by the equations of motion under quasi-static assumption:

$$\frac{\partial \sigma_{ij}(\mathbf{x}, t)}{\partial x_i} = 0, \quad (2.37)$$

the kinematic equations for infinitesimal deformation:

$$\varepsilon_{ij}(\mathbf{x}, t) = \frac{1}{2} \left(\frac{\partial u_i(\mathbf{x}, t)}{\partial x_j} + \frac{\partial u_j(\mathbf{x}, t)}{\partial x_i} \right), \quad (2.38)$$

the linear constitutive equations of the form:

$$\sigma_{ij}(\mathbf{x}, t) = F(\varepsilon_{ij}(\mathbf{x}, t)),$$

and boundary conditions:

$$\mathbf{u}(\mathbf{x}, t) = \vec{0}, \quad \mathbf{x} \in \partial\Omega_{out} \quad (2.39)$$

$$\sigma_{ij}(\mathbf{x}, t) \mathbf{n}_j^{in} = -g_i(\mathbf{x}, t), \quad \mathbf{x} \in \partial\Omega_{in} \quad (2.40)$$

where \mathbf{n}^{in} is an outward unit normal at \mathbf{x} , and $\mathbf{g}(\mathbf{x}, t)$ is a stress vector

$$\begin{bmatrix} g_1(\mathbf{x}, t) \\ g_2(\mathbf{x}, t) \end{bmatrix} = \frac{1}{t_1^2 + t_2^2} \begin{bmatrix} t_1 & t_2 \\ t_2 & -t_1 \end{bmatrix} \begin{bmatrix} 0 \\ -P(t) \end{bmatrix}$$

for \mathbf{t}^{in} is a unit tangent at \mathbf{x} pointing clockwise, and $P(t)$ represents the CSF pressure.

Elastic Problem

When the brain Ω is assumed to be homogeneous isotropic linear elastic, the constitutive equations in terms of the Young's modulus E and the Poisson ratio ν is

$$\sigma_{ij}(\mathbf{x}, t) = \frac{E\nu}{(1+\nu)(1-2\nu)} \varepsilon_{kk}(\mathbf{x}, t) \delta_{ij} + \frac{E}{(1+\nu)} \varepsilon_{ij}(\mathbf{x}, t). \quad (2.41)$$

Although it may be inaccurate to model the brain as a linear elastic material, it is studied here because it is an analogy to the viscoelastic model and helps to develop an analytical and numerical solution to the viscoelastic problem. Therefore, (2.37) to (2.41) are the set of equations used in Section 3.1 to obtain a numerical solution to the elastic problem. Note that time dependency in this problem exists only in the boundary condition. Thus, whether the pressure changes instantaneously or incrementally to a final pressure, their final solutions are identical.

Viscoelastic Problem

As mentioned in the previous section, brain tissue is generally considered to be homogeneous, isotropic, non-aging, nonlinear viscoelastic and nearly incompressible. Homogeneity, isotropy and the non-aging property are already assumed in deriving the viscoelastic constitutive equations in Section 2.3. To describe incompressibility, the bulk modulus K is assumed to be a large constant, and so the dilatation response of the brain tissue is elastic. For the shear response, the shear relaxation modulus $G(t - q)$ is assumed to be a linear viscoelastic model. For the viscoelastic problem, two different constitutive equations are used for different purposes.

First, for developing a numerical method, the integral constitutive equations with K and $G(t - q)$ are used

$$\begin{aligned}\sigma'_{ij}(\mathbf{x}, t) &= 2G(t - t_0)\varepsilon'_{ij}(\mathbf{x}, t_0) + \int_{t_0}^t 2G(t - s)\frac{d\varepsilon'_{ij}(\mathbf{x}, s)}{ds}ds \\ \sigma_{kk}(\mathbf{x}, t) &= 3K\varepsilon_{kk}(\mathbf{x}, t),\end{aligned}$$

where $G(t - s)$ is defined in (2.28). These two equations can be combined together using (2.2) and (2.5) to obtain

$$\begin{aligned}\sigma_{ij}(\mathbf{x}, t) &= \left[K\varepsilon_{kk}(\mathbf{x}, t) - \frac{2}{3} \left(G(t - t_0)\varepsilon_{kk}(\mathbf{x}, t_0) + \int_{t_0}^t G(t - s)\frac{d\varepsilon_{kk}(\mathbf{x}, s)}{ds}ds \right) \right] \delta_{ij} \\ &\quad + 2 \left(G(t - t_0)\varepsilon_{ij}(\mathbf{x}, t_0) + \int_{t_0}^t G(t - s)\frac{d\varepsilon_{ij}(\mathbf{x}, s)}{ds}ds \right)\end{aligned}\quad (2.42)$$

for $t \geq t_0$. Thus, (2.42) together with (2.37) to (2.40) are the set of model equations used in Section 3.2 to formulate a numerical model.

Second, to verify the correctness of the numerical solution, an analytical solution is needed. In this case, the differential constitutive equations are more convenient in finding an analytical solution because Laplace Transform can be applied. Thus, the following differential constitutive equations

$$\mathbf{P}_1 \sigma'_{ij}(\mathbf{x}, t) = \mathbf{Q}_1 \varepsilon'_{ij}(\mathbf{x}, t) \quad (2.43)$$

$$\sigma_{kk}(\mathbf{x}, t) = 3K \varepsilon_{kk}(\mathbf{x}, t) \quad (2.44)$$

together with (2.37) to (2.40) are the set of model equations for deriving an analytical solution in the next section.

2.6 Analytical Solutions

In general, it is not possible to find an analytical solution to the viscoelastic problem when Ω is an arbitrary geometry. But when Ω is assumed to be a horizontal cross-section of a thick-walled cylinder, an analytical solution exists in polar coordinates (r, θ) . See Figure 2.8. Let the radius of inside wall be $r = a$, and the radius of the outside wall be $r = b$. Then, the boundary conditions in polar coordinates are

$$\begin{aligned} \sigma_{rr}(r, \theta, t) &= -P(t) \\ \sigma_{\theta\theta}(r, \theta, t) &= 0 \end{aligned} \quad (2.45)$$

at $r = a$ and $0 \leq \theta \leq 2\pi$

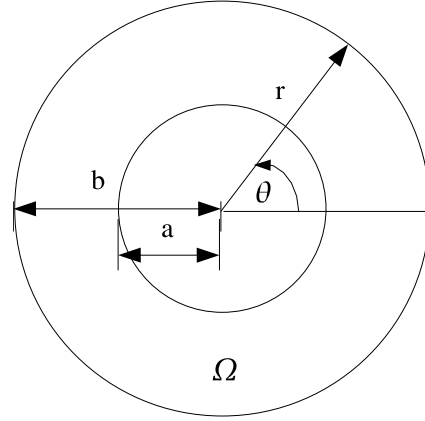
$$\begin{aligned} u_r(r, \theta, t) &= 0 \\ u_\theta(r, \theta, t) &= 0 \end{aligned} \quad (2.46)$$

at $r = b$ and $0 \leq \theta \leq 2\pi$.

Elastic Problem

The elastic problem for a thick-walled cylinder is a well-known example studied in many texts, and [47, Chapter 27] provides an example similar to the elastic problem in this thesis. Following the example in [47, Chapter 27], a general solution for the stress components are

$$\begin{aligned} \sigma_{rr}(r, \theta, t) &= \frac{A}{r^2} + 2C \\ \sigma_{\theta\theta}(r, \theta, t) &= -\frac{A}{r^2} + 2C, \end{aligned}$$

Figure 2.8: Domain Ω for analytical solutions.

and the displacements are

$$\begin{aligned} u_r(r, \theta, t) &= \frac{1}{E} \left(\frac{-(1+\nu)}{r} A + 2C(1-\nu-2\nu^2) \right) \\ u_\theta &= 0 \end{aligned}$$

for $a \leq r \leq b$ and $0 \leq \theta < 2\pi$, where the two unknowns A and C are determined by the two boundary conditions (2.45) and (2.46). It is easy to show they are

$$\begin{aligned} A &= -\frac{P(t)a^2b^2(1-2\nu)}{a^2+b^2(1-2\nu)}, \\ 2C &= -(P_0 + \frac{A}{a^2}). \end{aligned}$$

Hence, radial displacement has the final form

$$u_r(r, \theta, t) = P(t)a^2 \left(\frac{b}{r} - \frac{r}{b} \right) \frac{(1+\nu)(1-2\nu)}{E(a^2+b^2-2b^2\nu)}. \quad (2.47)$$

Viscoelastic Problem

Analytical solution to general viscoelastic problems are also studied in [15, Section 8.7], which uses a classical method called Correspondence Principle. Using this principle, the elastic counterpart to a viscoelastic problem must be solved first, and then take its Laplace

transform. In this case, the Laplace transform of (2.47) to give

$$\widehat{u}_r(r, \theta, s) = \frac{P_0}{s} a^2 \left(\frac{b}{r} - \frac{r}{b} \right) \frac{(1 + \nu)(1 - 2\nu)}{E(a^2 + b^2 - 2b^2\nu)}, \quad (2.48)$$

assuming $P(t) = P_0 H(t)$ for convenience, and where s represent the frequency domain. Then, the Laplace transform of the differential constitutive equations (2.43) and (2.44) are

$$\widehat{\mathbf{P}}_1(s) \widehat{\sigma}'_{ij}(\mathbf{x}, s) = \widehat{\mathbf{Q}}_1(s) \widehat{\varepsilon}'_{ij}(\mathbf{x}, s), \quad (2.49)$$

$$\widehat{\mathbf{P}}_2(s) \widehat{\sigma}_{kk}(\mathbf{x}, s) = \widehat{\mathbf{Q}}_2(s) \widehat{\varepsilon}_{kk}(\mathbf{x}, s), \quad (2.50)$$

and in particular, let the shear response be described by a simple Maxwell Solid model with one relaxation time

$$\begin{aligned} \widehat{\mathbf{P}}_1 &= 1 + p_1 s & \widehat{\mathbf{Q}}_1 &= 2(q_0 + q_1 s) \\ \widehat{\mathbf{P}}_2 &= 1 & \widehat{\mathbf{Q}}_2 &= 3K \end{aligned}, \quad (2.51)$$

where $q_1 > p_1 q_0$, and p_1 , q_0 , q_1 and K are some constants that describes an arbitrary material. The differential constitutive (2.49) and (2.50) are now algebraic relations, and if the following substitutions are made, they become identical with the constitutive equations of the elastic counterpart (2.41)

$$E \rightarrow \frac{3\widehat{\mathbf{Q}}_1\widehat{\mathbf{Q}}_2}{2\widehat{\mathbf{P}}_1\widehat{\mathbf{Q}}_2 + \widehat{\mathbf{Q}}_1\widehat{\mathbf{P}}_2}, \quad (2.52)$$

$$v \rightarrow \frac{\widehat{\mathbf{P}}_1\widehat{\mathbf{Q}}_2 - \widehat{\mathbf{Q}}_1\widehat{\mathbf{P}}_2}{2\widehat{\mathbf{P}}_1\widehat{\mathbf{Q}}_2 + \widehat{\mathbf{Q}}_1\widehat{\mathbf{P}}_2}. \quad (2.53)$$

Substitute the viscoelastic parameters (2.51) into (2.52) and (2.53) which then substitute into the transformed elastic solution (2.48) to obtain the transformed viscoelastic solution

$$\widehat{u}_r(r, \theta, s) = \frac{3P_0 a^2 (b^2 - r^2)}{r} \frac{1 + p_1 s}{s [(6a^2 p_1 K + 2a^2 q_1 + 6b^2 q_1) s + 6a^2 K + 2a^2 q_0 + 6b^2 q_0]}. \quad (2.54)$$

Then, take the inverse Laplace transform of this equation to obtain the analytical solution of the viscoelastic problem

$$u_r(r, \theta, r) = \frac{3P_0 a^2 (b^2 - r^2)}{r} \left[\frac{1}{\beta} + \left(\frac{p_1}{\alpha} - \frac{1}{\beta} \right) e^{-\frac{\beta}{\alpha} t} \right],$$

where

$$\alpha = 6a^2p_1K + 2a^2q_1 + 6b^2q_1$$

$$\beta = \beta = 6a^2K + 2a^2q_0 + 6b^2q_0.$$

Chapter 3

Numerical Method

The finite element method is often used to solve elliptic partial differential equations, and the elastic problem described in Chapter 2 is a classical application of finite element method. Moreover, because of the similarity between the elastic and viscoelastic problem, finite element method can also be applied to the viscoelastic problem for space discretization.

In this chapter, the concepts of finite element method are introduced in Section 3.1 using the elastic problem as an example first. Then, in Section 3.2, the viscoelastic problem is discretized in space using the same finite element method, and its time domain is discretized using finite difference and trapezoidal rule. Next, image segmentation and grid generation are discussed in Section 3.3, since the computational meshes used in numerical simulations are generated using a medical image of a patient's brain.

Once the numerical methods for solving the two problems and for generating computational meshes are developed, the numerical solution is compared with the analytical solution in Section 3.4. Finally, the stability of the numerical method for the viscoelastic problem is studied in Section 3.5.

3.1 Finite Element Method for the Elastic Problem

From Chapter 2, the model equations for the elastic problem are

$$\frac{\partial \sigma_{ij}(\mathbf{x}, t)}{\partial x_j} = 0, \quad (3.1)$$

$$\varepsilon_{ij}(\mathbf{x}, t) = \frac{1}{2} \left(\frac{\partial u_i(\mathbf{x}, t)}{\partial x_j} + \frac{\partial u_j(\mathbf{x}, t)}{\partial x_i} \right), \quad (3.2)$$

$$\sigma_{ij}(\mathbf{x}, t) = \frac{Ev}{(1+v)(1-2v)} \varepsilon_{kk}(\mathbf{x}, t) \delta_{ij} + \frac{E}{(1+v)} \varepsilon_{ij}(\mathbf{x}, t), \quad (3.3)$$

and the boundary conditions are

$$\mathbf{u}(\mathbf{x}, t) = 0, \quad \mathbf{x} \in \partial\Omega_{out}, \quad (3.4)$$

$$\sigma_{ij}(\mathbf{x}, t) \mathbf{n}_j^{in} = -g_i(\mathbf{x}, t), \quad \mathbf{x} \in \partial\Omega_{in}, \quad (3.5)$$

where \mathbf{n}^{in} is the outward unit normal at \mathbf{x} on $\partial\Omega_{in}$, and $\mathbf{g}(\mathbf{x}, t)$ is a stress vector.

In this section, the three main steps of finite element method are introduced with the elastic problem. The first step is to set up a weak formulation of the problem. The second step is to discretize the weak formulation. Lastly, elementary stiffness matrix and load vector are assembled to form a system of equations that solves for displacement. For more information about finite element method for the elastic problem, see [6] and [49].

3.1.1 Step 1: Weak Formulation

Let $\mathcal{H}^1(\Omega)$ be the usual Sobolev space of functions whose generalized derivatives of order at most 1 are squared integrable, that is they belong to $\mathcal{L}_2(\Omega)$, and a product space be $(\mathcal{H}^1(\Omega))^2 = \mathcal{H}^1(\Omega) \times \mathcal{H}^1(\Omega)$. Let a trial space for the elastic problem be given by

$$\mathcal{V} = \{ \mathbf{v}(\mathbf{x}) \in (\mathcal{H}^1(\Omega))^2, \mathbf{v}(\mathbf{x}) = 0 \text{ on } \partial\Omega_{out} \}.$$

Let $\mathbf{v}(\mathbf{x}) = (v_1(\mathbf{x}), v_2(\mathbf{x})) \in \mathcal{V}$ be a test vector function. Spatial and temporal dependence are omitted in the following derivation for convenience. Take the scalar product of the system (3.1) with the test vector function \mathbf{v} , and integrate over Ω gives

$$\int_{\Omega} \frac{\partial \sigma_{ij}}{\partial x_j} v_i d\mathbf{x} = 0. \quad (3.6)$$

The repeated index in this equation sums over $i = 1, 2$ and $j = 1, 2$, to give a scalar, since $\frac{\partial \sigma_{ij}}{\partial x_j}$ is a divergence of a tensor which gives a vector, and so the scalar product of $\frac{\partial \sigma_{ij}}{\partial x_j}$ and \mathbf{v} gives a scalar. Then substitute the following product identity,

$$\frac{\partial}{\partial x_j} (\sigma_{ij} v_i) = v_i \frac{\partial \sigma_{ij}}{\partial x_j} + \sigma_{ij} \frac{\partial v_i}{\partial x_j},$$

into (3.6), and it becomes

$$\int_{\Omega} \frac{\partial}{\partial x_j} (\sigma_{ij} v_i) d\mathbf{x} - \int_{\Omega} \sigma_{ij} \frac{\partial v_i}{\partial x_j} d\mathbf{x} = 0. \quad (3.7)$$

Apply the Divergence Theorem to the first term of (3.7), and get

$$\int_{\Omega} \frac{\partial}{\partial x_j} (\sigma_{ij} v_i) d\mathbf{x} = \int_{\partial\Omega_{in}} v_i \sigma_{ij} \mathbf{n}_j^{in} ds + \int_{\partial\Omega_{out}} v_i \sigma_{ij} \mathbf{n}_j^{out} ds,$$

where \mathbf{n}^{out} is a unit normal at \mathbf{x} on $\partial\Omega_{out}$ pointing outward. Since $\mathbf{v} \in \mathcal{V}$ which implies $\mathbf{v} = 0$ on $\partial\Omega_{out}$, the second term on the right hand side is zero. Then using the Neumann boundary condition (3.5), the first term of the right hand side becomes $-\int_{\partial\Omega_{in}} v_i g_i ds$. Thus, the first term of (3.7) becomes

$$\int_{\Omega} \frac{\partial}{\partial x_j} (\sigma_{ij} v_i) dx = - \int_{\partial\Omega_{in}} v_i g_i ds. \quad (3.8)$$

Next, consider the second term of equation (3.7), its integrand can be written using the fact that $\sigma_{ij} = \sigma_{ji}$ as follows

$$\begin{aligned} \sigma_{ij} \frac{\partial v_i}{\partial x_j} &= \sigma_{ij} \frac{1}{2} \left(\frac{\partial v_i}{\partial x_j} + \frac{\partial v_i}{\partial x_j} \right) \\ &= \frac{1}{2} \left(\sigma_{ij} \frac{\partial v_i}{\partial x_j} + \sigma_{ij} \frac{\partial v_i}{\partial x_j} \right) \\ &= \frac{1}{2} \left(\sigma_{ij} \frac{\partial v_i}{\partial x_j} + \sigma_{ji} \frac{\partial v_j}{\partial x_i} \right) \\ &= \sigma_{ij} \varepsilon_{ij}(\mathbf{v}) \end{aligned} \quad (3.9)$$

where $\varepsilon_{ij}(\cdot) = \frac{1}{2} \left(\frac{\partial \cdot}{\partial x_j} + \frac{\partial \cdot}{\partial x_i} \right)$ is treated as an functional operator on $v(\mathbf{x})$. So using (3.8) and (3.9), (3.7) becomes

$$\int_{\partial\Omega_{in}} v_i g_i ds + \int_{\Omega} \sigma_{ij}(\mathbf{u}) \varepsilon_{ij}(\mathbf{v}) d\mathbf{x} = 0 \quad (3.10)$$

where $\sigma_{ij}(\mathbf{x}, t)$ is written as $\sigma_{ij}(\mathbf{u})$ to emphasize its dependence on the unknown displacement $\mathbf{u}(\mathbf{x}, t)$.

Since σ_{ij} and ε_{ij} are symmetric, the stress tensor σ and the strain tensor ε can be written as:

$$\sigma = \begin{bmatrix} \sigma_{11} & \sigma_{12} \\ \sigma_{12} & \sigma_{22} \end{bmatrix}, \quad \varepsilon = \begin{bmatrix} \varepsilon_{11} & \varepsilon_{12} \\ \varepsilon_{12} & \varepsilon_{22} \end{bmatrix}.$$

Define the stress vector, $\boldsymbol{\sigma}$, as

$$\boldsymbol{\sigma} = \begin{bmatrix} \sigma_{11} \\ \sigma_{22} \\ \sigma_{12} \end{bmatrix}, \quad (3.11)$$

and define the strain vector, $\boldsymbol{\varepsilon}$, as

$$\boldsymbol{\varepsilon}(\mathbf{u}) = \begin{bmatrix} \varepsilon_{11} \\ \varepsilon_{22} \\ 2\varepsilon_{12} \end{bmatrix} = \begin{bmatrix} \frac{\partial u_1}{\partial x_1} \\ \frac{\partial u_2}{\partial x_2} \\ \frac{\partial u_1}{\partial x_2} + \frac{\partial u_2}{\partial x_1} \end{bmatrix}. \quad (3.12)$$

Then, in vector notation, (3.10) is

$$\int_{\partial\Omega_{in}} \mathbf{v}^T \mathbf{g} ds + \int_{\Omega} \boldsymbol{\varepsilon}(\mathbf{v})^T \boldsymbol{\sigma}(\mathbf{u}) dx = 0. \quad (3.13)$$

Note that the factor of 2 in the strain vector is introduced to account for the duplicate products in summation of $\sigma_{ij}(\mathbf{u})\varepsilon_{ij}(\mathbf{v})$.

Lastly, rewrite the constitutive equation (3.3) in terms of stress and strain vector, using a constitutive matrix, D ,

$$\boldsymbol{\sigma}(\mathbf{u}) = D\boldsymbol{\varepsilon}(\mathbf{u})$$

where

$$D = \frac{E}{(1+v)(1-2v)} \begin{bmatrix} 1-v & v & 0 \\ v & 1-v & 0 \\ 0 & 0 & \frac{1-2v}{2} \end{bmatrix}.$$

The factor of $\frac{1}{2}$ in the matrix D is introduced to account for the factor of 2 in the strain vector. Substituting $\boldsymbol{\sigma}(\mathbf{u}) = D\boldsymbol{\varepsilon}(\mathbf{u})$ into (3.13) gives

$$\int_{\Omega} \boldsymbol{\varepsilon}^T(\mathbf{v}) D \boldsymbol{\varepsilon}(\mathbf{u}) dx = - \int_{\partial\Omega_{in}} \mathbf{v}^T \mathbf{g} ds.$$

Therefore, the weak formulation for the 2D linear elasticity problem is:

Find $\mathbf{u}(\mathbf{x}, t) \in \mathcal{V}$ at each $t \in I$ such that

$$a(\mathbf{u}, \mathbf{v}) = L(\mathbf{v}, t) \quad \forall \mathbf{v}(\mathbf{x}) \in \mathcal{V}, \quad (3.14)$$

where $a(\mathbf{u}, \mathbf{v})$ is called a bilinear operator,

$$a(\mathbf{u}, \mathbf{v}) = \int_{\Omega} \boldsymbol{\varepsilon}^T(\mathbf{v}) D \boldsymbol{\varepsilon}(\mathbf{u}) dx, \quad (3.15)$$

and $L(\mathbf{v}, t)$ is called the load operator,

$$L(\mathbf{v}, t) = - \int_{\partial\Omega_{in}} \mathbf{v}^T \mathbf{g}(t) ds. \quad (3.16)$$

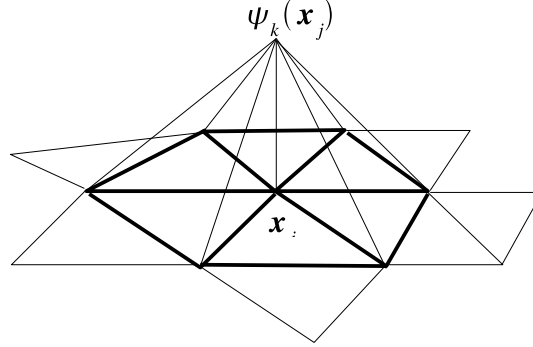
Note the load operator depends on time through $\mathbf{g}(t)$. The Dirichlet boundary condition is imposed on \mathbf{u} implicitly by requiring $\mathbf{u} \in \mathcal{V}$. The solution of (3.14) is called a weak solution because of the transfer of spatial derivatives from \mathbf{u} onto the test function \mathbf{v} , thus weaker regularity is required for \mathbf{u} . For information about the existence and uniqueness of solution to this weak formulation (3.14), see Appendix A.

3.1.2 Step 2: Discretizing the Weak Formulation

The second step is to discretize the weak formulation. First, discretize the domain Ω by dividing it into a set of non-overlapping element so that the approximation of Ω is

$$\Omega_h = T^1 \cup T^2 \dots \cup T^E,$$

where T^e denotes the e^{th} element, and E denotes the total number of elements in Ω_h . The element could be any simple polygon, and it is a triangle in this thesis. The vertices of a

Figure 3.1: $\psi_k(\mathbf{x})$ of \mathcal{V}_h at $\mathbf{x} = \mathbf{x}_j$

triangle are called nodes, and P denotes the total number of nodes in Ω_h . Then, the j^{th} node is denoted by $\mathbf{x}_j = (x_j, y_j)$, and j is referred as the global index of a node.

Let \mathcal{V}_h be a finite-dimensional subspace of \mathcal{V} . Define \mathcal{V}_h as

$$\mathcal{V}_h = \{\mathbf{v} : v_i \in C^0(\Omega), v_i|_{T^e} \in P_1(\mathfrak{R}^2), \text{ and } v_i = 0 \text{ on } \partial\Omega_{out}, \text{ for } i = 1, 2\}$$

where $\mathbf{v}|_{T^e}$ means the restriction of \mathbf{v} over region T^e , and $P_1(\mathfrak{R}^2)$ is the space of linear polynomials in 2-D. Thus, the space \mathcal{V}_h consists of all continuous vector functions that are linear polynomials over each element T^e and vanish on $\partial\Omega_{out}$.

Let the basis functions of \mathcal{V}_h be the column vectors of a $2 \times 2P$ matrix, $\Psi(\mathbf{x})$,

$$\Psi(\mathbf{x}) = \begin{bmatrix} \psi_1(\mathbf{x}) & 0 & \psi_2(\mathbf{x}) & 0 & \dots & \psi_P(\mathbf{x}) & 0 \\ 0 & \psi_1(\mathbf{x}) & 0 & \psi_2(\mathbf{x}) & \dots & 0 & \psi_P(\mathbf{x}) \end{bmatrix}$$

with components $\psi_k(\mathbf{x}) \in P_1(\mathfrak{R}^2)$, $k = 1, \dots, P$, such that

$$\psi_k(\mathbf{x}_j) = \begin{cases} 1 & \text{if } k = j \\ 0 & \text{if } k \neq j \end{cases}.$$

Figure 3.1 shows $\psi_k(\mathbf{x})$ is a linear function over an element T^e , and the support of $\psi_k(\mathbf{x})$ consists of the elements with the common node \mathbf{x}_k .

Since the basis functions of \mathcal{V}_h are the columns of $\Psi(\mathbf{x})$, let the i^{th} column be $\Psi_i(\mathbf{x})$ so that for $i = 1 \dots 2P$

$$\Psi_i(\mathbf{x}) = \Psi(\mathbf{x})\hat{e}_i$$

where \widehat{e}_i is the i^{th} column of a $2P \times 2P$ identity matrix. Then, the weak formulation (3.14) is equivalent to

$$a(\mathbf{u}, \Psi_i) = L(\Psi_i, t) \quad \text{for } i = 1 \dots 2P.$$

where the test function $\mathbf{v}(\mathbf{x})$ is replaced with $\Psi_i(\mathbf{x})$. This gives $2P$ equations to solve for $2P$ unknowns.

Let $\mathbf{u}_h \in \mathcal{V}_h$ be the approximation of \mathbf{u} . The displacement vector at \mathbf{x}_j , $\mathbf{u}_h(\mathbf{x}_j, t)$, are the unknowns, and $\mathbf{u}_h(\mathbf{x}, t)$ can be written in vector form as

$$\mathbf{u}_h(\mathbf{x}, t) = \Psi(\mathbf{x})\mathbf{U}(t), \quad (3.17)$$

where $\mathbf{U}(t)$ is a vector of length $2P$. This implies $\mathbf{u}_h(\mathbf{x}, t)$ is a linear combinations of the basic vector of \mathcal{V}_h , and \mathbf{u}_h is a piecewise linear function over Ω_h . So, $\mathbf{U}(t)$ is a decomposition of $\mathbf{u}_h(\mathbf{x}, t)$ in the basis vectors of V_h . at time t , and it is called the global displacement vector. It consists of all displacement vectors at every nodes at time t . For example, the displacement along x and y direction at the node \mathbf{x}_k is

$$\mathbf{u}_h(\mathbf{x}_k, t) = \begin{bmatrix} U_{2k-1}(t) \\ U_{2k}(t) \end{bmatrix}.$$

In the bilinear form (3.15), the strain vector associated with \mathbf{u}_h is

$$\boldsymbol{\varepsilon}(\mathbf{u}_h) = \mathbf{B}\mathbf{U}(t) \quad (3.18)$$

where \mathbf{B} is a $3 \times 2P$ matrix defined by

$$\mathbf{B} = \begin{bmatrix} \frac{\partial \psi_1(\mathbf{x})}{\partial x_1} & 0 & \dots & \frac{\partial \psi_P(\mathbf{x})}{\partial x_1} & 0 \\ 0 & \frac{\partial \psi_1(\mathbf{x})}{\partial x_2} & \dots & 0 & \frac{\partial \psi_P(\mathbf{x})}{\partial x_2} \\ \frac{\partial \psi_1(\mathbf{x})}{\partial x_2} & \frac{\partial \psi_1(\mathbf{x})}{\partial x_1} & \dots & \frac{\partial \psi_P(\mathbf{x})}{\partial x_2} & \frac{\partial \psi_P(\mathbf{x})}{\partial x_1} \end{bmatrix}.$$

Since $\psi_k(\mathbf{x})$ are linear polynomial, \mathbf{B} is a constant matrix. Similarly, the strain vector associated with the test function $\Psi_i(\mathbf{x})$ is

$$\boldsymbol{\varepsilon}(\Psi_i(\mathbf{x})) = \mathbf{B}\widehat{e}_i. \quad (3.19)$$

Then, after replacing the test function $\mathbf{v}(\mathbf{x})$ with $\Psi_i(\mathbf{x})$, substitute (3.18) and (3.19) into (3.15) and (3.16), the bilinear operator and load operator becomes

$$\begin{aligned} a(\mathbf{u}_h(\mathbf{x}, t), \Psi_i(\mathbf{x})) &= \hat{e}_i^T \left(\int_{\Omega_h} \mathbf{B}^T \mathbf{D} \mathbf{B} \, d\mathbf{x} \right) \mathbf{U}(t), \\ L(\Psi_i(\mathbf{x}), \mathbf{g}(\mathbf{x}, t)) &= -\hat{e}_i^T \int_{\partial\Omega} \mathbf{N}^T(\mathbf{x}) \mathbf{g}(\mathbf{x}, t) \, ds. \end{aligned}$$

Define

$$\mathbf{K} = \int_{\Omega_h} \mathbf{B}^T \mathbf{D} \mathbf{B} \, d\mathbf{x} \quad (3.20)$$

as the global stiffness matrix of size $2P \times 2P$, and

$$\mathbf{L}(t) = - \int_{\partial\Omega_{in}} \Psi^T(\mathbf{x}) \mathbf{g}(\mathbf{x}, t) \, ds \quad (3.21)$$

as the global load vector of length $2P$. Thus, the weak formulation (3.14) is discretized as

$$\hat{e}_i^T \left(\int_{\Omega_h} \mathbf{B}^T \mathbf{D} \mathbf{B} \, d\mathbf{x} \right) \mathbf{U}(t) = -\hat{e}_i^T \int_{\partial\Omega} \Psi^T(\mathbf{x}) \mathbf{g}(\mathbf{x}, t) \, ds \quad \forall i,$$

which is a system of equations

$$\mathbf{K} \mathbf{U}(t) = \mathbf{L}(t).$$

Thus, finding the weak solution at time t is equivalent to solving a system of equations.

3.1.3 Step 3: Assembling the Elementary Matrix and Vector

The last step is to construct the basis vector functions, the elementary stiffness matrices and load vectors, and assemble the elementary matrix and vector together to form a global system. Consider a single triangle, T^e , and let the 3 nodes on T^e be \mathbf{x}_a , \mathbf{x}_b and \mathbf{x}_c , where $a, b, c \in \{1 \dots P\}$. Then, let the displacements of these 3 nodes be represented by an elementary displacement vector, $\mathbf{U}^e(t)$, where

$$\mathbf{U}^e(t) = \begin{bmatrix} U_{2a-1}(t) \\ U_{2a}(t) \\ U_{2b-1}(t) \\ U_{2b}(t) \\ U_{2c-1}(t) \\ U_{2c}(t) \end{bmatrix},$$

and the piecewise continuous function, $\mathbf{u}_h(\mathbf{x}, t)$, over the region T^e is defined as

$$\mathbf{u}_h(\mathbf{x}, t)|_{T^e} = \begin{bmatrix} \psi_a(\mathbf{x}) & 0 & \psi_b(\mathbf{x}) & 0 & \psi_c(\mathbf{x}) & 0 \\ 0 & \psi_a(\mathbf{x}) & 0 & \psi_b(\mathbf{x}) & 0 & \psi_c(\mathbf{x}) \end{bmatrix} \mathbf{U}^e(t). \quad (3.22)$$

To build the basis functions $\psi_i(\mathbf{x})$, let $\psi_a(\mathbf{x})$, $\psi_b(\mathbf{x})$ and $\psi_c(\mathbf{x})$ be

$$\begin{aligned} \psi_a(\mathbf{x}) &= \alpha_a + \beta_a x + \gamma_a y \\ \psi_b(\mathbf{x}) &= \alpha_b + \beta_b x + \gamma_b y \\ \psi_c(\mathbf{x}) &= \alpha_c + \beta_c x + \gamma_c y \end{aligned} \quad (3.23)$$

Apply the matrix multiplication in (3.22), and $\mathbf{u}_h(\mathbf{x}, t)|_{T^e}$ can be rewritten as

$$\mathbf{u}_h(\mathbf{x}, t)|_{T^e} = \begin{bmatrix} p_1 + p_2 x + p_3 y \\ q_1 + q_2 x + q_3 y \end{bmatrix} \quad (3.24)$$

where the coefficients p_1, p_2, p_3, q_1, q_2 and q_3 are to be determined. For $i = a, b, c$, $\mathbf{u}_h(\mathbf{x}_i, t)|_{T^e} = \begin{bmatrix} U_{2i-1} \\ U_{2i} \end{bmatrix}$, and (3.24) gives

$$\begin{bmatrix} 1 & x_a & y_a \\ 1 & x_b & y_b \\ 1 & x_c & y_c \end{bmatrix} \begin{bmatrix} p_1 \\ p_2 \\ p_3 \end{bmatrix} = \begin{bmatrix} U_{2a-1} \\ U_{2b-1} \\ U_{2c-1} \end{bmatrix}.$$

for the first component of \mathbf{u}_h . Let A be the matrix on the left hand side of the above equation. If A is invertible, then

$$\begin{aligned} p_1 &= \sum_{i=a}^c U_{2i-1} \alpha_i \\ p_2 &= \sum_{i=a}^c U_{2i-1} \beta_i \\ p_3 &= \sum_{i=a}^c U_{2i-1} \gamma_i \end{aligned}$$

where

$$\begin{aligned} \alpha_a &= \frac{x_b y_c - x_c y_b}{\det(A)} & \alpha_b &= \frac{x_c y_a - x_a y_c}{\det(A)} & \alpha_c &= \frac{x_a y_b - x_b y_a}{\det(A)} \\ \beta_a &= \frac{y_b - y_c}{\det(A)} & \beta_b &= \frac{y_c - y_a}{\det(A)} & \beta_c &= \frac{y_a - y_b}{\det(A)} \\ \gamma_a &= \frac{x_b - x_c}{\det(A)} & \gamma_b &= \frac{x_c - x_a}{\det(A)} & \gamma_c &= \frac{x_a - x_b}{\det(A)} \end{aligned} \quad (3.25)$$

If A is non-invertible, the triangle is degenerate and has zero area, which will not be considered. The same idea is applied to the second component of $\mathbf{u}_h(\mathbf{x})|_{T^e}$. Therefore, α_i , β_i and γ_i in (3.23) are found, and $\mathbf{u}_h(\mathbf{x}, t)|_{T^e}$ is defined as a linear polynomial over T^e .

Recall the strain vector over the whole domain Ω_h is defined in (3.18) using the matrix \mathbf{B} . Then, over the element T_e , the elementary strain vector is defined as

$$\boldsymbol{\varepsilon}(\mathbf{u}_h)|_{T^e} \doteq \boldsymbol{\varepsilon}^e = \mathbf{B}^e \mathbf{U}^e, \quad (3.26)$$

where \mathbf{B}^e can be evaluated using (3.23) and (3.25)

$$\begin{aligned} \mathbf{B}^e &= \begin{bmatrix} \frac{\partial \psi_a(\mathbf{x})}{\partial x} & 0 & \frac{\partial \psi_b(\mathbf{x})}{\partial x} & 0 & \frac{\partial \psi_c(\mathbf{x})}{\partial x} & 0 \\ 0 & \frac{\partial \psi_a(\mathbf{x})}{\partial y} & 0 & \frac{\partial \psi_b(\mathbf{x})}{\partial y} & 0 & \frac{\partial \psi_c(\mathbf{x})}{\partial y} \\ \frac{\partial \psi_a(\mathbf{x})}{\partial y} & \frac{\partial \psi_a(\mathbf{x})}{\partial x} & \frac{\partial \psi_b(\mathbf{x})}{\partial y} & \frac{\partial \psi_b(\mathbf{x})}{\partial x} & \frac{\partial \psi_c(\mathbf{x})}{\partial y} & \frac{\partial \psi_c(\mathbf{x})}{\partial x} \end{bmatrix} \\ &= \begin{bmatrix} \beta_a & 0 & \beta_b & 0 & \beta_c & 0 \\ 0 & \gamma_a & 0 & \gamma_b & 0 & \gamma_c \\ \gamma_a & \beta_a & \gamma_b & \beta_b & \gamma_c & \beta_c \end{bmatrix} \end{aligned}$$

Now, the elementary stiffness matrix is defined as

$$\mathbf{K}^e = \int_{T^e} (\mathbf{B}^e)^T \mathbf{D} \mathbf{B}^e d\mathbf{x} = (\mathbf{B}^e)^T \mathbf{D} \mathbf{B}^e \left(\frac{1}{2} |\det(A)| \right).$$

Since $(\mathbf{B}^e)^T \mathbf{D} \mathbf{B}^e$ is constant over T^e , the evaluation of the integral is exact, and the area of T^e is $\frac{1}{2} |\det(A)|$.

Let the set $EdgesIn$ contain the global index of the nodes on the boundary $\partial\Omega_{in}$. Approximate $\partial\Omega$ as a polygonal curve, then the global load vector (3.21) is approximated by piecewise line integrals

$$\mathbf{L}(t) \approx \sum_{i \in EdgesIn} \int_{\mathbf{x}_i}^{\mathbf{x}_{i+1}} \begin{bmatrix} \psi_i(\mathbf{x}) & 0 \\ 0 & \psi_i(\mathbf{x}) \\ \psi_{i+1}(\mathbf{x}) & 0 \\ 0 & \psi_{i+1}(\mathbf{x}) \end{bmatrix} \begin{bmatrix} g_1(\mathbf{x}, t) \\ g_2(\mathbf{x}, t) \end{bmatrix} ds.$$

Since $\psi_i(\mathbf{x})$ is a linear function on the line segment from \mathbf{x}_i to \mathbf{x}_{i+1} , the elementary load

vector over an boundary segment is

$$\mathbf{L}^e = \int_{\mathbf{x}_i}^{\mathbf{x}_{i+1}} \begin{bmatrix} \psi_i(\mathbf{x})g_1 \\ \psi_i(\mathbf{x})g_2 \\ \psi_{i+1}(\mathbf{x})g_1 \\ \psi_{i+1}(\mathbf{x})g_2 \end{bmatrix} ds \approx \frac{|\mathbf{x}_{i+1} - \mathbf{x}_i|}{2} \begin{bmatrix} g_1 \\ g_2 \\ g_1 \\ g_2 \end{bmatrix}$$

where the vector $\mathbf{g} = [g_1, g_2]^T$ is evaluated at the mid-point of the boundary segment.

After the elementary stiffness matrix \mathbf{K}^e and the elementary load vector \mathbf{L}^e are computed for each element, they are assembled to form the global stiffness matrix \mathbf{K} and global load vector \mathbf{L} according to how each element is connected together.

All remains is to apply the Dirichlet boundary condition (3.4), which is $\mathbf{u}(\mathbf{x}) = 0$ for $\mathbf{x} \in \partial\Omega_{out}$. Let the set *EdgesOut* contain the global index of the nodes on the boundary $\partial\Omega_{out}$. Then truncate the global stiffness matrix and global load vector by setting the entries of the corresponding rows and columns to zero; *i.e.* for $j \in \text{EdgesOut}$

$$\begin{aligned} \mathbf{K}_{2j,k} = \mathbf{K}_{2j-1,k} &= 0 \quad \text{for } k = 1 \dots 2P \\ \mathbf{K}_{k,2j} = \mathbf{K}_{k,2j-1} &= 0 \quad \text{for } k = 1 \dots 2P \\ \mathbf{L}_{2j} = \mathbf{L}_{2j-1} &= 0 \end{aligned}$$

Let the truncated stiffness matrix be $\tilde{\mathbf{K}}$, and let the truncated load vector be $\tilde{\mathbf{L}}$, so solving the system

$$\tilde{\mathbf{K}}\tilde{\mathbf{U}}(t) = \tilde{\mathbf{L}}$$

gives the displacement vector $\tilde{\mathbf{U}}(t)$ for the interior nodes and the boundary nodes on $\partial\Omega_{in}$. This system of equations can be solved by iterative methods or direct methods. In this thesis, this system is solved by Gaussian elimination through LU factorization.

3.2 Numerical Solution for the Viscoelastic Problem

Finite element method is also used to discretized the viscoelastic problem in space. In addition, the viscoelastic problem requires a time stepping scheme for its time-dependent constitutive equations. These constitutive equations are the only difference between the two

problems, for both problems have the same equations of motions, kinematic equations and boundary conditions. Recall from Section 2.5, the time dependent constitutive equation for viscoelastic problem is

$$\begin{aligned} \sigma_{ij}(\mathbf{x}, t) = & \left[K\varepsilon_{kk}(\mathbf{x}, t) - \frac{2}{3} \left(G(t - t_0)\varepsilon_{kk}(\mathbf{x}, t_0) + \int_{t_0}^t G(t - s) \frac{d\varepsilon_{kk}(\mathbf{x}, s)}{ds} ds \right) \right] \delta_{ij} \\ & + 2 \left(G(t - t_0)\varepsilon_{ij}(\mathbf{x}, t_0) + \int_{t_0}^t G(t - s) \frac{d\varepsilon_{ij}(\mathbf{x}, s)}{ds} ds \right). \end{aligned} \quad (3.27)$$

In this section, the viscoelastic problem is first discretized in space using finite element method, which gives a semi-discretization. Then, it is discretized in time using finite difference and trapezoidal rule, which results in a full discretization. This numerical technique is discussed thoroughly in the work of Shaw *el at.* such as [34], [19] and [36], and in the Ph. D. thesis of Chinviriyasit, [6].

3.2.1 Semi-Discretization

Similar to the elastic problem, a weak formulation for the viscoelastic problem is required. Following the same procedure as in Section 3.1.1, take a scalar product of $\frac{\partial \sigma_{ij}}{\partial x_j}$ with a test function $\mathbf{v}(\mathbf{x}) \in \mathcal{V}$, integrate over Ω , and apply the Divergence Theorem to obtain a weak formulation. Then, consider the same finite dimensional space \mathcal{V}_h and the same displacement $\mathbf{u}_h(\mathbf{x}, t)$, the semi-discrete weak formulation is to find $\mathbf{u}_h(\mathbf{x}, t) \in \mathcal{V}_h$, at t , such that

$$\int_{\Omega} \boldsymbol{\varepsilon}^T(\mathbf{v}) \boldsymbol{\sigma}(\mathbf{u}_h) d\mathbf{x} = - \int_{\partial\Omega_{in}} \mathbf{v}^T \mathbf{g} ds \quad (3.28)$$

for all $\mathbf{v}(\mathbf{x}) \in \mathcal{V}_h$.

Then, omitting spatial dependence, rewrite (3.27) using stress and strain vectors as

follows:

$$\begin{aligned} \boldsymbol{\sigma}(t) = & \begin{bmatrix} K & K & 0 \\ K & K & 0 \\ 0 & 0 & 0 \end{bmatrix} \boldsymbol{\varepsilon}(t) - \begin{bmatrix} \frac{2}{3} & \frac{2}{3} & 0 \\ \frac{2}{3} & \frac{2}{3} & 0 \\ 0 & 0 & 0 \end{bmatrix} (G(t-t_0)\boldsymbol{\varepsilon}(t_0)) \\ & + \int_{t_0}^t G(t-s) \frac{d\boldsymbol{\varepsilon}(s)}{ds} ds \Bigg) + \begin{bmatrix} 2 & 0 & 0 \\ 0 & 2 & 0 \\ 0 & 0 & 1 \end{bmatrix} (G(t-t_0)\boldsymbol{\varepsilon}(t_0)) \\ & + \int_{t_0}^t G(t-s) \frac{d\boldsymbol{\varepsilon}(s)}{ds} ds \Bigg) \end{aligned}$$

or

$$\boldsymbol{\sigma}(t) = D_K \boldsymbol{\varepsilon}(t) + D_G G(t-t_0) \boldsymbol{\varepsilon}(t_0) + \int_{t_0}^t D_G G(t-s) \frac{d\boldsymbol{\varepsilon}(s)}{ds} ds, \quad (3.29)$$

where D_K and D_G are constitutive matrices

$$D_K = \begin{bmatrix} K & K & 0 \\ K & K & 0 \\ 0 & 0 & 0 \end{bmatrix}, \quad D_G = \begin{bmatrix} \frac{4}{3} & \frac{-2}{3} & 0 \\ \frac{-2}{3} & \frac{4}{3} & 0 \\ 0 & 0 & 1 \end{bmatrix}.$$

Noting $\boldsymbol{\sigma}(t) = \boldsymbol{\sigma}(\mathbf{u}_h(t))$, substitute (3.29) into (3.28). Assume it is permissible to interchange the order of integration, and replace the test function $\mathbf{v}(\mathbf{x})$ with $\Psi_i(\mathbf{x})$, the basis vector function of \mathcal{V}_h , the semi-discrete weak formulation for the viscoelastic problem is:

Find $\mathbf{u}_h(\mathbf{x}, t) \in \mathcal{V}_h$ for each $t \in \mathcal{I}$ such that

$$\begin{aligned} & \int_{\Omega_h} \boldsymbol{\varepsilon}^T(\Psi_i) (D_K \boldsymbol{\varepsilon}(\mathbf{u}_h(t)) + D_G G(t-t_0) \boldsymbol{\varepsilon}(\mathbf{u}_h(t_0))) d\mathbf{x} \\ & + \int_{t_0}^t \int_{\Omega_h} \boldsymbol{\varepsilon}^T(\Psi_i) D_G G(t-s) \frac{d\boldsymbol{\varepsilon}(\mathbf{u}_h(s))}{ds} d\mathbf{x} ds = - \int_{\partial\Omega_{in}} \mathbf{g}(t) ds \end{aligned} \quad (3.30)$$

for $i = 1 \dots 2P$.

Note that when the constitutive equations (3.27) are used, this weak formulation is not defined with a bilinear operator. However, the weak formulation can be written with a

different form of constitutive equations such that a bilinear operator is defined, and existence and uniqueness of solution to the weak formulation can be shown. See Appendix A for details.

Replace $\mathbf{u}_h(\mathbf{x}, t)$, $\boldsymbol{\varepsilon}(\mathbf{u}_h(\mathbf{x}, t))$ and $\boldsymbol{\varepsilon}(\Psi_i(\mathbf{x}))$ in (3.30) with their expressions in (3.17), (3.18) and (3.19), and obtain

$$\begin{aligned} & \widehat{e}_i \int_{\Omega_h} \mathbf{B}^T (D_K \mathbf{B} \mathbf{U}(t) + D_G G(t - t_0) \mathbf{B} \mathbf{U}(t_0)) d\mathbf{x} + \int_{t_0}^t \widehat{e}_k \int_{\Omega_h} \mathbf{B}^T D_G G(t - s) \mathbf{B} \frac{d\mathbf{U}(s)}{ds} d\mathbf{x} ds \\ = & -\widehat{e}_i \int_{\partial\Omega_{in}} \mathbf{N}^T(\mathbf{x}) \mathbf{g}(\mathbf{x}, t) ds \end{aligned}$$

for $k = 1 \dots 2P$. Since D_K , D_G and \mathbf{B} are constant matrices, and $G(t - q)$ is a scalar, the above equation becomes

$$A_K \mathbf{U}(t) + A_G G(t - t_0) \mathbf{U}(t_0) + A_G \int_{t_0}^t G(t - s) \frac{d\mathbf{U}(s)}{ds} ds = \mathbf{L}(t), \quad (3.31)$$

where A_K and A_G are $2P \times 2P$ stiffness matrices defined as

$$A_K = \int_{\Omega} \mathbf{B}^T D_K \mathbf{B} d\mathbf{x}, \quad A_G = \int_{\Omega_h} \mathbf{B}^T D_G \mathbf{B} d\mathbf{x}.$$

These two matrices are assembled in the same way as in Section 3.1.3. Therefore, (3.31) is a system of integral equations solving for $\mathbf{U}(t)$ which is the global displacement vector at time t .

3.2.2 Fully Discrete Formulation

Next, discretize the continuous time domain \mathcal{I} into $\mathcal{I}_h = \{t_0, \dots, t_k, \dots, t_J\}$ with constant time step $\Delta t = t_k - t_{k-1}$. Let $\mathbf{U}^k = \mathbf{U}(t_k)$ be the global displacement vector at time t_k . As discussed in Section 2.5, the shear relaxation modulus $G(t - s)$ follows the generalized Maxwell Solid model and has the form

$$G(t - s) = g_0 + \sum_{i=1}^N g_i e^{-\frac{t-s}{\tau_i}} \quad (3.32)$$

for $s < t$. Substitute the relaxation modulus (3.32) in the system of integral equations (3.31), and change the order of integration and summation to obtain

$$A_K \mathbf{U}^k + A_G G(t_k - t_0) \mathbf{U}^0 + A_G \int_{t_0}^{t_k} g_0 \frac{d\mathbf{U}(s)}{ds} ds + A_G \sum_{i=1}^N \left(\int_{t_0}^{t_k} g_i e^{-\frac{t_k-s}{\tau_i}} \frac{d\mathbf{U}(s)}{ds} ds \right) = \mathbf{L}(t). \quad (3.33)$$

At time t_0 , the displacement vector \mathbf{U}^0 in (3.33) is simply found by solving

$$(A_K + A_G G(0)) \mathbf{U}^0 = L(0)$$

because both integral terms in (3.33) vanish.

At time t_k , the first integral of (3.33) can be evaluated and simplified to

$$A_G \int_{t_0}^{t_k} g_0 \frac{d\mathbf{U}(s)}{ds} ds = A_G g_0 (\mathbf{U}^k - \mathbf{U}^0),$$

and (3.33) becomes

$$(A_K + A_G g_0) \mathbf{U}^k + A_G \sum_{i=1}^N g_i e^{-\frac{t_k-t_0}{\tau_i}} \mathbf{U}^0 + A_G \sum_{i=1}^N \left(\int_{t_0}^{t_k} g_i e^{-\frac{t_k-s}{\tau_i}} \frac{d\mathbf{U}(s)}{ds} ds \right) = \mathbf{L}(t). \quad (3.34)$$

At this point, the numerical method for evaluating the integrals in (3.34) strongly depends on the form of the relaxation functions. Fortunately, these functions have a special form which renders the problem simpler. In this case, $G(t-s)$ is non-aging as discussed in Section 2.3.2. Also, the time dependent terms of $G(t-s)$, $g_i e^{-\frac{t-s}{\tau_i}}$, are separable, so that the following Lemma can be applied to evaluate the integrals.

Lemma 1. *Assume $\chi(t-s)$ is separable, such that $\chi(t-s) = \chi^a(t)\chi^b(s)$ for some $\chi^a(t)$ and $\chi^b(s)$. Let*

$$\theta(t) = \int_0^t \chi(t-s) ds.$$

Then

$$\theta(t + \Delta t) = \int_t^{t+\Delta t} \chi((t + \Delta t) - s) ds + \frac{\chi^a(t + \Delta t)}{\chi^a(t)} \theta(t).$$

Proof.

$$\begin{aligned}
\theta(t + \Delta t) &= \int_0^{t+\Delta t} \chi(t + \Delta t - s) ds \\
&= \int_t^{t+\Delta t} \chi(t + \Delta t - s) ds + \int_0^t \chi^a(t + \Delta t) \chi^b(s) ds \\
&= \int_t^{t+\Delta t} \chi(t + \Delta t - s) ds + \frac{\chi^a(t + \Delta t)}{\chi^a(t)} \int_0^t \chi^a(t) \chi^b(s) ds \\
&= \int_t^{t+\Delta t} \chi(t + \Delta t - s) ds + \frac{\chi^a(t + \Delta t)}{\chi^a(t)} \theta(t)
\end{aligned}$$

□

This lemma gives a recurrence relationship for evaluating the integral in (3.34), which is desirable in developing numerical schemes. With this property, the memory requirement and operation counts of a numerical program remain constant throughout the time stepping. Without this property, evaluating the integral in (3.34) requires storing the solutions \mathbf{U}^k at every time step and evaluating the integrand k times at time t_k ; thus, both memory requirement and operation counts increase rapidly [19]. To use Lemma 1, let $\chi_i^a(t) = g_i e^{-\frac{t}{\tau_i}}$ and $\chi_i^b(s) = e^{\frac{s}{\tau_i}} \frac{d\mathbf{U}(s)}{ds}$.

Then, suppose for $1 \leq i \leq N$

$$\theta_i(t_{k-1}) = \int_{t_0}^{t_{k-1}} g_i e^{-\frac{t_{k-1}-s}{\tau_i}} \frac{d\mathbf{U}(s)}{ds} ds$$

are known from previous time step t_{k-1} . Apply Lemma 1 to the last integral term of (3.34) to obtain

$$\sum_{i=1}^N \left(\int_{t_0}^{t_k} g_i e^{-\frac{t_k-s}{\tau_i}} \frac{d\mathbf{U}(s)}{ds} ds \right) = \sum_{i=1}^N \left[\int_{t_{k-1}}^{t_k} g_i e^{-\frac{t_k-s}{\tau_i}} \frac{d\mathbf{U}(s)}{ds} ds + e^{-\frac{\Delta t}{\tau_i}} \theta_i(t_{k-1}) \right]. \quad (3.35)$$

All that remains is to find an approximation for evaluating the integral

$$\int_{t_{k-1}}^{t_k} g_i e^{-\frac{t_k-s}{\tau_i}} \frac{d\mathbf{U}(s)}{ds} ds.$$

First, apply the midpoint rule on $\frac{d\mathbf{U}(s)}{ds}$. Then approximate it with finite difference for $t \in [t_{k-1}, t_k]$, and finally apply trapezoidal rule for numerical integration [36, 34] as follows

$$\begin{aligned}
\int_{t_{k-1}}^{t_k} g_i e^{-\frac{t_k-s}{\tau_i}} \frac{d\mathbf{U}(s)}{ds} ds &\approx \int_{t_{k-1}}^{t_k} g_i e^{-\frac{t_k-s}{\tau_i}} ds \frac{d\mathbf{U}(t_{k-1} + \frac{\Delta t}{2})}{ds} \\
&\approx \int_{t_{k-1}}^{t_k} g_i e^{-\frac{t_k-s}{\tau_i}} ds \left(\frac{\mathbf{U}^k - \mathbf{U}^{k-1}}{\Delta t} \right) \\
&\approx \frac{1}{2} \Delta t \left(g_i + g_i e^{-\frac{\Delta t}{\tau_i}} \right) \left(\frac{\mathbf{U}^k - \mathbf{U}^{k-1}}{\Delta t} \right) \\
&= \frac{1}{2} g_i \left(1 + e^{-\frac{\Delta t}{\tau_i}} \right) (\mathbf{U}^k - \mathbf{U}^{k-1})
\end{aligned} \tag{3.36}$$

where \mathbf{U}^{k-1} is known from previous time step. After substituting (3.35) and (3.36) into (3.34), \mathbf{U}^k is found by solving the following system of equations

$$\begin{aligned}
(A_K + A_G \mathbf{g}_0) \mathbf{U}^k + A_G \left(\sum_{i=1}^N g_i e^{-\frac{t_k-t_0}{\tau_i}} \right) \mathbf{U}^0 \\
+ A_G \sum_{i=1}^N \left[\frac{1}{2} g_i \left(1 + e^{-\frac{\Delta t}{\tau_i}} \right) (\mathbf{U}^k - \mathbf{U}^{k-1}) + e^{-\frac{\Delta t}{\tau_i}} \theta_i(t_{k-1}) \right] = \mathbf{L}(t_k)
\end{aligned}$$

or

$$A(t_k) \mathbf{U}^k = b(t_k) \tag{3.37}$$

where

$$A(t_k) = \left(A_K + A_G \left(\mathbf{g}_0 + \sum_{i=1}^N \frac{1}{2} g_i \left(1 + e^{-\frac{\Delta t}{\tau_i}} \right) \right) \right), \tag{3.38}$$

$$\begin{aligned}
b(t_k) &= L(t_{k+1}) - A_G \left(\sum_{i=1}^N g_i e^{-\frac{t_k-t_0}{\tau_i}} \right) \mathbf{U}^0 - A_G \sum_{i=1}^N e^{-\frac{\Delta t}{\tau_i}} \theta_i(t_{k-1}) \\
&\quad + \sum_{i=1}^N \frac{1}{2} g_i \left(1 + e^{-\frac{\Delta t}{\tau_i}} \right) \mathbf{U}^{k-1}.
\end{aligned} \tag{3.39}$$

Once \mathbf{U}^k is found, $\theta_i(t_k)$, which is

$$\begin{aligned}
\theta_i(t_k) &= \int_{t_{k-1}}^{t_k} g_i e^{-\frac{t_k-s}{\tau_i}} \frac{d\mathbf{U}(s)}{ds} ds + e^{-\frac{\Delta t}{\tau_i}} \theta_i(t_{k-1}) \\
&\approx \frac{1}{2} g_i \left(1 + e^{-\frac{\Delta t}{\tau_i}} \right) (\mathbf{U}(t_k) - \mathbf{U}(t_{k-1})) + e^{-\frac{\Delta t}{\tau_i}} \theta_i(t_{k-1}),
\end{aligned} \tag{3.40}$$

is computed and stored for the next time step.

Finally, the pseudo-code for solving the viscoelastic problem is outlined in Algorithm 1.

3.2.3 Computing Stress and Strain

Once the displacement vectors are found at every nodes, the state of stress and strain are computed to provide a better understanding of the behaviour of the viscoelastic material. Since $\mathbf{u}_h(\mathbf{x}, t)$ are linear piecewise functions, the components of strain tensor which involves the first derivative of $\mathbf{u}_h(\mathbf{x}, t)$ are constant within an element. The components of the stress tensor are also constant within the element since it is a function of the strain tensor. The volumetric strain, volumetric stress and the principle stress and directions are also computed. In this case, it is common to assign all these variables at the centroid of an element [49], since they are constant within an element.

Given an elementary displacement vector, the elementary strain vector $\boldsymbol{\varepsilon}^e$ is simply given by (3.26). Then, the complete strain tensor at the element, ε_{ij}^e , is determined from the components of $\boldsymbol{\varepsilon}^e$ and the fact that $\varepsilon_{13}^e = \varepsilon_{23}^e = \varepsilon_{33}^e = 0$ for plane strain.

Note that the strain computed above is Cauchy's infinitesimal strain tensor, which is the linear part of the Green's strain tensor defined by (2.1). The nonlinear part is assumed to be small and omitted in the mathematical model. But once the displacement is found, it is beneficial to compute the nonlinear part and check how small it really is, which will be done in Chapter 4. Denote $\tilde{\varepsilon}_{ij}$ as the nonlinear part of Green's strain tensor, which is

$$\tilde{\varepsilon}_{ij} = \frac{\partial u_\alpha}{\partial x_i} \frac{\partial u_\alpha}{\partial x_j}. \quad (3.41)$$

The first derivative of displacements for each element are

$$\begin{aligned} \frac{\partial u_1}{\partial x_1} &= \begin{bmatrix} \beta_a & 0 & \beta_b & 0 & \beta_c & 0 \end{bmatrix} \mathbf{U}_e \\ \frac{\partial u_2}{\partial x_1} &= \begin{bmatrix} 0 & \beta_a & 0 & \beta_b & 0 & \beta_c \end{bmatrix} \mathbf{U}_e \\ \frac{\partial u_1}{\partial x_2} &= \begin{bmatrix} \gamma_a & 0 & \gamma_b & 0 & \gamma_c & 0 \end{bmatrix} \mathbf{U}_e \\ \frac{\partial u_2}{\partial x_2} &= \begin{bmatrix} 0 & \gamma_a & 0 & \gamma_b & 0 & \gamma_c \end{bmatrix} \mathbf{U}_e. \end{aligned}$$

Algorithm 1 Fully discrete algorithm for the viscoelastic problem

1. Given:
 2. a finite element mesh Ω_h
 - (a) Bulk modulus K and Shear Relaxation Modulus $G(t - q)$
 - (b) CSF pressure $P(t)$
 3. Define the constitutive matrices D_K and D_G .
 4. Assemble the Global Stiffness Matrices A_K and A_G .
 5. Apply Dirichlet Boundary condition by removing some rows and columns of A_K and A_G .
 6. For $t = 0$ to t_J
 - (a) Set up the Load Vector $L(t)$
 - (b) When $t = 0$
 - i. Solve $(A_k + A_G G(0)) \mathbf{U}(0) = L(0)$
 - ii. Set $\theta_i(0) = 0$ for $1 \leq i \leq N$
 - (c) When $t_k > 0$
 - i. Solve $A(t_k) \mathbf{U}(t_k) = b(t_k)$ where $A(t_k)$ and $b(t_k)$ are defined in (3.38) and (3.39).
 - ii. Compute $\theta_i(t_k)$ for $1 \leq i \leq N$ according to (3.40).
-

where β_i and γ_i are defined in (3.25) and the derivatives are also constant over an element. Then, the components $\tilde{\varepsilon}_{ij}^e$ are computed at each element according to (3.41) using the above derivatives, and the fact that $\tilde{\varepsilon}_{13}^e = \tilde{\varepsilon}_{23}^e = \tilde{\varepsilon}_{33}^e = 0$ for plane strain.

The elementary stress vector is determined by substituting the elementary strain vector into constitutive equations (3.29), which can be rewritten using $\theta_i(t_k)$ as follows since it is computed and stored at every time,

$$\begin{aligned} \boldsymbol{\sigma}^e(\mathbf{x}, t_k) &= D_K \boldsymbol{\varepsilon}^e(\mathbf{x}, t_k) + D_G G(t_k - t_0) \boldsymbol{\varepsilon}^e(\mathbf{x}, t_0) \\ &\quad + D_G g_0 (\boldsymbol{\varepsilon}^e(\mathbf{x}, t_0) - \boldsymbol{\varepsilon}^e(\mathbf{x}, t_k)) + D_G B^e \boldsymbol{\theta}_i^e(t_k), \end{aligned} \quad (3.42)$$

where $\boldsymbol{\theta}_i^e(t_k)$ is the elementary $\theta_i(t_k)$, a vector of length 6 representing the value of $\theta_i(t_k)$ at the 3 nodes of an element.

Then, the complete stress tensor at the element, σ_{ij}^e , can be determined from the components of $\boldsymbol{\sigma}^e$, and the fact that $\sigma_{13}^e = \sigma_{23}^e = 0$ and σ_{33}^e defined as follows. Substituting $\varepsilon_{33}^e = 0$ in the constitutive equations (3.27) for σ_{33}^e gives

$$\begin{aligned} \sigma_{33}^e &= K (\varepsilon_{11}^e(\mathbf{x}, t_k) + \varepsilon_{22}^e(\mathbf{x}, t_k)) - \frac{2}{3} (G(t_k - t_0) (\varepsilon_{11}^e(\mathbf{x}, t_0) + \varepsilon_{22}^e(\mathbf{x}, t_0)) \\ &\quad \int_{t_0}^t G(t-s) \frac{d(\varepsilon_{11}^e(\mathbf{x}, s) + \varepsilon_{22}^e(\mathbf{x}, s))}{ds} ds). \end{aligned}$$

Rewriting this equation using $\theta_i(t_k)$ by letting $\varphi_i^e(t_k) = \mathbf{B}^e \boldsymbol{\theta}_i^e(t_k)$, which is a vector of length 3. Letting $\varphi_{i1}(t_k)$ be the first component of this vector, the above equation is

$$\begin{aligned} \sigma_{33}^e &= K [\varepsilon_{11}^e(\mathbf{x}, t_k) + \varepsilon_{22}^e(\mathbf{x}, t_k)] - \frac{2}{3} \left[G(t_k - t_0) (\varepsilon_{11}^e(\mathbf{x}, t_0) + \varepsilon_{22}^e(\mathbf{x}, t_0)) \right. \\ &\quad \left. g_0 (\varepsilon_{11}^e(\mathbf{x}, t_0) + \varepsilon_{22}^e(\mathbf{x}, t_0) - \varepsilon_{11}^e(\mathbf{x}, t_k) - \varepsilon_{22}^e(\mathbf{x}, t_k)) + \sum_i^N \varphi_{i1}(t_k) + \varphi_{i2}(t_k) \right] \end{aligned} \quad (3.43)$$

Once the stress tensor σ_{ij}^e is found, volumetric strain and stress are computed according to (2.3) and (2.6) respectively, and principle stresses and directions are computed according to (2.4). Lastly, since the element is a triangle, and the centroid of an triangle, (x_C, y_C) , is defined as

$$\begin{aligned} x_C &= \frac{1}{3}(x_a + x_b + x_c), \\ y_C &= \frac{1}{3}(y_a + y_b + y_c), \end{aligned}$$

where (x_a, y_a) , (x_b, y_b) and (x_c, y_c) are the 3 nodes of the triangles.

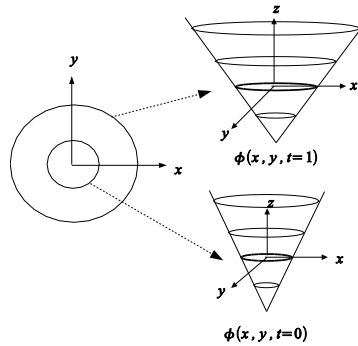


Figure 3.2: Visualization of the level set function $z = \phi(x, y, t)$ and its zero level set $\phi = 0$.

3.3 Grid Generation from an Image

To simulate a brain with hydrocephalus accurately, the geometry of a computational mesh Ω_h should resemble the geometry of a brain as much as possible. Furthermore, since each patient's brain is different from another, Ω_h should be customized for each individual patient. This is possible if the computational mesh Ω_h is generated from a medical image of a patient's brain, such that the two boundaries of Ω_h accurately represents the boundary of a patient's skull and ventricles. In 2D, these two boundaries are curves, and the method to trace a curve is called segmentation, which can be done using the level set method. Once two boundaries are identified and represented with a signed distance function, a triangular mesh can be created using a grid generation program, called DistMesh¹. In this section, the level set method and the grid generation program are briefly introduced.

A simple closed curve in 2D can be described by a level set of a surface in 3D, and the level set method is a way to evolve the surface such that its level set becomes a curve of interest. Let this curve be $\xi(t)$, and let the corresponding level set function be $\phi(x, y, t)$ such that its zero level set is the curve,

$$\xi(t) = \{(x, y) \mid \phi(x, y, t) = 0\}.$$

For example, the level set function $z = \phi(x, y, t) = x^2 + y^2 - (t + 1)^2$ is a cone in xyz -space, and its zero level set $\phi(x, y, t) = 0$ is a circle of radius $t + 1$ at time t . See Figure 3.2.

¹<http://www-math.mit.edu/~persson/mesh/>

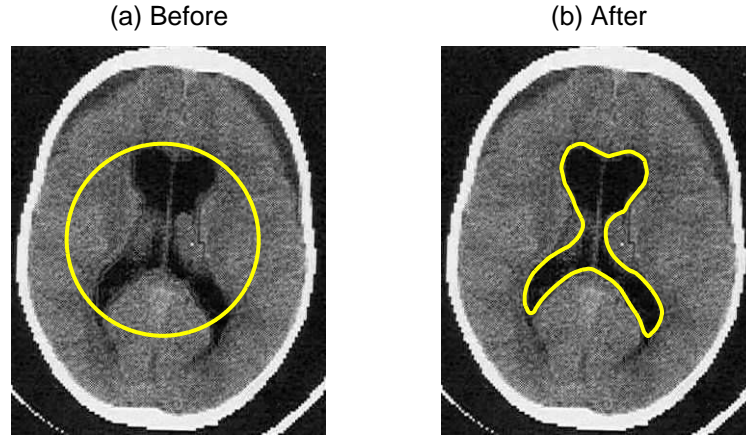


Figure 3.3: To segment the ventricles, start with a simple signed distance function as in (a), then evolve the function to match the ventricles as in (b).

Then, the level set function evolves according to the following partial differential equation

$$\frac{\partial \phi(x, y, t)}{\partial t} + F |\nabla \phi(x, y, t)| = 0, \quad (3.44)$$

where $F = F(x, y)$ describes the speed of the evolving curves in the normal direction. To segment a curve from an image, select the intensity value of the image pixels which lies on the curve of interest, and define an initial simple level set function $\phi(x, y, 0)$ that lies within, intersects or enclose the curve of interest. Then, evolves the level set function by solving (3.44) numerically, such that points inside the curve move outward, and the point outside move inward, until the zero level set becomes the desired curve. See Figure 3.3. The program that performed segmentation in this thesis is written by West for his Master's thesis [48].

Once the two level set functions, ϕ_s and ϕ_v , that represent the boundary of skull and ventricles are found, they are combined into one function, according to

$$\phi(x, y) = \max(\phi_s(x, y), -\phi_v(x, y)), \quad (3.45)$$

so that the region of interest is represented by negative value of $\phi(x, y)$. This region is where the triangular mesh will be. See Figure 3.4 and Figure 3.5.

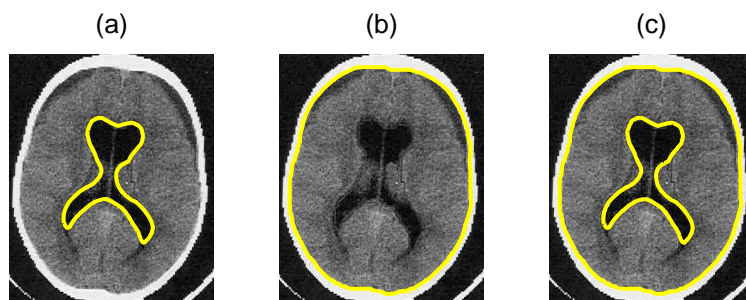


Figure 3.4: (a) Segmentation of the ventricles. (b) Segmentation of the skull. (c) Combine (a) and (b).

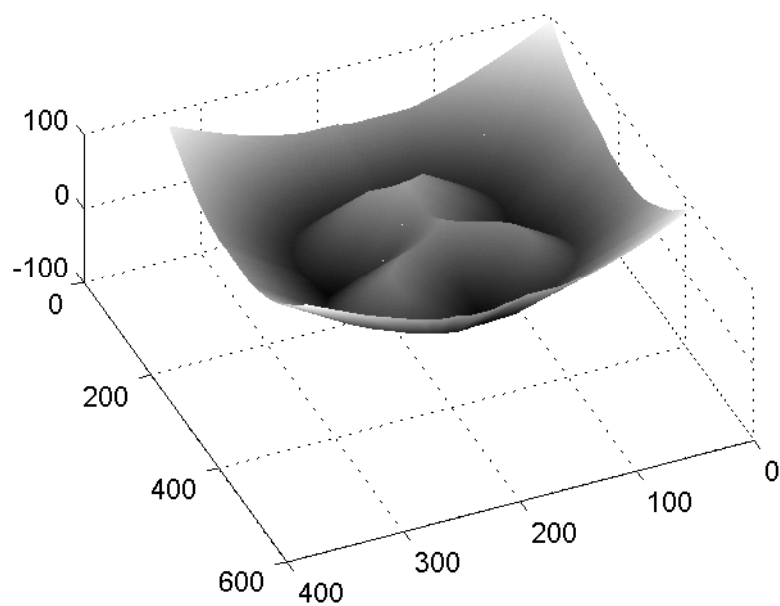


Figure 3.5: The final level set function, where the region with negative distance is the region of interest.

Next, the grid generation program, DistMesh, uses the combined level set function $\phi(x, y)$ to generate a triangular mesh. First, a random distribution of nodes is created over a computational domain, then by evaluating $\phi(x, y)$ at each node, the program eliminates the nodes that are outside the region of interest.

The goal of any mesh generation program is to have equilateral triangles, and DistMesh accomplished this goal by considering the triangular mesh to be a mechanical structure. The nodes of a triangular mesh are assumed to be connected by an elastic spring, so that force exists to extend or compress the length between two nodes. There are also forces on the boundaries to keep a node inside. When this structure of springs are confined by the two boundaries and equilibrium of forces is reached, the triangles should be equilateral. Denote $F(\mathbf{x}_i)$ as the sum of external boundary force and internal spring force at node \mathbf{x}_i . Equilibrium of force implies $F(\mathbf{x}) = 0$, which is solved as a system of ordinary differential equations with an artificial time dependence

$$\frac{d\mathbf{x}}{dt} = F(\mathbf{x}).$$

This equation is solved iteratively until $\frac{d\mathbf{x}}{dt}$ is close to zero, and the final result is a triangular mesh that resembles the geometry of a patient's brain. See Figure 3.6. DistMesh is written by Persson for his Ph. D. thesis [30].

3.4 Compare with Analytical Solution

In this section, the numerical algorithm is validated by comparing the numerical solutions with the analytical solutions discussed in Section 2.6. The computational mesh Ω_h and boundary conditions are set to be the same as those of the analytical solution. That is, Ω_h is an annulus with inner radius, $a = 10mm$, and outer radius, $b = 20mm$, and the pressure at the inner boundary is constant, $P(t) = P_0$. In general, the analytical solution is not identical to the numerical solution because of numerical error, but this error is usually bounded and can be estimated.

First, the program for the elastic problem is validated with five different mesh sizes in two test cases, where the parameters P_0 , E and ν are different. The numerical error

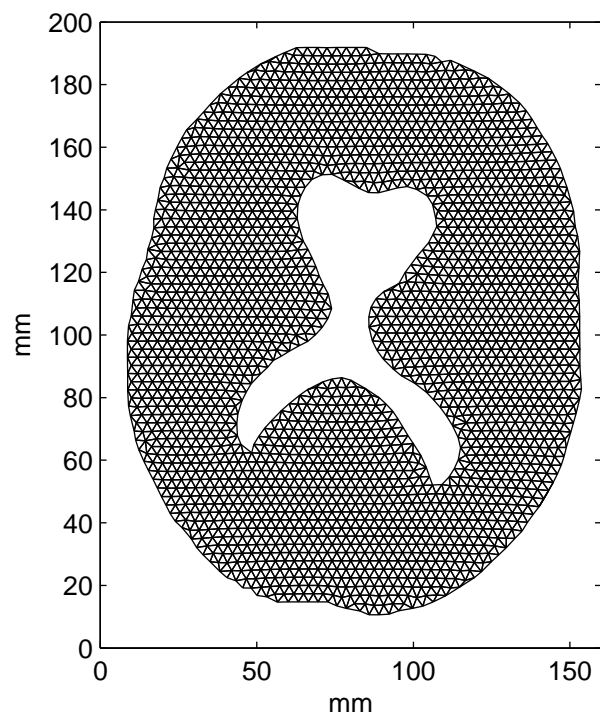


Figure 3.6: A triangular mesh of a patient's brain

between the numerical and analytical solutions is estimated in the following theorem found in [20]:

Theorem 1. *Let $\mathbf{u} \in \mathcal{C}^0(\Omega_h \cup \partial\Omega_h)$ be the analytical solution. Let \mathbf{u}_h be the numerical solution. Let the mesh size h be the longest side of all triangles in Ω_h . There is an absolute constant C independent of \mathbf{u} and h such that numerical error $e(h)$ is bounded by*

$$e(h) = \|\mathbf{u} - \mathbf{u}_h\|_{\mathcal{L}_2(\Omega)} \leq Ch^2 |\mathbf{u}|_{\mathcal{H}^2(\Omega)}$$

where $\|\cdot\|_{\mathcal{L}_2(\Omega)}$ is the \mathcal{L}_2 -norm

$$\|\varphi(\mathbf{x})\|_{\mathcal{L}_2(\Omega)} = \left[\int_{\Omega} |\varphi(\mathbf{x})|^2 d\mathbf{x} \right]^{\frac{1}{2}},$$

and $|\cdot|_{\mathcal{H}^2(\Omega)}$ is a semi-norm, that measure the \mathcal{L}_2 -norm of only second partial derivatives,

$$|\varphi(\mathbf{x})|_{\mathcal{H}^2(\Omega)} = \left[\int_{\Omega} |D^2\varphi(\mathbf{x})|^2 d\mathbf{x} \right]^{\frac{1}{2}}.$$

This theorem shows that the error bound between the analytical and numerical solution, measured by \mathcal{L}_2 -norm, is proportional to h^2 , so that when the mesh size is reduced by half, the error is reduced at least by a fourth. Note that, in general, the error estimate depends on the order of the basic functions and how is $e(h)$ estimated. Since the basic functions is linear and $e(h)$ is measured by \mathcal{L}_2 -norm, the error is order 2 in space. If h is the mesh size of mesh Ω_h , and $\frac{h}{2}$ is the mesh size of mesh $\Omega_{\frac{h}{2}}$, then the ratio between their numerical errors

$$\begin{aligned} \frac{e(\frac{h}{2})}{e(h)} &\leq \frac{C (\frac{h}{2})^2 |\mathbf{u}|_{\mathcal{H}^2(\Omega_h)}}{Ch^2 |\mathbf{u}|_{\mathcal{H}^2(\Omega_{\frac{h}{2}})}} \\ &= \frac{1}{4}. \end{aligned}$$

Thus, the power of h^2 indicates the convergence rate of the numerical solution as the mesh size decreases.

In Section 2.6, the analytical solution for the radial displacement $u_r(r, \theta)$ is found, but it is defined in polar coordinates. So, node \mathbf{x}_j is converted into (r_j, θ_j) , and then $u_r(r_j, \theta_j)$

is evaluated and projected along the x and y axes to obtain

$$\begin{bmatrix} \mathbf{u}_{2j} \\ \mathbf{u}_{2j-1} \end{bmatrix} = \begin{bmatrix} u_r(r_j, \theta_j) \cos \theta_j \\ u_r(r_j, \theta_j) \sin \theta_j \end{bmatrix}.$$

which are two components of the vector \mathbf{u} , and \mathbf{u} is compared with the global displacement vector \mathbf{U} of the numerical method. Then, the error $\|\mathbf{u} - \mathbf{u}_h\|_{\mathcal{L}_2(\Omega)}$ is approximated by $d_1(h)$, which is

$$\|\mathbf{u} - \mathbf{u}_h\|_{\mathcal{L}_2(\Omega)} \simeq d_1(h) = \left[\sum_{i=1}^{2P} |\mathbf{u}_i - \mathbf{U}_i|^2 h^2 \right]^{\frac{1}{2}}. \quad (3.46)$$

Consider five different meshes Ω_h , where the mesh size h is reduced by half between each mesh. Then, $d_1(h)$ and the ratio between the consecutive values of $d_1(h)$ are computed for each mesh and for the two test cases.

In Test Case 1, where $P_0 = 200Pa$, $E = 600Pa$ and $\nu = 0.25$, the ratio between consecutive values of $d_1(h)$ is shown in Table 3.1, and the ratio is consistently close to 0.25 which matches with the estimated value. Therefore, the program gives a correct solution to the elastic problem. In Test Case 2, where $P_0 = 10^6 Pa$, $E = 3.07 \times 10^5 Pa$ and $\nu = 0.49$, the ratio between consecutive values of $d_1(h)$ is shown in Table 3.2, and it is approaching 0.25 slowly. Since the convergence rate approaches 0.25 slower in Test Case 2 compared with Test Case 1, this suggests the numerical error $e(h)$ depends on the Poisson's ratio and the mesh size. Also, when $\nu = 0.49$, the material is nearly incompressible, and the problem is slightly ill-conditioned. In fact, in the study of hydrocephalus using consolidation theory, Tenti *et al* [46], have shown that the stress components of an poroelastic solid approaches an indeterminate form of $\frac{0}{0}$ as $\nu \rightarrow 0.5$.

Next, the program that solves the viscoelastic problem is also verified with the analytical solution found in Section 2.6. There are several error estimates for the viscoelastic problem. In [34], it is shown that, there exist a constant $C \geq 0$ that is depending on \mathbf{u}_h but not on h and Δt such that $\|\mathbf{u} - \mathbf{u}_h\|_{\mathcal{H}^1(\Omega)} \leq C(h^2 + \Delta t^2)$ for $t_k \in \mathcal{I}_h$. This shows convergence rate in space and in time; however, it is more difficult to demonstrate this convergence rate numerically.

Hence, the following norm is used in measuring the numerical error

$$\|\phi(x, t)\|_{\mathcal{L}_2(\mathcal{I}; \mathcal{L}_2(\Omega))} = \left(\int_0^t \|\phi(x, t)\|_{\mathcal{L}_2(\Omega)}^2 dt \right)^{\frac{1}{2}}, \quad (3.47)$$

Test Case 1	h (mm)	$d_1(h) \simeq \ \mathbf{u} - \mathbf{u}_h\ _{\mathcal{L}_2(\Omega)}$	$\frac{d_1(h_i)}{d_1(h_{i-1})}$
h_1	5	3.12×10^{-6}	-
h_2	2.5	6.44×10^{-7}	0.21
h_3	1.25	1.58×10^{-7}	0.24
h_4	0.625	4.24×10^{-8}	0.27
h_5	0.313	1.03×10^{-8}	0.24

Table 3.1: Test Case 1 for the elastic problem: $P_0 = 200Pa$, $E = 600Pa$ and $\nu = 0.25$

Test Case 1	h (mm)	$d_1(h) \simeq \ \mathbf{u} - \mathbf{u}_h\ _{\mathcal{L}_2(\Omega)}$	$\frac{d(h_i)}{d(h_{i-1})}$
h_1	5	1.10×10^{-5}	-
h_2	2.5	3.67×10^{-6}	0.33
h_3	1.25	1.03×10^{-6}	0.28
h_4	0.625	2.80×10^{-7}	0.27
h_5	0.313	6.58×10^{-8}	0.23

Table 3.2: Test Case 2 for the elastic problem: $P_0 = 10^6Pa$, $E = 3.07 \times 10^5Pa$, and $\nu = 0.49$

Test Case	h (mm)	$d_2(h) \simeq \ \mathbf{u} - \Pi_h \mathbf{u}\ _{\mathcal{L}_2(0,T;\mathcal{L}_2(\Omega))}$	$\frac{d_2(h_i)}{d_2(h_{i-1})}$
h_1	5	1.66×10^{-4}	-
h_2	2.5	3.88×10^{-5}	0.23
h_3	1.25	9.65×10^{-6}	0.25
h_4	0.625	2.63×10^{-6}	0.27
h_5	0.313	6.47×10^{-7}	0.25

Table 3.3: Test Case 1 for the viscoelastic problem: $K = 1Pa$, $p_1 = 1s$, $q_1 = 1Pa \cdot s$, $q_0 = 0.1Pa$, and $P(t) = 1Pa$.

and check if there is a consistent convergence rate.

Let $\|\mathbf{u} - \mathbf{u}_h\|_{\mathcal{L}_2(\mathcal{I};\mathcal{L}_2(\Omega))}$ be approximated by $d_2(h)$,

$$\|\mathbf{u} - \mathbf{u}_h\|_{\mathcal{L}_2(0,T;\mathcal{L}_2(\Omega))} \simeq d_2(h) = \left[\sum_{k=1}^J |d_1(h)|^2 \Delta t \right]^{\frac{1}{2}},$$

where $d_1(h)$ is defined in (3.46). In a test case, the pressure is $P(t) = 1Pa$, for $0 < t < 50s$, the bulk modulus $K = 1Pa$, the parameters of the shear relaxation modulus is $p_1 = 1s$, $q_1 = 1Pa \cdot s$ and $q_0 = 0.1Pa$. Hence, relaxation time $\tau_R = p_1 = 1s$, and so the time step is set as $\Delta t = 0.1\tau_R$. Table 3.3 shows the ratios between consecutive values of $d_2(h)$. This ratio is consistently close to 0.25; thus, the time-stepping component of the viscoelastic program is correct and its convergence rate in space is h^2 .

To illustrates this convergence in space visually, Figure 3.7 shows the analytical solution at the inner radius, $\mathbf{u}_r(r = a, t)$, and the numerical solution at the inner boundary, $\mathbf{u}_h(|\mathbf{x}| = a, t)$ for three different mesh size. As the mesh size decreases, it is shown that the numerical solution becomes closer to the analytical solution.

3.5 Stability Analysis

In this section, the stability of the numerical method for solving the viscoelastic problem is studied. When a numerical method is stable, an error in the numerical solution is bounded in time. Suppose there is an error, ϵ , in the first solution \mathbf{U}^0 , so that the perturbed solution

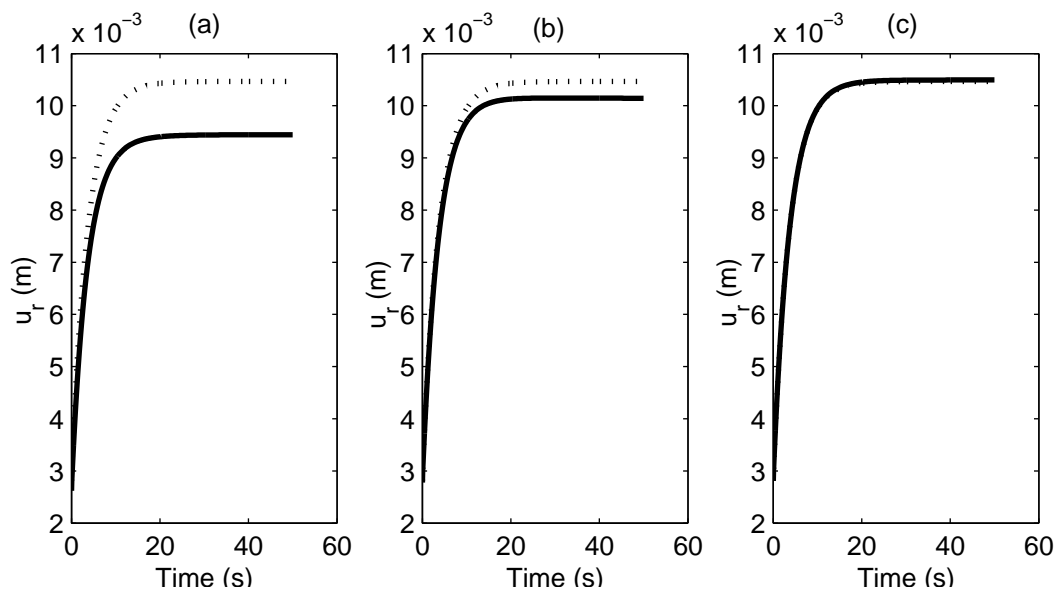


Figure 3.7: Comparison between analytical and numerical solution of the viscoelastic problem. Solid line represents numerical solution and dotted line represents analytical solution. In case (a), the mesh size is $h=5\text{mm}$; in case (b), $h=2.5\text{mm}$; in case (c), $h=1.25\text{mm}$. For all these cases, $\Delta t = 0.1\tau_R$

is $\tilde{\mathbf{U}}^0 = \mathbf{U}^0 + \epsilon$. Then, since the solution at $t = t_k$ depends on all solutions at previous time steps, \mathbf{U}^k is also perturbed, $\tilde{\mathbf{U}}^k = \mathbf{U}^k + \epsilon_k$. If ϵ_k is bounded, then the numerical method is stable. To determine the form of ϵ_k , the explicit form for the solution U^k is required.

Note that the solution for the viscoelastic problem at $t > t_0$ is found by solving (3.34), which is restated here for convenience

$$(A_K + A_G g_0) \mathbf{U}^k + A_G \sum_{i=1}^N g_i e^{-\frac{t_k - t_0}{\tau_i}} \mathbf{U}^0 + A_G \sum_{i=1}^N \left(\int_{t_0}^{t_k} g_i e^{-\frac{t_k - s}{\tau_i}} \frac{d\mathbf{U}(s)}{ds} ds \right) = \mathbf{L}(t). \quad (3.48)$$

For simplicity, let $N = 1$ and $t_0 = 0$, and then discretize this equation in time without using recurrence relationship Lemma 1. When $t_k = k\Delta t$, the integral term of (3.48) is divided into $k - 1$ terms, where each is approximated by a finite difference and trapezoidal rule as discussed in Section 3.2.2

$$\begin{aligned} & \int_0^{t_k} g e^{-\frac{t_k - s}{\tau}} \frac{d\mathbf{U}}{ds} ds \\ \approx & \int_0^{t_1} g e^{-\frac{t_k - s}{\tau}} \frac{d\mathbf{U}}{ds} ds + \dots + \int_{t_{k-1}}^{t_k} g e^{-\frac{t_k - s}{\tau}} \frac{d\mathbf{U}}{ds} ds \\ \approx & \frac{1}{2} g_1 \left(e^{-\frac{(k-1)\Delta t}{\tau_1}} + e^{-\frac{k\Delta t}{\tau_1}} \right) (\mathbf{U}^1 - \mathbf{U}^0) + \dots + \frac{1}{2} g_1 \left(1 + e^{-\frac{\Delta t}{\tau_1}} \right) (\mathbf{U}^k - \mathbf{U}^{k-1}) \\ = & \frac{1}{2} g_1 e^{-\frac{(k-1)\Delta t}{\tau_1}} \left(1 + e^{-\frac{\Delta t}{\tau_1}} \right) (\mathbf{U}^1 - \mathbf{U}^0) + \dots + \frac{1}{2} g_1 \left(1 + e^{-\frac{\Delta t}{\tau_1}} \right) (\mathbf{U}^k - \mathbf{U}^{k-1}). \end{aligned} \quad (3.49)$$

Assuming \mathbf{U}^0 is known, find an explicit form for the solutions, \mathbf{U}^1 , \mathbf{U}^2 and \mathbf{U}^3 . For $t_1 = \Delta t$, using (3.49) to discretize (3.48) gives

$$(A_K + A_G g_0) \mathbf{U}^1 + A_G g_1 e^{-\frac{\Delta t}{\tau_1}} \mathbf{U}^0 + A_G \frac{1}{2} g_1 \left(1 + e^{-\frac{\Delta t}{\tau_1}} \right) (\mathbf{U}^1 - \mathbf{U}^0) = L(\Delta t).$$

Solving this equation for \mathbf{U}^1 gives

$$\mathbf{U}^1 = F^{-1} L(t_1) + F^{-1} A_G \frac{1}{2} g_1 \left(1 - e^{-\frac{\Delta t}{\tau_1}} \right) \mathbf{U}^0, \quad (3.50)$$

where

$$F = A_K + A_G \left(g_0 + \frac{1}{2} g_1 \left(1 + e^{-\frac{\Delta t}{\tau_1}} \right) \right).$$

For $t_2 = 2\Delta t$, \mathbf{U}^2 is found similarly by solving the following

$$(A_K + A_G g_0) \mathbf{U}^2 + A_G g_1 e^{-\frac{2\Delta t}{\tau_1}} \mathbf{U}^0 + A_G \left(\frac{1}{2} g_1 e^{-\frac{\Delta t}{\tau_1}} \left(1 + e^{-\frac{\Delta t}{\tau_1}} \right) (\mathbf{U}^1 - \mathbf{U}^0) + \frac{1}{2} g_1 \left(1 + e^{-\frac{\Delta t}{\tau_1}} \right) (\mathbf{U}^2 - \mathbf{U}^1) \right) = L(2\Delta t),$$

so \mathbf{U}^2 is

$$\mathbf{U}^2 = F^{-1} L(2\Delta t) + F^{-1} A_G \frac{1}{2} g_1 \left(1 - e^{-\frac{2\Delta t}{\tau_1}} \right) \mathbf{U}^1 + F^{-1} A_G \frac{1}{2} g_1 e^{-\frac{\Delta t}{\tau_1}} \left(1 - e^{-\frac{\Delta t}{\tau_1}} \right) \mathbf{U}^0. \quad (3.51)$$

And for $t_3 = 3\Delta t$, \mathbf{U}^3 is found after some lengthy algebraic calculation,

$$\begin{aligned} \mathbf{U}^3 &= F^{-1} L(3\Delta t) + F^{-1} A_G \frac{1}{2} g_1 \left(1 - e^{-\frac{2\Delta t}{\tau_1}} \right) \mathbf{U}^2 + F^{-1} A_G \frac{1}{2} g_1 e^{-\frac{\Delta t}{\tau_1}} \left(1 - e^{-\frac{2\Delta t}{\tau_1}} \right) \mathbf{U}^1 \\ &\quad + F^{-1} A_G \frac{1}{2} g_1 e^{-\frac{2\Delta t}{\tau_1}} \left(1 - e^{-\frac{\Delta t}{\tau_1}} \right) \mathbf{U}^0. \end{aligned} \quad (3.52)$$

If $\tilde{\mathbf{U}}^0 = \mathbf{U}^0 + \epsilon$, then from (3.50) the perturbed $\tilde{\mathbf{U}}^1$ is

$$\tilde{\mathbf{U}}^1 = \mathbf{U}^1 + F^{-1} A_G \frac{1}{2} g_1 \left(1 - e^{-\frac{\Delta t}{\tau_1}} \right) \epsilon.$$

Define the matrix B as

$$\begin{aligned} B &= F^{-1} A_G \frac{1}{2} g_1 \left(1 - e^{-\frac{\Delta t}{\tau_1}} \right) \\ &= \left[A_K + A_G \left(g_0 + \frac{1}{2} g_1 \left(1 + e^{-\frac{\Delta t}{\tau_1}} \right) \right) \right]^{-1} A_G \frac{1}{2} g_1 \left(1 - e^{-\frac{\Delta t}{\tau_1}} \right). \end{aligned} \quad (3.53)$$

If $\tilde{\mathbf{U}}^0 = \mathbf{U}^0 + \epsilon$ and $\tilde{\mathbf{U}}^1 = \mathbf{U}^1 + B\epsilon$, then from (3.51) the perturbed $\tilde{\mathbf{U}}^2$ is

$$\begin{aligned} \tilde{\mathbf{U}}^2 &= \mathbf{U}^2 + F^{-1} A_G \frac{1}{2} g_1 \left(1 - e^{-\frac{2\Delta t}{\tau_1}} \right) B\epsilon + F^{-1} A_G \frac{1}{2} g_1 e^{-\frac{\Delta t}{\tau_1}} \left(1 - e^{-\frac{\Delta t}{\tau_1}} \right) \epsilon \\ &= \mathbf{U}^2 + F^{-1} A_G \frac{1}{2} g_1 \left(1 - e^{-\frac{2\Delta t}{\tau_1}} \right) B\epsilon + e^{-\frac{\Delta t}{\tau_1}} B\epsilon \\ &= \mathbf{U}^2 + \left[F^{-1} A_G \frac{1}{2} g_1 \left(1 - e^{-\frac{2\Delta t}{\tau_1}} \right) + e^{-\frac{\Delta t}{\tau_1}} I \right] B\epsilon. \end{aligned}$$

Define the matrix C as

$$\begin{aligned} C &= F^{-1} A_G \frac{1}{2} g_1 \left(1 - e^{-\frac{2\Delta t}{\tau_1}} \right) + e^{-\frac{\Delta t}{\tau_1}} I \\ &= \left[A_K + A_G \left(g_0 + \frac{1}{2} g_1 \left(1 + e^{-\frac{\Delta t}{\tau_1}} \right) \right) \right]^{-1} A_G \frac{1}{2} g_1 \left(1 - e^{-\frac{2\Delta t}{\tau_1}} \right) + e^{-\frac{\Delta t}{\tau_1}} I. \end{aligned} \quad (3.54)$$

where I is the identity matrix. Similarly, after some lengthy algebraic calculation, the perturbed $\tilde{\mathbf{U}}^3$ can be found to be

$$\tilde{\mathbf{U}}^3 = \mathbf{U}^3 + C^2 B \epsilon.$$

In general, if $\tilde{\mathbf{U}}^0 = \mathbf{U}^0 + \epsilon$, then the perturbed solution at $t = t_k$ is given by

$$\tilde{\mathbf{U}}^k = \mathbf{U}^k + C^k B \epsilon.$$

When the numerical scheme is stable, the error at $\epsilon_k = C^k B \epsilon$ is bounded for all time. The error ϵ_k to be bounded if and only if

$$\|B\|_2 \leq 1 \quad (3.55)$$

$$\|C\|_2 \leq 1. \quad (3.56)$$

Since B and C are non-symmetric, it turns out to be quite difficult to prove (3.55) and (3.56). Instead, the eigenvalues of B and C are considered in the following Lemma, since a necessary condition for stability requires the eigenvalues of B and C to be less than 1.

Lemma 2. *Let λ_B be eigenvalues of B defined by (3.53), and let λ_C be the eigenvalues of C defined by (3.54). Then, $\lambda_B < 1$ and $\lambda_C < 1$.*

Proof. To show $\lambda_B < 1$, let

$$\begin{aligned} D &= A_K + A_G g_0 \\ E &= A_G \frac{1}{2} \left(1 + e^{-\frac{\Delta t}{\tau_1}} \right) \\ G &= A_G \frac{1}{2} \left(1 - e^{-\frac{\Delta t}{\tau_1}} \right), \end{aligned}$$

so that $B = (D + E)^{-1} G$. Let v be the corresponding eigenvector of λ_B . Then

$$\begin{aligned} (D + E)^{-1} Gv &= \lambda_B v \\ Gv &= \lambda_B (D + E)v \\ v^T Gv &= \lambda_B (v^T Dv + v^T Ev) \\ \lambda_B &= \frac{v^T Gv}{v^T Dv + v^T Ev}. \end{aligned} \quad (3.57)$$

By the definition of E and G , $v^T E v > v^T G v$, for $\Delta t > 0$. Therefore, by (3.57), $\lambda_B < 1$.

To show $\lambda_C < 1$, rewrite C as

$$C = \left[A_K + A_G \left(g_0 + \frac{1}{2} g_1 \left(1 + e^{-\frac{\Delta t}{\tau_1}} \right) \right) \right]^{-1} A_G \frac{1}{2} g_1 \left(1 + e^{-\frac{\Delta t}{\tau_1}} \right) \left(1 - e^{-\frac{\Delta t}{\tau_1}} \right) + e^{-\frac{\Delta t}{\tau_1}} I.$$

Then,

$$C = (D + E)^{-1} E \left(1 - e^{-\frac{\Delta t}{\tau_1}} \right) + e^{-\frac{\Delta t}{\tau_1}} I.$$

Let the eigenvalue and corresponding eigenvector of $(D + E)^{-1} E$ be λ and w . Then

$$\begin{aligned} (D + E)^{-1} E w &= \lambda w \\ w^T E w &= \lambda (w^T D w + w^T E w) \\ \lambda &= \frac{w^T E w}{w^T D w + w^T E w}, \end{aligned}$$

which implies $\lambda < 1$. Then, the eigenvalue of C is

$$\begin{aligned} \lambda_C &= \lambda \left(1 - e^{-\frac{\Delta t}{\tau_1}} \right) + e^{-\frac{\Delta t}{\tau_1}} \\ &= \lambda + (1 - \lambda) e^{-\frac{\Delta t}{\tau_1}} \\ &< \lambda + (1 - \lambda) \\ &= 1, \end{aligned}$$

for $\Delta t > 0$. Therefore, $\lambda_C < 1$. □

Note that $\lambda_B < 1$, and $\lambda_C < 1$ are necessary condition for stability, since the perturbed solution is given by $\tilde{\mathbf{U}}^k = \mathbf{U}^k + C^k B \epsilon$. Suppose there is an eigenvalue of C where $\lambda_C > 1$ and the corresponding eigenvector is v_C . If ϵ happens to be $B^{-1} v_C$, then the error at time t_k is

$$\begin{aligned} \epsilon_k &= C^k B \epsilon \\ &= C^k v_C \\ &= \lambda_C^k v_C, \end{aligned}$$

which implies the error ϵ_k will grow unbound. So, $\lambda_C < 1$ is a necessary condition for stability.

Chapter 4

Numerical Studies

Now that the viscoelastic model of the brain can be solved numerically, and a realistic computational mesh can be generated, numerical experiments are conducted to provide a better understanding of the biomechanics of hydrocephalus. By changing the pressure $P(t)$, one can simulate different conditions for a brain with hydrocephalus.

In this chapter, some background information about the numerical experiments are first introduced. Then, three numerical studies are conducted. First, the state of stress of the brain tissue as the ventricles expand are observed. Then, the role of viscoelastic properties in modeling hydrocephalus is investigated. Lastly, the movement of the ventricular wall after the shunting procedure is studied. In addition to these studies, the limitation of the infinitesimal deformation and linear viscoelasticity are investigated.

4.1 Background Information

For the following numerical experiments, the chosen computational mesh, material parameters for the elastic and viscoelastic problem and the time step are described as follows.

4.1.1 Computational Mesh

In the following experiments, simple computational mesh, such as an annulus, are generated using a MATLAB's toolbox called `pdetool`. Other computational meshes are generated

from medical images of actual patients with hydrocephalus using the methods discussed Section 3.3. These images were obtained from the database of the hydrocephalus group at the Hospital for Sick Children in Toronto, and they were also used in West's thesis [48]. The images are taken before and after a shunting procedure of 8 patients, typically a year apart, and the 8 patients are identified as Patient A to Patient H. An image taken before the surgery is referred as the pre-shunt image and after the surgery as the post-shunt image. However, little is known about the actual length scale of these images. Therefore, they are roughly scaled to the average size of a human head, which is 140mm in width and 167 mm in length [2].

Among these set of images, only a few were used to generated a computational mesh in this thesis. The mesh size of the generated meshes are: $h = 2.08mm$ from a post-shunt image of Patient A, $h = 2.11mm$ from a post-shunt image of Patient C, $h = 2.14$ from a post-shunt image of Patient H, and $h = 1.56mm$ from a pre-shunt of Patient D.

4.1.2 Material Parameter for the Elastic and Viscoelastic Problem

The parameter for the elastic constitutive equations are the Young's modulus E and the Poisson's ratio ν , and they are

$$\begin{aligned} E &= 10KPa \\ \nu &= 0.49. \end{aligned} \tag{4.1}$$

This value of Young's modulus also used in [21, 29] to describe the elasticity of the brain tissue. To describe that fact that the tissue is nearly incompressible, the Poisson's ratio is chosen to be close to 0.50.

The viscoelastic constitutive equations require a value for the bulk modulus K and a function for shear relaxation modulus $G(t)$ of the brain tissue. As mention in Section 2.4, the shear relaxation modulus $G(t)$ is taken from [18], and it is

$$G(t) = g_0 + g_1 e^{-\frac{t}{\tau_1}} + g_2 e^{-\frac{t}{\tau_2}}, \tag{4.2}$$

where $g_0 = 717Pa$, $g_1 = 430Pa$, $\tau_1 = 1.82s$, $g_2 = 405Pa$ and $\tau_2 = 29.8s$. Two values for the bulk modulus are considered in the following experiments. One of them is $K = 2100MPa$,

taken from the studies of traumatic brain injury [3, 8, 32]. The other value is $K = 166\text{KPa}$, calculated from setting E and ν to be (4.1) in

$$K = \frac{E}{3(1 - 2\nu)}. \quad (4.3)$$

4.1.3 Time Step

Although a small time step gives greater accuracy, it also takes a longer computational time. So, different time steps were tested for the gain in accuracy. In two test cases that solves the viscoelastic problem, two different time steps are used, $\Delta t = 60s$ and $\Delta t = 600s$. The result shows that the resulting displacement is identical for the first 5 non-zero digits. Thus, having the greater time step does not cause a noticeable difference in the solution, but it reduces computational time by $\frac{1}{12}$. So, $\Delta t = 600s$ is used in the following experiment, unless it is stated otherwise.

4.2 State of Stress of Brain Tissue

When hydrocephalus develops and the ventricles expand, the state of stress of the brain tissue changes. The region of high stress may indicates areas where the brain tissue is damaged. In this section, the state of stress of the brain tissue is studied in a numerical experiment where the pressure increases to simulate the development of hydrocephalus using a realistic geometry of the brain.

In this experiment, the computation domain Ω_h is generated from a post-shunt image of Patient A, and the pressure $P(t)$ is increased linearly 0 to 3000Pa ($306\text{mmH}_2\text{O}$) over 8 hours of simulated time. The shear modulus $G(t)$ is defined by (4.2), and the bulk modulus is $K = 166\text{KPa}$.

The result of this experiment is shown in Figure 4.1. Figure 4.1(a) shows the original shape of Ω_h , and Figure 4.1(b) shows the resulting geometry of Ω_h after 8 hours of simulated time. Comparing Figure 4.1(a) and Figure 4.1(b), the greatest displacement occurs on the ventricular wall, and it is 1.5 mm.

The volumetric stress is also computed at every element and is shown in Figure 4.2 in mmH_2O . Since the values on the colour bar of this figure are negative, the volumetric stress

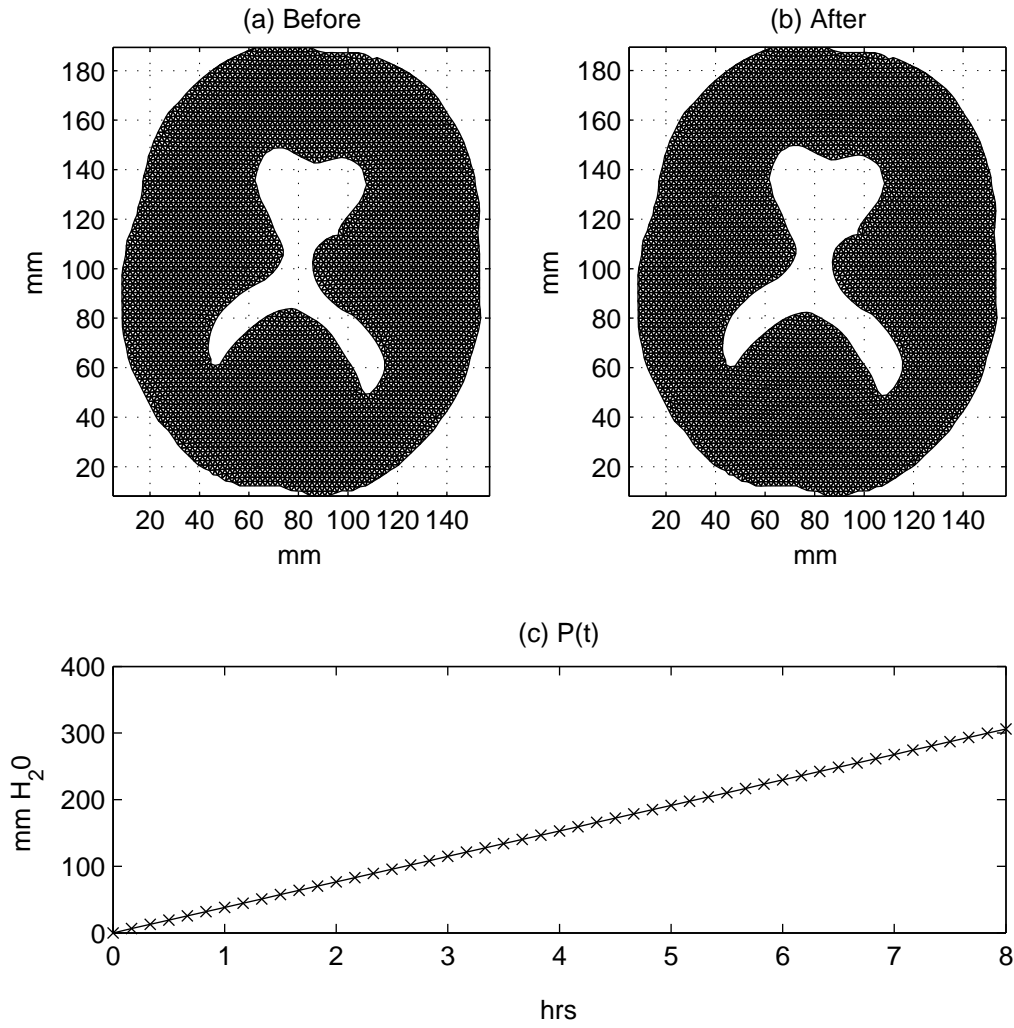


Figure 4.1: (a) The original shape of Ω_h . (b) The resulted shape of Ω_h after 8 hours of simulated time. (c) The pressure $P(t)$ at the ventricular wall which linearly increases over 8 hours.

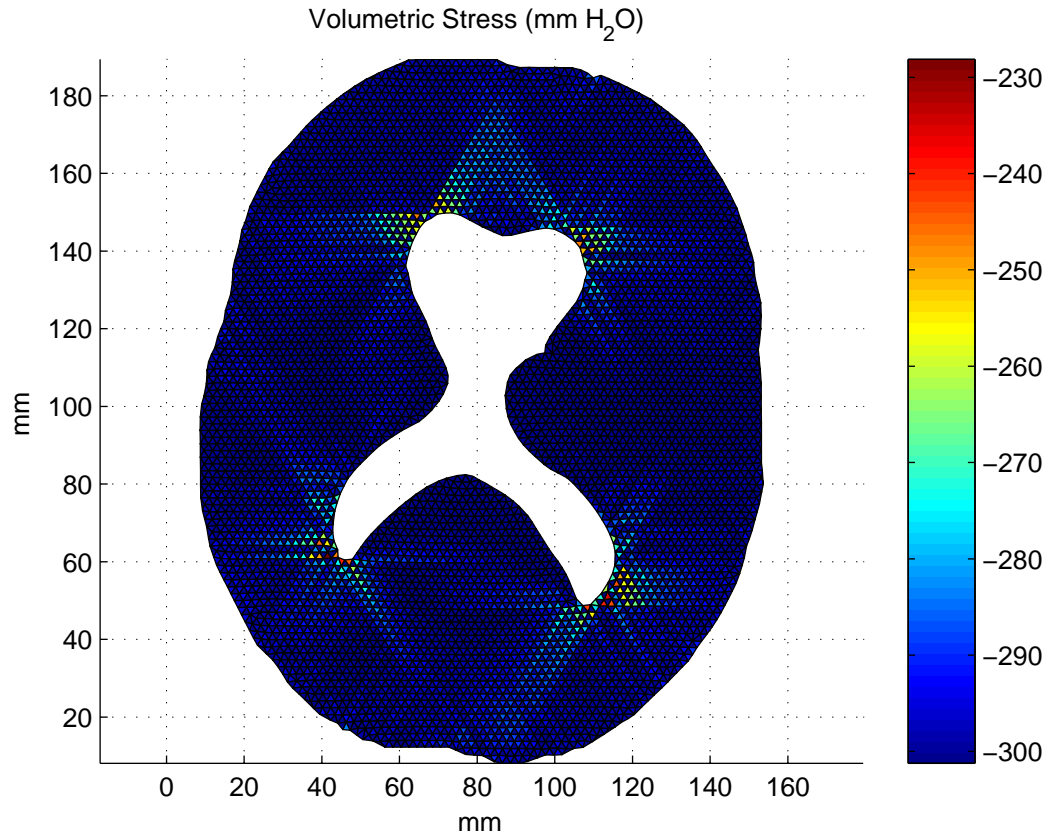


Figure 4.2: Volumetric stress of the resulted Ω_h at day 14.

is negative at every element which implies the brain tissue is compressed everywhere. The figure also shows that volumetric stress at the anterior and posterior ventricular horns are different from other region. In particular, near these regions, elements with high value of stress are next to elements with low value of stress. So, principle stresses and directions are computed to investigate further. This observation at the two horns is consistently observed in meshes of different resolution, thus the principle stress and direction are computed on a coarser grid, which allows the principle directions to display clearly.

The computed principle stress and directions along with the volumetric stress near one of the anterior horns are shown Figure 4.3. Figure 4.3(a) shows the volumetric stress and Figure 4.3(b) shows the corresponding principle stress and its direction. The arrows in black

represents the principle directions, and its length indicates the magnitude of the principle stress. In Figure 4.3(a), two elements with very different magnitude in volumetric stress are indicated by two arrows in red. The corresponding elements are indicated with two red arrows in Figure 4.3(b), which shows the principle stress of one element, represented by the length of arrows, is slightly larger than the other.

It is unclear why elements so close to each other are compressed by slightly different amount. Such observation is only found in regions of near anterior and posterior ventricular horns, regions where the ventricular wall has the same concavity. Since this observation is also found in a simple mesh that is annulus with the finest mesh, $h = 0.313mm$, of this thesis. This observation may be due to a numerical difficulties described in [25]. “Severe numerical difficulties are encountered for incompressible or nearly incompressible materials because small volumetric strains cause large volumetric stress due to the high effective bulk modulus. Thus, the hydrostatic part of the stress tensor is very sensitive to computed fluctuations in the hydrostatic strain, which leads to numerical instability in the finite element simulation. [25]”

Although the exact distribution of volumetric stress may be unclear, the above experiment shows that the state of stress of brain tissue is compressive everywhere. This result is different from the numerical result of Peña *et. al.* in [29], where they describe the tissue as poroelastic solid filled with fluid and study edema¹. In their numerical simulation, they computed the mean effective stress of the poroelastic solid and found that there is a region of expansive stresses surrounding the anterior and posterior horns, and a region of compressive stress in the concave region of the ventricles system. They conclude that fluid accumulates in the region of expansive stress, resulting in edema.

Comparing the results in [29] and in this thesis, their difference in the state of stress highlights the difference between the two ways of modeling the brain tissue. The pressure and simulated time in this thesis are set to be the same as those in [29]. The bulk modulus K is calculated from E and ν , where the value E is same as the value in [29]. The difference between the two models is that, in [29], the tissue is modeled as an inhomogeneous material, and so the poroelastic solid requires a lower Poisson’s ratio ($\nu = 0.3$). But, in this thesis, the tissue is model as a homogeneous material, and so a higher Poisson’s ratio ($\nu = 0.49$) is

¹Edema is a feature of acute stages of hydrocephalus where CSF accumulates in the brain tissue.

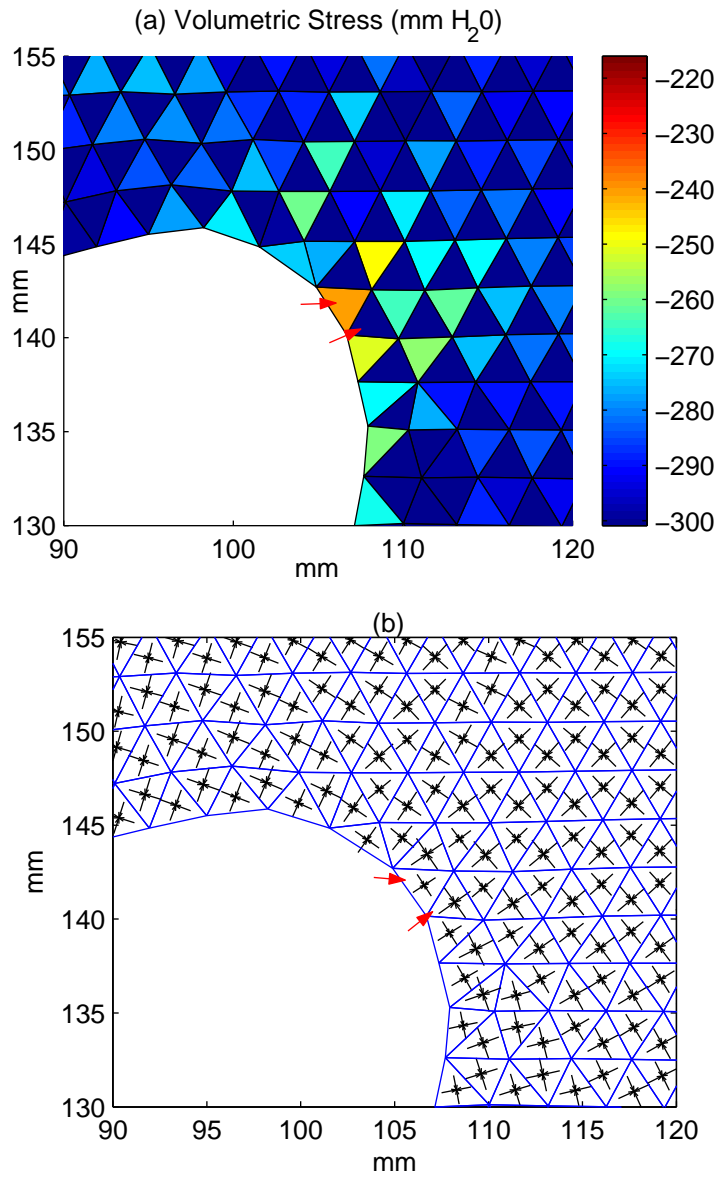


Figure 4.3: (a) The volumetric stress at one of the anterior horns. (b) The corresponding principle stress and direction, where the principle direction is represented by an arrow, and the magnitude of a principle stress is represented by the length of an arrow.

necessary. Interestingly, when a lower Poisson's ratio is tested for the viscoelastic problem, the state of stress is both compressive and expansive in regions similar to [29]. Thus, the difference in the type of stress observed is due to the way incompressibility is modeled, and these two biomechanical models of the brain tissue provide different information about the state of stress for the brain with hydrocephalus, which provide different view on how brain tissue is damaged.

4.3 Material Parameter for the Viscoelastic Problem

Many experiments conducted to determine the material property of brain tissue use a viscoelastic model to fit the experimental data, and most of experiments were designed to mimic the loading conditions of traumatic brain injury. Using the material parameters derived from such experiments, how does this viscoelastic model of brain tissue play a role in modeling hydrocephalus? In this section, the effect of the bulk modulus and shear modulus of the viscoelastic model are investigated.

4.3.1 Choice of Bulk Modulus

When $G(t)$ is fixed and defined by (4.2), the choice of bulk modulus has a direct influence on the pressure $P(t)$ required to move the ventricular wall. Although the bulk modulus is known to be a large number to describe a nearly incompressible tissue, it is unclear how large it should be for modeling hydrocephalus. In the study of brain traumatic injury, the value of bulk modulus is usually around $K = 2100MPa$, but is it appropriate for modeling hydrocephalus? The effects of different values for K is investigated in the following two experiments.

In these two experiments, the computational mesh Ω_h is generated from a post-shunt image of Patient A, and different value of pressure is used such that both experiment gives the similar magnitude in displacement. In the first experiment, where $K = 2100MPa$, $P(t)$ is increased from 0 to $30MPa$ over 8 hours of simulated time with $\Delta t = 200s$. The numerical result shows that the greatest displacement that occurs on the ventricular wall is $1.60mm$. Moreover, the average volumetric stress over Ω_h is $-29.98MPa$ or $-3.06 \times 10^6 mmH_2O$. In the second experiment, where $K = 166KPa$, $P(t)$ is increased from 0

to $3000Pa$ over 8 days of simulated time with $\Delta t = 200s$. The numerical result shows that the greatest displacement is $1.55mm$, and the average volumetric stress is $-2952Pa$ or $-300mmH_2O$.

Thus, the above two numerical experiments shows that the higher bulk modulus requires a higher pressure to move the ventricular wall, and the resultant state of stress is also higher. To illustrate which value of K is probable, let's relate the state of stress with the intracranial pressure (ICP) of the brain. Intracranial pressure is the pressure exerted by the brain, CSF and the brain's blood supply on the closed skull cavity, and it is usually $100-180mmH_2O$ for a healthy individual[33]. From the definition of ICP, it is permissible that ICP and the state of stress has the same order of magnitude, for it is assumed here that the viscoelastic material is homogeneous describing all material inside the skull cavity. So, in the case where $K = 2100MPa$, the state of stress shown in the numerical experiment is significantly higher than the normal value of ICP, and the ventricular wall have only moved by $1.60mm$. Therefore, in modeling hydrocephalus, it is unlikely that the patient's brain can suffer such high states of stress over a long period of time, and such high state of stress in brain trauma may only last a few seconds. Thus, between these two values for the bulk modulus, it is more reasonable to consider the bulk modulus to be $166KPa$, and the bulk modulus for modeling traumatic brain injury is not suitable.

4.3.2 Choice of Shear Modulus

The viscoelastic model is different from the elastic models because of the time dependent shear response of the tissue. To study the role of the time-dependent shear modulus in modeling hydrocephalus, the numerical result of the viscoelastic problem is compared with those of the elastic problem in the following two numerical experiments.

But first, to fairly compare the two problems, their dilatation responses are set to be the same, such that they both describes the same degree of incompressibility. That is, the Young's modulus and the Poisson's ratio of the elastic problem are defined in (4.1), and the bulk modulus of the viscoelastic problem is defined by (4.3) using E and ν to give $K = 166KPa$. However, the shear modulus $G(t)$ is defined in (4.2), and the constant shear modulus of the elastic problem is $G = \frac{E}{2(1+\nu)} = 3356Pa$, which is larger in magnitude compared to $G(t)$ and will make a difference to their response.

In the first experiment, the pressure is set to be

$$\begin{aligned} P(t) &= 1000 (H(t) - H(t - 600)) Pa \\ &= 102 (H(t) - H(t - 600)) mmH_2O \end{aligned}$$

for $0 \leq t \leq 1200s$ as shown in Figure 4.4, and $\Delta t = 10s$. Also, the computational mesh is an annulus with an inner radius $a = 35mm$ and an outer radius of $b = 70mm$, so that the outer diameter is close the length scale of a human brain. The mesh size is $h = 1.25mm$. Thus, with such simple geometry, the radial displacement at the inner boundary can be computed easily from the displacements $\mathbf{u}_h = (u_1, u_2)$ at node \mathbf{x}_a that lies on the inner boundary. The resulting radial displacement from a numerical experiment at the inner boundary is computed by

$$u_r(r = a, t) = \sqrt{u_{h1}(\mathbf{x}_a, t)^2 + u_{h2}(\mathbf{x}_a, t)^2}.$$

The numerical result for radial displacements of the two problems are shown in Figure 4.5. Figure 4.5(a) shows $u_r(r = a, t)$ of viscoelastic material, which is slightly different from $u_r(r = a, t)$ of elastic material at $t = 0$ and $t = 600$, as shown in Figure 4.5(b). The elastic response is instantaneous and time independent. That is, when pressure is applied, the displacement becomes non-zero immediately. When the applied pressure is removed, the displacement becomes zero immediately which implies Ω_h has returned to its original shape. For the viscoelastic problem, the viscoelastic response is time dependent as a result of the time dependent shear modulus. But since the relaxation times of the shear modulus are short, and the magnitude of the shear modulus is small compared to that of the bulk modulus, the dependent response is short and soon dominated by the elastic dilatational response. Then, when the applied pressure is removed, the displacement of the viscoelastic problem decreases rapidly to zero in time.

Moreover, when volumetric stress is computed at $t = 590s$, the distribution of the stress for the two problems over Ω_h is also similar, as shown in Figure 4.6. Note that the value of volumetric stress is higher for the viscoelastic case, but this is consequence of the higher displacement for the viscoelastic case compared to the elastic case. The average volumetric stress in space is $-99.9mmH_2O$ for the viscoelastic case and $-93.5mmH_2O$ for the elastic case.

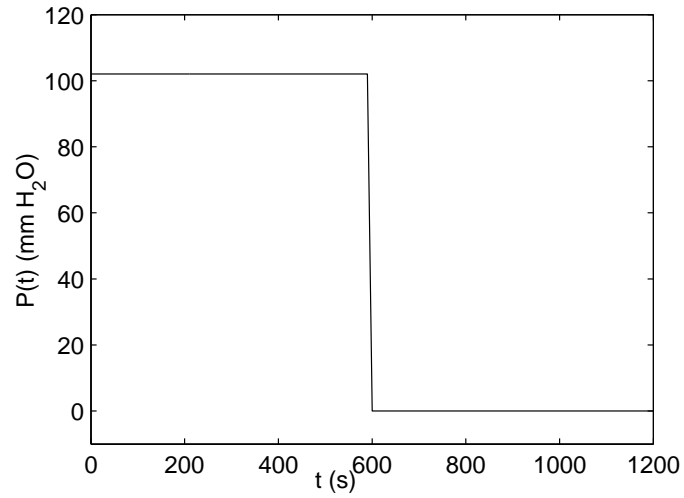
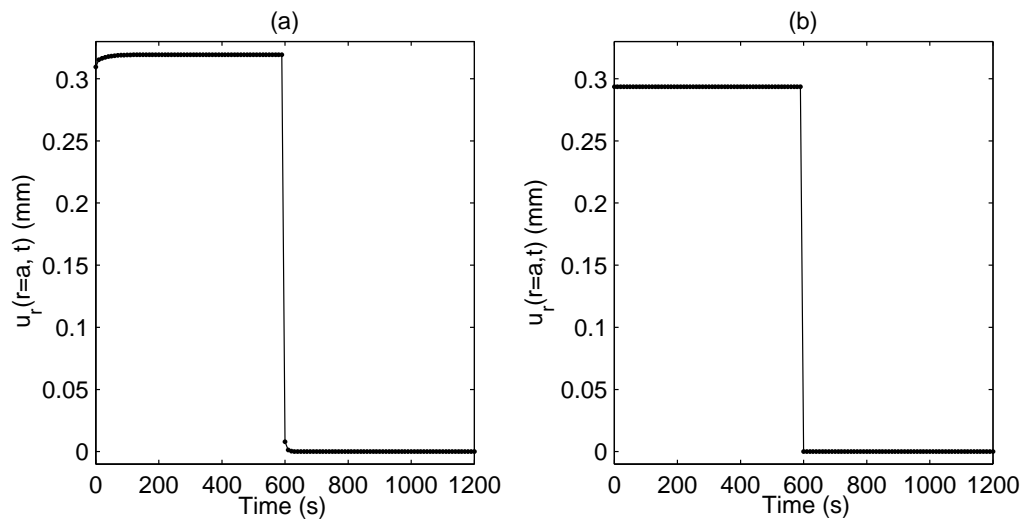
Figure 4.4: Pressure $P(t)$ as a function of time

Figure 4.5: The radial displacement at the inner boundary when the material is (a) viscoelastic, and (b) elastic.

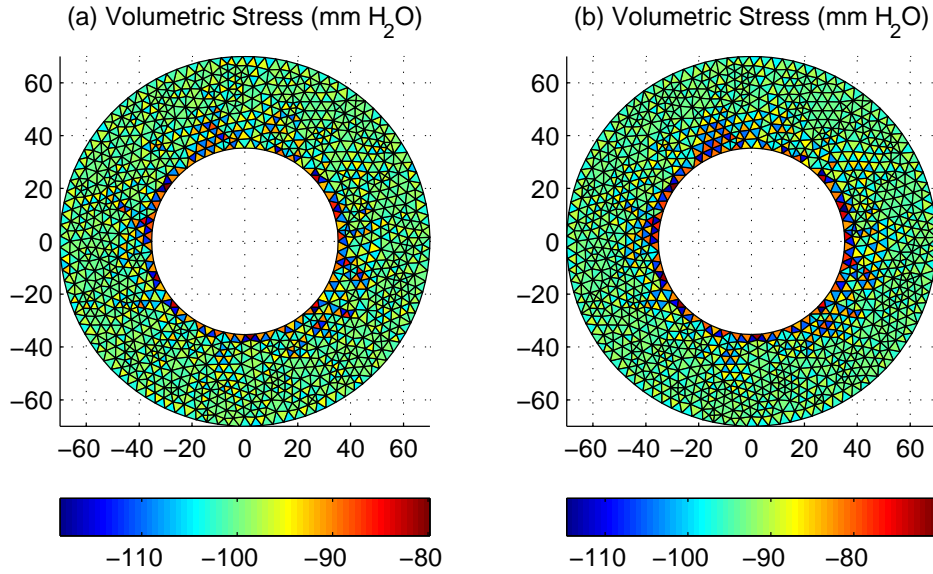


Figure 4.6: The volumetric stress of (a) the viscoelastic problem at $t = 590s$, and (b) the elastic problem at $t = 590s$.

In the second experiment, the two problems are compared with a realistic geometry of the ventricular wall, and a realistic time scale and pressure. The computational domain Ω_h is generated from a post-shunt image of Patient C. $P(t)$ is increased linearly from 0 to $9000Pa$ over 14 days of simulated time. The material parameters K , $G(t)$, E and ν are the same as the previous experiment.

The numerical result of the second experiment shows that, at day 14, the greatest displacement around the ventricular wall is $4.73mm$ for the elastic problem and $5.12mm$ for the viscoelastic problem. Because the difference in displacement is small, the shapes of the ventricular wall for the two problems are nearly identical. Figure 4.7 shows the boundaries of the original mesh and the boundaries of the deformed mesh for the two problems.

From the observations of these two numerical experiments, the displacement, strain and stress response of the elastic and viscoelastic problems are very similar, and they have a small difference in magnitude since their magnitude in shear modulus are different. Moreover, when a realistic geometry is used, the shape of their deformed ventricles are

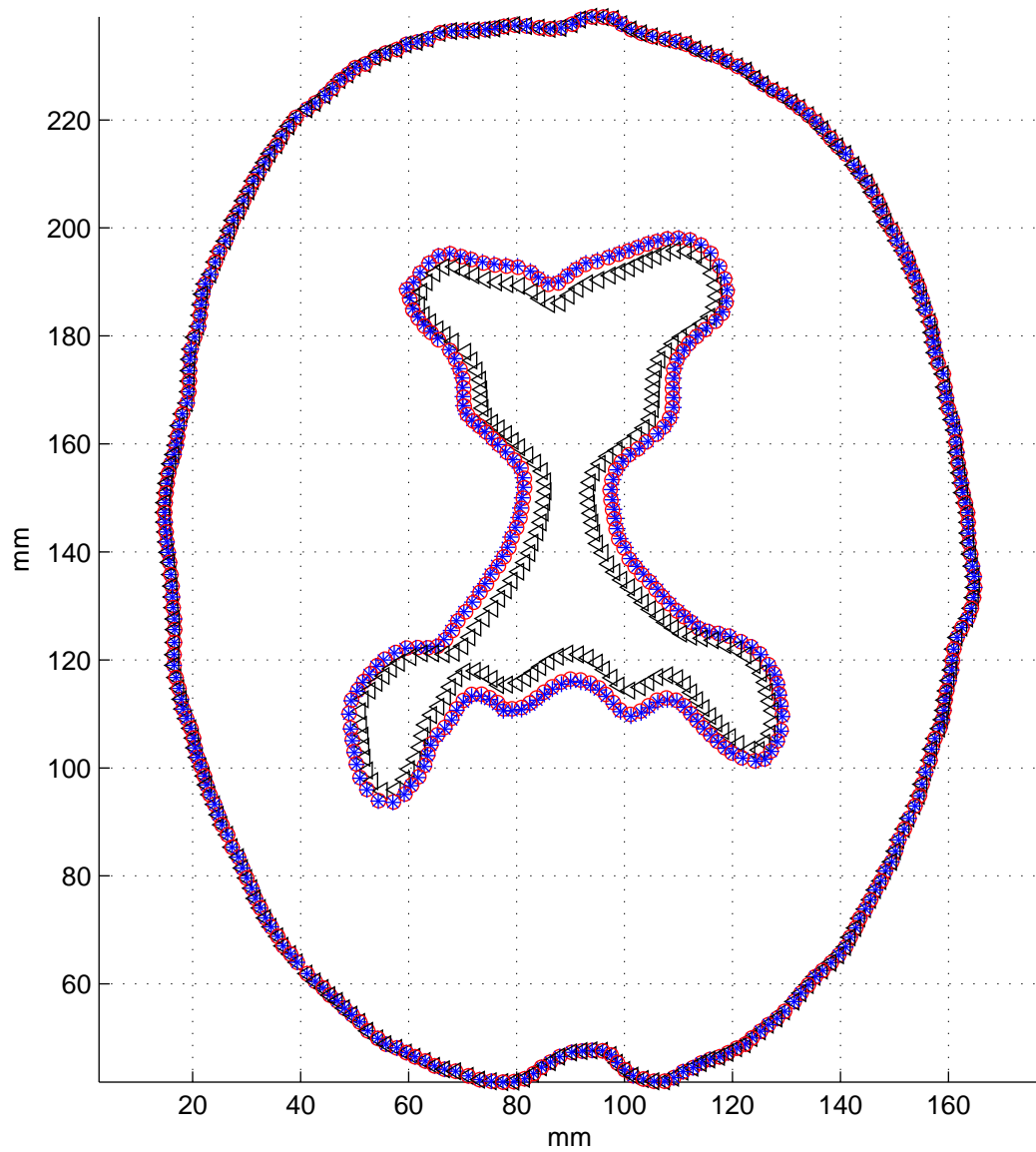


Figure 4.7: The symbol “ Δ ” outlines the original boundaries of Ω_h . The symbol “*” outlines the deformed boundaries of Ω_h of the viscoelastic problem. The symbol “o” outlines the deformed boundaries of Ω_h of the elastic problem.

similar. This is because both problems describe their dilatation response as elastic, and have the same degree of incompressibility. Another reason is that the relaxation time of the shear modulus $G(t)$ is short, and its magnitude is small compared to the magnitude of the bulk modulus. In [9], several forms of the shear modulus $G(t)$ are summarized, and the one with the greatest magnitude is three times bigger than the current shear modulus used. However, it is still small compared to the bulk modulus. Also, the longest relaxation time is 80s found in [12] with a quasi-linear model, but it is still short compared to the time scale of hydrocephalus. Thus, given the current material parameters for the linear viscoelastic model of brain tissue, the description of brain tissue response is similar to the elastic description in modeling hydrocephalus.

4.4 Movement of the Ventricular Wall

Since the success of a shunting procedure depends on the placement of the shunt, it is beneficial to know how the ventricular wall will move inward when a shunt is placed. It would even be better if the shape of the ventricular wall can be predicted. In this section, the movement of the ventricular wall is studied as the pressure increases and decreases. Then, the challenge to predict the shape of the ventricular wall is addressed.

4.4.1 Movement of the Ventricular Wall

If the ventricular wall and the skull were two concentric circles, then as the pressure changes, the radius of ventricular wall would change but it would still remain a circle. Since the ventricular wall and the skull are not circles, how the ventricular wall expands and shrinks is unclear. To study how the ventricular wall shrinks after a shunting procedure, the development and treatment of hydrocephalus is simulated by increasing and then decreasing the pressure, and then the displacement made by the ventricular wall is observed.

Three experiments are conducted using the viscoelastic model with three computation meshes Ω_h generated from a post-shunt image of Patient A, Patient C and Patient H. The pressure $P(t)$ increases linearly, then becomes stationary, and then decreases linearly

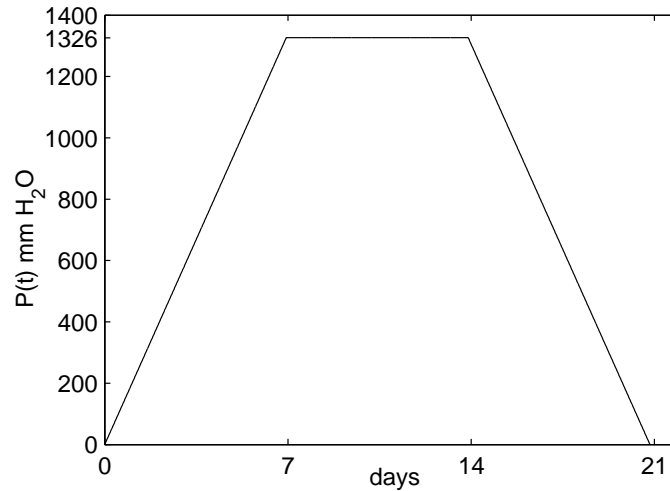


Figure 4.8: Pressure $P(t)$ as a function of time

within three weeks, as shown in Figure 4.8. Also, the shear modulus $G(t)$ is defined in (4.2), and the bulk modulus $K = 166\text{KPa}$.

Figure 4.9, Figure 4.10, and Figure 4.11 show the outline of the boundaries of the three meshes at day 14 and day 21, which describe the displacement made by the ventricular wall as it moves inward. In all three figures, the displacement around the ventricular wall is non uniform. In particular, the regions where the displacement is greatest are where the ventricular wall is concave and are furthest away from the skull. Similarly, the regions where the displacement are smallest are where the ventricular wall is convex and are closest to the skull. This shows the different regions of ventricular wall are moving at different speeds.

Such observation is useful in the research conducted by West in [48], where the level set method is used to simulate the ventricular motion. This method requires information about how the ventricular wall moves, and West tried both uniform speed and curvature dependent speed. The observation of these experiments shows that the speed is definitely not uniform, even when the deformation is small. When the deformation is small such as those shown in this experiment, the motion of the ventricular wall is influenced by the concavity of the wall and the distance between the ventricular wall and the skull. It is not clear which of these two factors plays a more important role, since the wall is usually

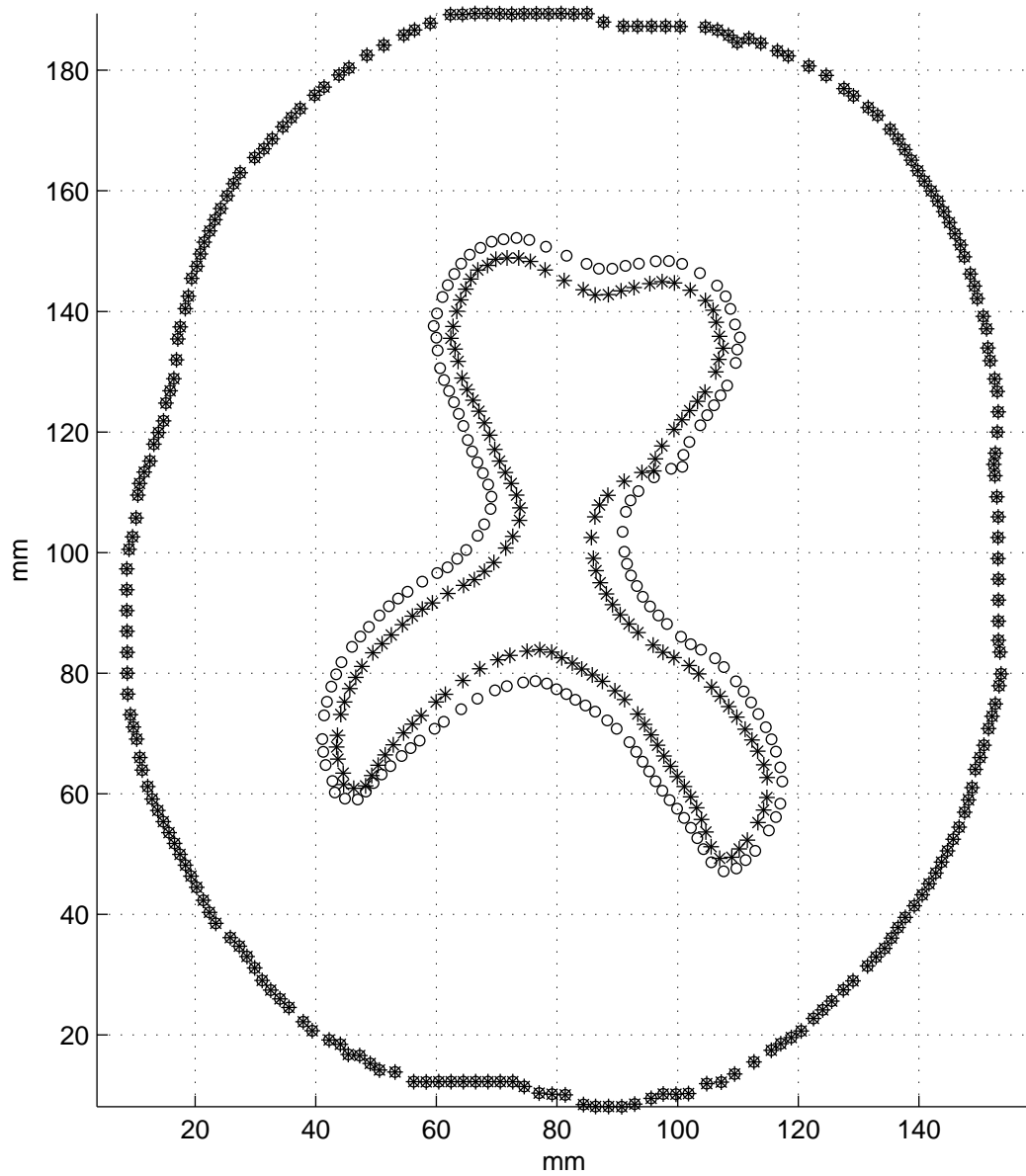


Figure 4.9: Ω_h represent the brain of Patient A. The symbol “o” outlines the boundaries of Ω_h at day 14. The symbol “*” outlines the boundaries of Ω_h at day 21.

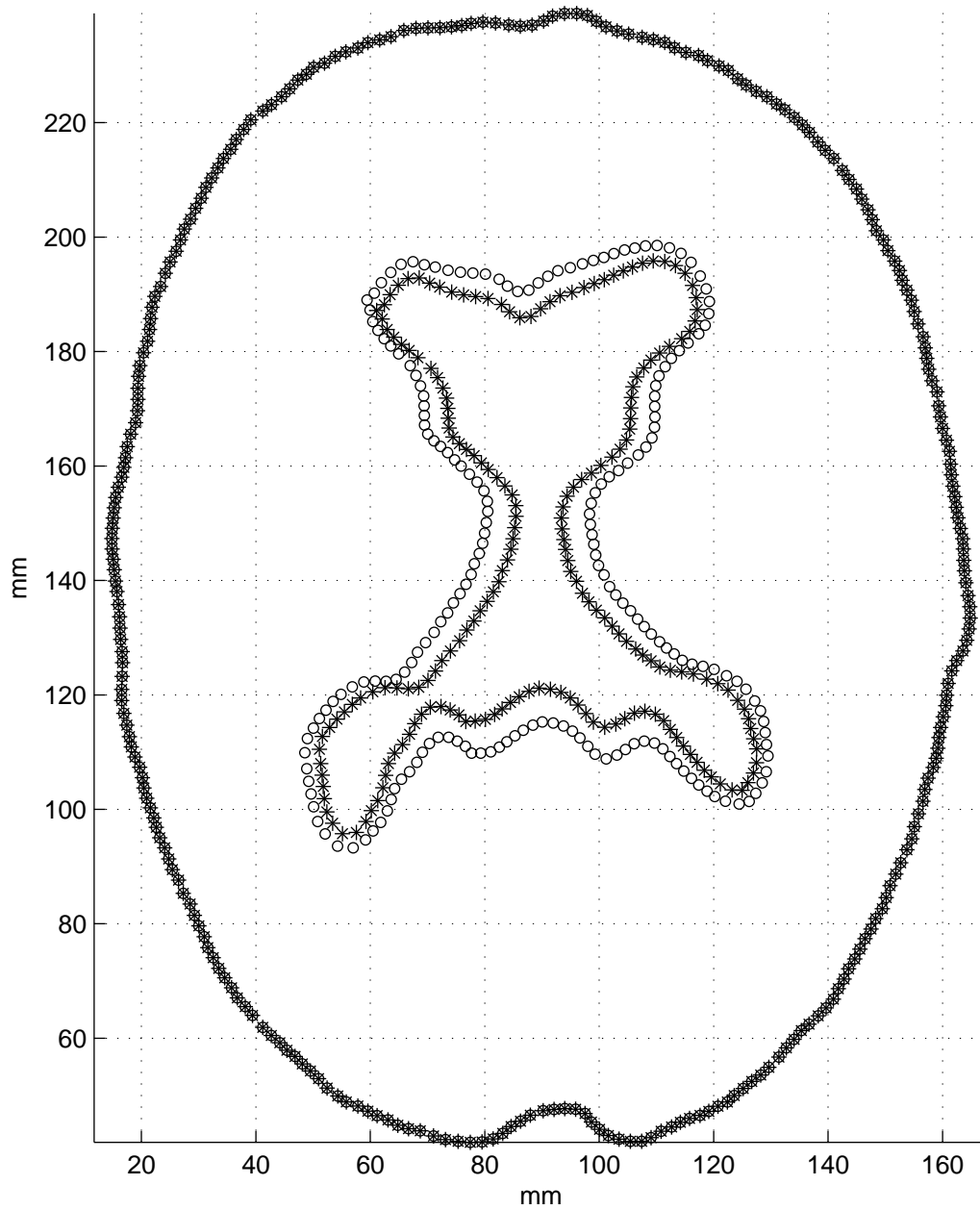


Figure 4.10: Ω_h represent the brain of Patient C. The symbol “o” outlines the boundaries of Ω_h at day 14. The symbol “*” outlines the boundaries of Ω_h at day 21.

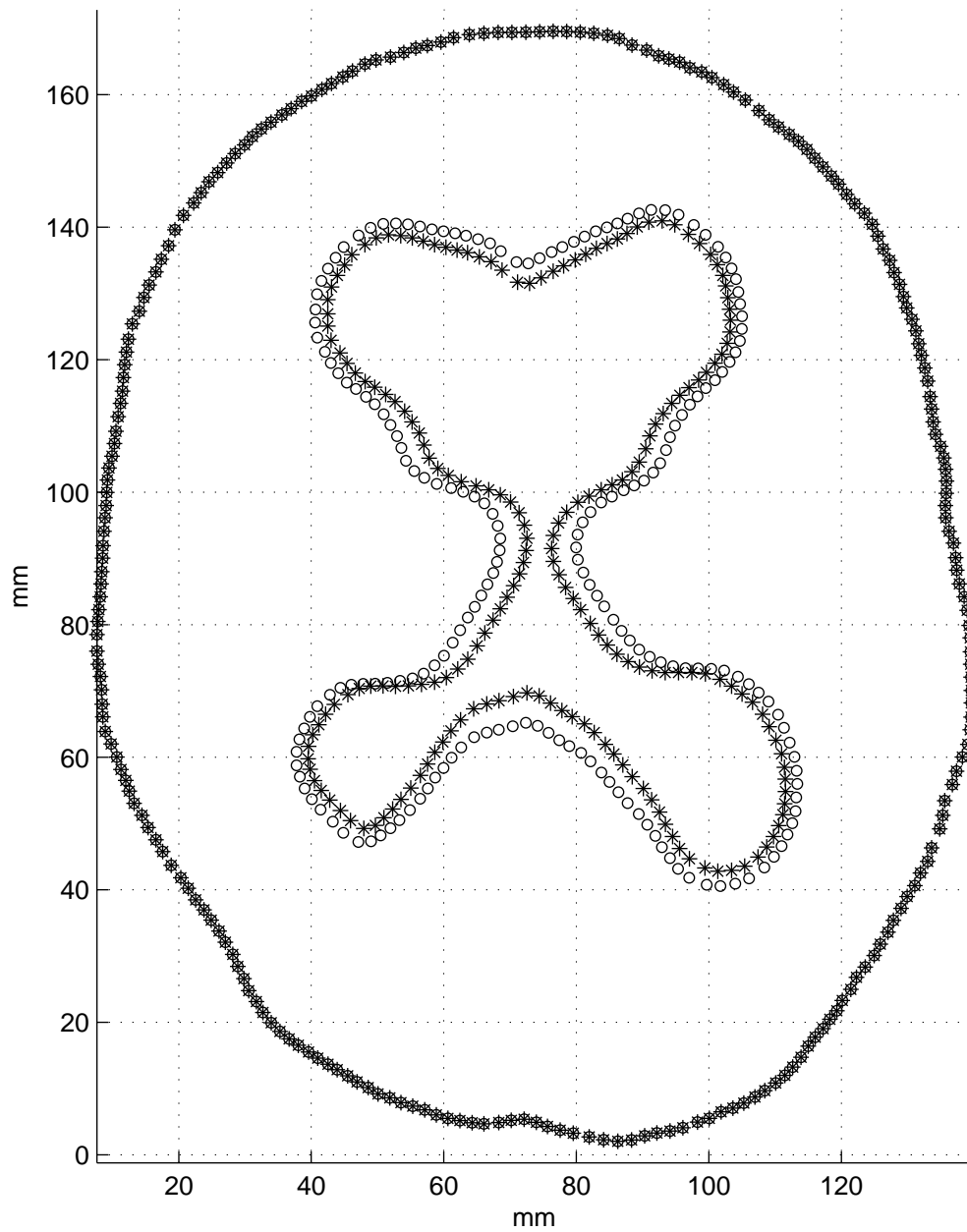


Figure 4.11: Ω_h represents the brain of Patient H. The symbol “o” outlines the boundaries of Ω_h at day 14. The symbol “*” outlines the boundaries of Ω_h at day 21.

concave when it is far from the skull.

4.4.2 Predicting the Shape of Ventricles During Treatment

When a shunting procedure is needed, medical images are taken of the enlarged ventricular, and the surgeon decides on the shunt placement based on these images. It would be beneficial if the position of the shrinking ventricles can be predicted by a numerical simulation, so that an optimal placement can be decided before surgery. It seems that such simulation could be performed by decreasing the pressure in the numerical model developed in this thesis; however, it is found to be more difficult.

To illustrate, an experiment is conducted using a computational mesh generated from a pre-shunt image of Patient D, which describes an enlarged ventricles. Then, the pressure is decreased linearly from 0 to -18000Pa or $-1836\text{mmH}_2\text{O}$ in 14 days. The shear modulus $G(t)$ is defined in (4.2) and the bulk modulus $K = 166\text{KPa}$.

Figure 4.12(a) shows the original geometry of the enlarged ventricles, and Figure 4.12(b) shows the resulted geometry at day 14. Comparing these two figures, the ventricular wall have moved inward and become very close to each other in some region, and the ventricles surrounding the frontal and occipital horns remain dilated. This observation is different from what is actually observed in the post-shunt image. Figure 4.13(a) and Figure 4.13(b) show the pre-shunt and post-shunt image of Patient D respectively. The post-shunt image shows the overall size of the ventricles is reduced, and the regions near the frontal and occipital horns have also reduced in size, which is not the case in the numerical experiment.

What is missing in the numeral simulation that leads to this discrepancy is the state of stress and strain of the deformed brain of Patient D. Like all previous experiments, the mathematical model considers the initial geometry as the natural original shape of the brain, and once it is deformed, the stress and strain become non-zeros. Thus this experiment is pulling the ventricular wall inwards, instead of allowing the compressed brain tissue to restore its shape. Therefore, it is incorrect to model the treatment of hydrocephalus simply by decreasing the pressure. More information is needed about the state of stress and strain of a patient's brain. Unfortunately, current technology does not enable one to measure the state of stress and strain of a human brain. Even if it is possible, the viscoelastic model of the brain would require the entire history of the deformation.

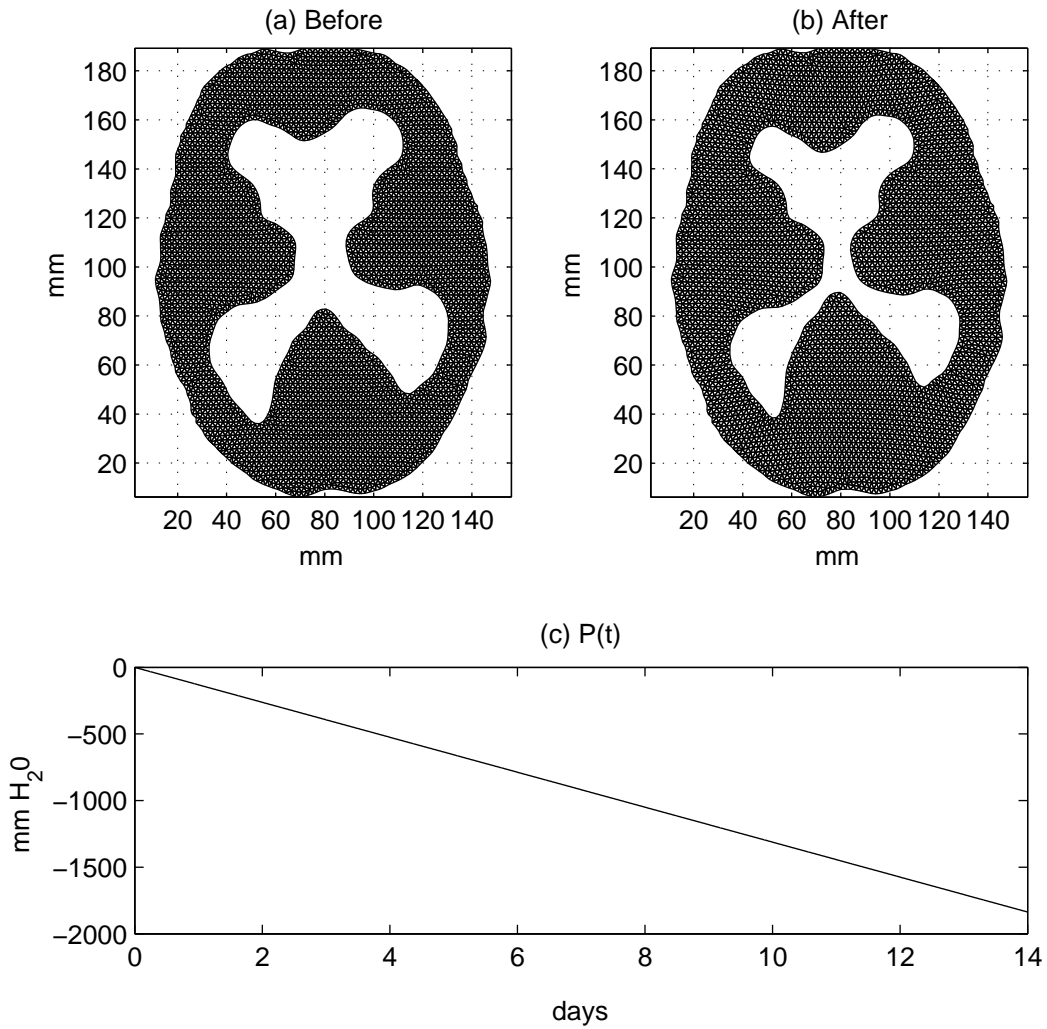


Figure 4.12: (a) The original shape of Ω_h . (b) The resulted shape of Ω_h after 14 days of simulated time. (c) The pressure $P(t)$ at the ventricular wall which linearly decreases over 14 days.

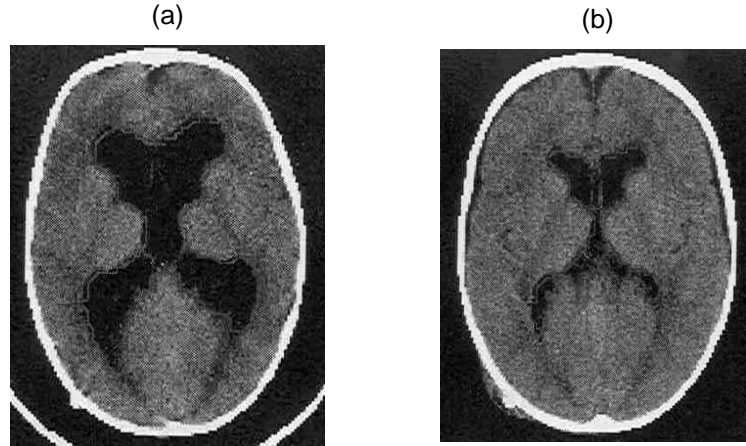


Figure 4.13: (a) a pre-shunt image of Patient C. (b) a post-shunt image of Patient C.

4.5 Assumptions of Linearity

In formulating the mathematical model for hydrocephalus, the assumption of linearity is used twice: first, the deformation is assumed to be small enough such that the Cauchy's infinitesimal strain tensor is used; second, the stress and strain relationship of the material is assumed to be linear. Most behaviour of a material is nearly linear over a certain ranges of stress, strain and time, but over a larger range of these variable, the use of linear theory will gives only a poor approximation of the actual behaviour of the material. Thus, in this section, an acceptable range of strain over which linear theory may be employed is discussed.

First, the infinitesimal deformation approximation is discussed, and the limitation of this approximation is that the deformation resulting from a numerical experiment should not be too large. Since this assumption requires that the nonlinear part of the Green's strain tensor $\tilde{\varepsilon}_{ij}$ to be small compare to the Cauchy's infinitesimal strain tensor ε_{ij} , the ratio between $\tilde{\varepsilon}_{ij}$ and ε_{ij} provides a good indication of the validity of this assumption. Consider the following ratio κ

$$\kappa = \frac{\frac{1}{N} \sum_{e=1}^N (|\text{trace}(\tilde{\varepsilon}_{ij}^e)|)}{\frac{1}{N} \sum_{e=1}^N (|\text{trace}(\varepsilon_{ij}^e)|)}, \quad (4.4)$$

where N is the total number of elements, and ε_{ij}^e and $\tilde{\varepsilon}_{ij}^e$ are computed as described in Section 3.2.3.

To set a reasonable bound on κ , four experiments with progressively larger deformation are performed. Since both the elastic and viscoelastic problems made the same assumption, it is sufficient to conduct these experiments with only the elastic problem. The computation domain Ω_h is generated from a post-shunt image of Patient A, and the Young's modulus and Poisson's ratio are defined in (4.1). Then, the pressure of the four experiments are $10KPa$, $20KPa$, $40KPa$ and $80KPa$, so that the deformation between each experiment is increased.

The result of these four experiments are shown in Figure 4.14. Figure 4.14(a) shows the original ventricles shape of Ω_h . Figure 4.14(b), (c), (d) and (e) shows the deformed geometry of Ω_h , the maximum displacement and the ratio κ for the four experiments, which is becoming larger between each experiment. Figure 4.14(b) shows the result of the first experiment, where the ventricles are slightly enlarged with a maximum displacement of 4.71mm, and the ratio κ is 0.13. This implies the magnitude of the nonlinear terms, that are excluded in the mathematical model, is roughly 13% of the magnitude of the linear terms. Similarly for the next experiment, with a larger deformation and displacement as shown in Figure 4.14(c), the ratio κ is already 0.27 implying a greater magnitude of the nonlinear strain tensor is excluded. Thus, when a deformation gives $\kappa > 0.50$ as shown in Figure 4.14(d) and Figure 4.14(e), the use of infinitesimal strain tensor surely yield a poor approximation of the actual behaviour of the material.

To ensure the nonlinear terms $\tilde{\varepsilon}_{ij}^e$ is small enough in numerical experiments of this thesis, the ratio κ is computed and bounded above by 0.15. This value is chosen because it is small enough such that the experiments give sufficiently noticeable changes in the shape of the ventricles.

Lastly, the assumption of linear viscoelasticity is discussed. According to [12], the linear viscoelastic model is insufficient to describe the brain tissue if the strain is greater than 40%. Thus, the average volumetric strain over Ω_h is computed and observed. It is found that as long as the ratio $\kappa < 0.15$, the resulting strain of an experiment will not exceed 40%. Thus, as long as the deformation is infinitesimal, the use of the linear viscoelastic model is acceptable. Therefore, since the ratio κ and volumetric strain of the numerical

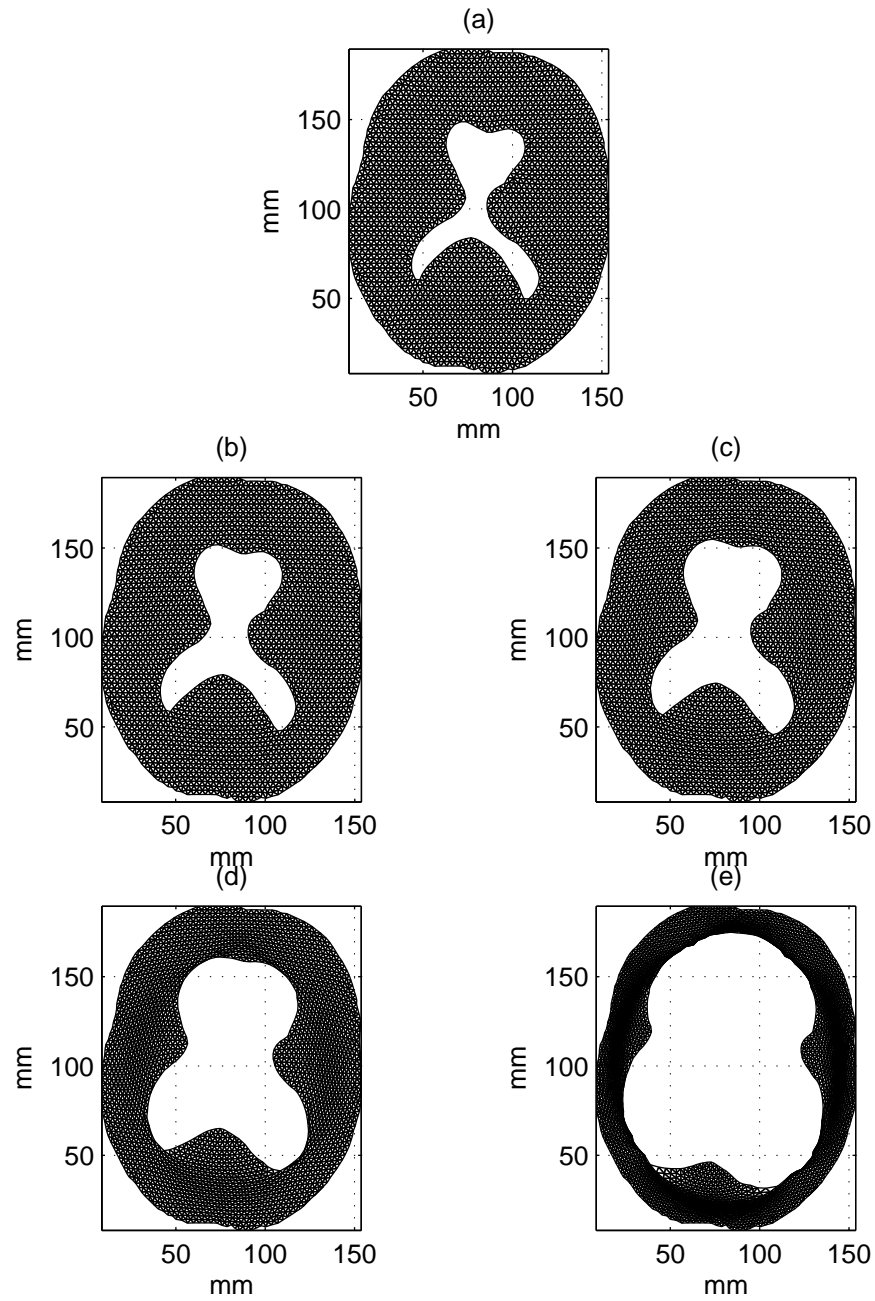


Figure 4.14: (a) The original shape of Ω_h . The deformed Ω_h with parameters (b) $P(t) = 10\text{KPa}$, $\max \mathbf{u} = 4.70\text{mm}$, and $\kappa = 0.13$, (c) $P(t) = 20\text{KPa}$, $\max \mathbf{u} = 9.41\text{mm}$, and $\kappa = 0.27$, (d) $P(t) = 40\text{KPa}$, $\max \mathbf{u} = 18.82\text{mm}$, and $\kappa = 0.54$. (e) $P(t) = 80\text{KPa}$, $\max \mathbf{u} = 37.64\text{mm}$, and $\kappa = 1.09$.

experiments in this thesis are bounded, the experiments in this thesis give an accurate approximation of infinitesimal deformations.

Chapter 5

Conclusions

5.1 Summary

In this thesis, the viscoelastic model for studying hydrocephalus is described, and finite element method and a time-stepping scheme for solving this model is presented. Analytical solution is also found when the geometry of brain is a cylinder, and the numerical solution is validated with the analytical solution. The elastic model is also introduced to assist the development of analytical and numerical solution. Also, realistic computational mesh are generated using level set method and a program called DistMesh. Numerical stability of the time-stepping scheme is also studied.

Using the generated computational meshes, three numerical studies related to hydrocephalus are conducted. In one of these studies, the state of stress of the brain tissue when hydrocephalus develops is investigated and found to be compressive everywhere in the brain. However, in [29], the state of stress is found to be both compressive and expansive when the brain tissue is modeled as a poroelastic solid filled with fluid. Consequently, the two approaches give a different description on how the brain tissue may be damaged.

In another study, the role of viscoelastic material in modeling hydrocephalus is investigated. When the tissue is described with a bulk modulus that is used in brain traumatic injury, the volumetric stress of tissue is significantly much higher compared to normal ICP. Hence this suggests such bulk modulus might not be appropriate for modeling hydrocephalus. Also, the time dependent shear response of the tissue is very short compared to

a typical time scale of hydrocephalus, and the viscoelastic response is soon dominated by elastic response. Therefore, the time scale of current viscoelastic models may be suitable for brain traumatic injury, but it is insignificant in modeling hydrocephalus.

In the last study, the movement of the ventricles is observed when the pressure gradient increases and decreases, and it is found that the ventricular wall does not move uniformly inward, even when the deformation is small. When ventricles of different geometry are tested, it is found that the greatest displacement occurs in the region where the ventricular walls are concave and are furthest away from the skull. Moreover, it would be beneficial to predict the position of the ventricles before the shunt is implanted, but it is shown that the challenges lie in knowing the state of stress of the deformed brain.

5.2 Future work

There are a number of possible extensions to this work. An important one is to model large deformation by using the fully nonlinear Green's strain tensor, since the deformation of the brain is usually quite large when hydrocephalus develops. A large deformation can be described by a series of small deformation, and this subject is referred to as mechanics of incremental deformation. One can refer to [5] for a comprehensive reference on this subject. Finite element method has also been developed to model large deformation through incremental deformations, where each increment is solved using the method introduced in this thesis. [31, 28] are two excellent references to this subject. [24] provides a good summary of numerical methods for biomechanical models of soft tissue but it requires some knowledge of finite element method. Nonlinear constitutive equations could also be considered. Unless a viscoelastic model have a longer relaxation time, a nonlinear elastic model might be sufficient.

Another extension involves predicting the shape of ventricles. Since the state of stress and strain of the patient's brain is unknown, it is an ill-posed problem to predict the geometry of the ventricles as it shrinks. So, instead of trying to find a way to measure the state of stress of the tissue, one could try to find the initial geometry of the ventricles. Given an pre-shunt image, its original shape might be found by deforming an arbitrary shape with a possible pressure gradient, such that the deformed shape resembles the ventricles

on the pre-shunt image. Such an arbitrary shape should resemble the general shape of the normal ventricles. Then using this shape as the initial geometry, one could simulate the development and then the treatment of hydrocephalus. However, such an initial geometry may not be unique, so the initial shape could be chosen such that a function measuring the deformation is minimized. However, it is unclear how this function should be defined.

Other possible extensions include combining a compartmental model with the governing equations and extending the governing equations to 3D. A compartmental model describes the CSF volume and pressure relationship in the ventricles, and it would give a more realistic way to model the boundary condition at the ventricular wall. See [43, 39] for details. The numerical methods for grid generation methods can be applied for 3-D geometry.

Appendix A

Existence and Uniqueness of Solutions

For completeness, the conditions for the weak formulation of the two problems to have unique solution are stated. These conditions are discussed in [20] for the elastic problem, and in [34, 35] for the viscoelastic problem.

First, consider the Lax-Milgram Theorem which is often used in proving existence and uniqueness of solution to a weak formulation.

Theorem 2. *Lax-Milgram Theorem. Consider a weak formulation: find $\mathbf{u} \in \mathcal{V}$ such that $a(\mathbf{u}, \mathbf{v}) = L(\mathbf{v})$, $\forall \mathbf{v} \in \mathcal{V}$. Consider the following properties for $a(\mathbf{u}, \mathbf{v})$ and $L(\mathbf{v}, t)$*

1. $a(\mathbf{u}, \mathbf{v})$ is symmetric, i.e., $a(\mathbf{u}, \mathbf{v}) = a(\mathbf{v}, \mathbf{u})$, $\forall \mathbf{u}, \mathbf{v} \in \mathcal{V}$.
2. $a(\mathbf{u}, \mathbf{v})$ is continuous, i.e., there is a constant $m > 0$ such that $|a(\mathbf{u}, \mathbf{v})| \leq m \|\mathbf{u}\|_V \|\mathbf{v}\|_V$, $\forall \mathbf{u}, \mathbf{v} \in \mathcal{V}$.
3. $a(\mathbf{u}, \mathbf{v})$ is V -elliptic, i.e., there is a constant $\alpha > 0$ such that $a(\mathbf{v}, \mathbf{v}) \geq \alpha \|\mathbf{v}\|_V^2$, $\forall \mathbf{u}, \mathbf{v} \in \mathcal{V}$.
4. $L(\mathbf{v})$ is continuous, i.e., there is a constant $\Lambda > 0$ such that $|L(\mathbf{v})| \leq \Lambda \|\mathbf{v}\|_V$, $\forall \mathbf{u}, \mathbf{v} \in \mathcal{V}$.

When these property holds, the weak formulation has a unique solution.

Theorem 3. *Consider the weak formulation of the elastic problem (3.14). If the Young's modulus $E \geq 0$ and the Poisson's ratio $\nu \geq 0$, then the weak formulation of the elastic problem has a unique solution.*

Proof. It can be shown that $a(\mathbf{u}, \mathbf{v})$ and $L(\mathbf{v}, t)$ of (3.14) satisfies property 1, 2 and 4. Property 3 follows from Korn's inequality, provided that the Young's modulus, $E \geq 0$, and the Poisson's ratio $\nu \geq 0$. Therefore, the elastic problem has an unique solution according to Theorem 2. \square

To show that the weak formulation of the viscoelastic problem has a unique solution, the formulation needs to be written with a different form of constitutive equations, and it is derived in (2.35)

$$\begin{aligned} \sigma_{ij}(\mathbf{x}, t) &= \lambda(t - t_0)\varepsilon_{kk}(\mathbf{x}, t_0)\delta_{ij} + \mu(t - t_0)\varepsilon_{ij}(\mathbf{x}, t_0) \\ &+ \int_{t_0}^t \lambda(t - s)\frac{d\varepsilon_{kk}(\mathbf{x}, s)}{ds}\delta_{ij} + \mu(t - s)\frac{d\varepsilon_{ij}(\mathbf{x}, s)}{ds}ds. \end{aligned}$$

Using a relaxation matrix $D(t - s)$, this constitution equations become

$$\boldsymbol{\sigma}(\mathbf{x}, t) = D(t - t_0)\boldsymbol{\varepsilon}(\mathbf{x}, t_0) + \int_{t_0}^t D(t - s)\frac{d\boldsymbol{\varepsilon}(\mathbf{x}, s)}{ds}ds \quad (\text{A.1})$$

where

$$D(t - s) = \begin{bmatrix} \lambda + \mu & \lambda & 0 \\ \lambda & \lambda + \mu & 0 \\ 0 & 0 & \frac{\mu}{2} \end{bmatrix} (t - s).$$

Following the same procedure in Section 3.2.1, the resulted weak formulation can be defined neatly with a bilinear operator and a load operator.

Find $\mathbf{u}(\mathbf{x}, t) \in \mathcal{H}^1(\mathcal{I}, \mathcal{V})$ such that $\forall \mathbf{v} \in \mathcal{V}, \forall t \in \mathcal{I}$

$$\begin{aligned} &a(\lambda(t - t_0), \mu(t - t_0), \mathbf{u}(\mathbf{x}, t_0), \mathbf{v}(\mathbf{x})) + \int_{t_0}^t a\left(\lambda(t - s), \mu(t - s), \frac{d\mathbf{u}(\mathbf{x}, s)}{ds}, \mathbf{v}(\mathbf{x})\right) ds \\ &= L(\mathbf{v}(\mathbf{x})), \end{aligned} \quad (\text{A.2})$$

where the bilinear operator is

$$a(\lambda(t - q), \mu(t - q), \mathbf{u}(\mathbf{x}, q), \mathbf{v}(\mathbf{x})) = \int_{\Omega} \boldsymbol{\varepsilon}^T(\mathbf{v}(\mathbf{x}))D(t - q)\boldsymbol{\varepsilon}(\mathbf{u}(\mathbf{x}, t_0))d\mathbf{x},$$

and the load operator is

$$L(\mathbf{v}(\mathbf{x}), t) = - \int_{\partial\Omega} \mathbf{v}^T(\mathbf{x}) \mathbf{g}(\mathbf{x}, t) ds.$$

The Sobolev space $\mathcal{H}^1(\mathcal{I}, \mathcal{V})$ consists of all functions $\mathbf{u} \in L_2(\mathcal{I}, \mathcal{V})$ such that $\frac{d\mathbf{u}}{ds}$ exists in the weak sense and belongs to $\mathcal{L}_2(\mathcal{I}, \mathcal{V})$, and the norm of $\mathcal{L}_2(\mathcal{I}, \mathcal{V})$ is defined in (3.47). Another way to write the weak formulation is to use the alternate form of hereditary integral, as appeared in (2.30), and the resulted weak formulation is

$$\begin{aligned} & a(\lambda(0), \mu(0), \mathbf{u}(\mathbf{x}, t), \mathbf{v}(\mathbf{x})) - \int_{t_0}^t a\left(\frac{d\lambda(t-s)}{ds}, \frac{d\mu(t-s)}{ds}, \mathbf{u}(\mathbf{x}, s), \mathbf{v}(\mathbf{x})\right) ds \\ & = L(\mathbf{v}(\mathbf{x})). \end{aligned} \quad (\text{A.3})$$

Next, consider some properties of a stress relaxation function for the weak formulation (A.2) to have a unique solution.

Theorem 4. *Assume the stress relaxation function $\lambda(t - q)$ and $\mu(t - q)$ satisfy the following:*

1. *Positive Definiteness:* $\varphi(t - q) > 0, \forall t, t - q \in \mathcal{I}$.
2. *The fading memory hypothesis:* $\frac{d\varphi(t-q)}{dq} > 0, \forall t, t - q \in \mathcal{I}$. *This implies disturbances which occurred in the distant past have less influence on the present solution than those which occurred in the more recent past [12].*
3. *Regularity:* $\varphi(t - q) \in \mathcal{C}^\infty(\mathcal{I})$.
4. *Causality:* $\varphi(t - q) = 0 \forall q > t$ such that $t, q \in \mathcal{I}$. *This simply means future events does not affect present behaviour.*

then the bilinear operator $a(\lambda(t - q), \mu(t - q), \mathbf{u}_h(\mathbf{x}, q), \mathbf{v}(x))$ is V-elliptic, and the weak formulation has a unique solution

Proof. It is to check $a(\lambda(t - q), \mu(t - q), \mathbf{u}_h(\mathbf{x}, q), \mathbf{v}(\mathbf{x}))$ and $L(\mathbf{v}, t)$ of (A.2) satisfies property (1), (2) and (4) of Theorem 2. In addition, when $\lambda(t - q)$ and $\mu(t - q)$, satisfy the four assumptions, its bilinear operator is V-elliptic. Thus, it can be shown using the Picard iteration, detailed in [23], that (A.3) has an unique solution. Since (A.3) is mathematically equivalent to (A.2), (A.2) also has an unique solution[34]. \square

Note that when the spatial domain is discretized using finite element method, the weak formulation (A.2) is written as

$$A(t - t_0)\mathbf{U}(t_0) + \int_{t_0}^t A(t - s) \frac{d\mathbf{U}(s)}{ds} ds = L(t), \quad (\text{A.4})$$

where $A(t - s)$ is a stiffness matrix. The resulted equation is a Volterra system of integral equations of the first kind for $\mathbf{U}'(t)$.

Bibliography

- [1] *The Brain*. http://www.thebrain.mcgill.ca/flash/i/i_01/i_01_cr/i_01_cr_ana/i_01_cr_ana/i_01_cr_ana.html#2.
- [2] *Brain Facts and Figures*. <http://www.uib.no/med/avd/miapr/arvid/UiB50/anatomi/facts.htm>.
- [3] Toru Aida. *Study of Human Head Impact: Brain Tissue Constitutive Models*. PhD thesis, West Virginia University, 2000.
- [4] E.W. Billington and A. Tate. *The Physics of Deformation and Flow*. McGraw-Hill International Book Company, 1981.
- [5] Maurice A. Biot. *Mechanics of Incremental Deformations: Theory of Elasticity and Viscoelasticity of Initially Stressed Solids and Fluids, including Thermodynamic Foundations and Applications to Finite Strain*. John Wiley & Sons Inc., 1965.
- [6] Setta Chinviriyasit. *Numerical methods for treating quasistatic linear viscoelastic problems*. PhD thesis, Department of Mathematical Sciences, Brunel University, Uxbridge, England, 2001.
- [7] Cincinnati Children's Hospital Medical Center, <http://www.cincinnatichildrens.org/health/info/neurology/diagnose/hydrocephalus/htm>. *Conditions and diagnoses: Hydrocephalus*.
- [8] C.S. Cotter, P.K. Smolarkiewicz, and I.N. Szczyrba. A viscoelastic fluid model for brain injuries. *International Journal for Numerical Methods in Fluids*, 40:303–311, 2002.

- [9] Z.S. Couper and F. Albermani. Constitutive modeling of brain matter in traumatic brain injury. To appear in *Medical and Biological Engineering and Computing*.
- [10] B.R. Donnelly and J. Medige. Shear properties of human brain tissue. *Journal of Biomechanical Engineering*, 119:423–432, 1997.
- [11] J.M. Drake, J.R.W. Kestle, and S. Tuli. CSF shunts 50 years on-past,present and future. *Child's Nervious System*, 16:800–804, 2000.
- [12] Corina S. Drapaca. *Brain Biomechanics: Dynamical Morphology and Non-linear Viscoelastic Models of Hydrocephalus*. PhD thesis, University of Waterloo, 2002.
- [13] M.S. Estes and J.H. McElhaney. Response of brain tissue of compressive loading. *ASME paper*, 13:1–4, 1970.
- [14] William N. Findley, James S. Lai, and Kasif Onaran. *Creep and Relaxation of NonLinear Viscoelastic Material with an Introduction to Linear viscoelasticity*. North-Holland Publishing Company, 1976.
- [15] Wilhelm Flugge. *Viscoelasticity*. Baisdell Publishing Company, 1967.
- [16] Y.C. Fung. *Foundations of Solid Mechanics*. Prentice-Hall, Inc., 1965.
- [17] James E. Galford and James. H. McElhaney. A viscoelastic study of scalp, brain and dura. *Journal of Biomechanics*, 3:211–221, 1970.
- [18] Amit Gefen and Susan S. Margulies. Are in vivo and in situ brain tissue mechanically similar? *Journal of Biomechanics*, 37:1339–1352, 2004.
- [19] V. Janovsky, S. Shaw, M.K. Warby, and J.R. Whiteman. Numerical methods for treating problems of viscoelastic isotropic solid deformation. *Journal of Computational and Applied Mathematics*, 65:91–107, 1995.
- [20] Claes Johnson. *Numerical solution of partial differential equations by finite element method*. Cambridge University Press, 1987.

- [21] Mariusz Kaczmarek, Ravi P. Subramaniam, and Samuel R. Neff. The hydromechanics of hydrocephalus: steady-state solutions for cylindrical geometry. *Bulletin of Mathematical Biology*, 59(2):295–323, 1997.
- [22] Stelios K. Kyriacou, Ashraf Mohamed, Karol Miller, and Samuel Neff. Brain mechanics for neurosurgery: modelling issues. *Biomechan. Model. Mechanobiol.*, 1:151–164, 2002.
- [23] Peter Linz. *Analytical and Numerical Methods for Volterra Equations*. SIAM, 1985.
- [24] Walter Maurel, Yin Wu, Nagnenat Thalmann, and Daniel Thalmann. *Biomechanical Models for Soft Tissue Simulation*. Springer, 1998.
- [25] K.K. Mendis, R.L. Stalnaker, and S.H. Advani. A constitutive relationship for large deformation finite element modeling of brain tissue. *Journal of Biomechanical Engineering*, 117(279-285), 1995.
- [26] Karol Miller and Kiyoyuki Chinzei. Constitutive modelling of brain tissue: experiment and theory. *Journal of Biomechanics*, 30:1115–1121, 1997.
- [27] Tatsuya Nagashima, Norihiko Tamaki, Satoshi Matsumoto, Barry Horwitz, and Yasuyuki Seguchi. Biomechanics of hydrocephalus: a new theoretical model. *Neurosurgery*, 21:898–904, 1987.
- [28] J.T. Oden. *Finite Elements of Nonlinear Continua*. McGraw-Hill Book Company, 1972.
- [29] Alonso Pena, Malcolm D. Bolton, Helen Whitehouse, and John D. Pickard. Effects of brain ventricular shape on periventricular biomechanics: a finite element analysis. *Neurosurgery*, 45:107–118, July 1999.
- [30] Per-Olof Persson. *Mesh Generation for Implicit Geometries*. PhD thesis, Massachusetts Institute of Technology, 2005.
- [31] J.N. Reddy. *An Introduction to Nonlinear Finite Element Analysis*. Oxford University Press, 2004.

- [32] Jesse S. Ruan, Tawfik B. Khalil, and Albert I. King. Finite element modeling of direct head impact. *SAE paper*, (933114), 1993.
- [33] D. Schley, J. Billingham, and R.J. Marchbanks. A model of in-vivo hydrocephalus shunt dynamics for blockage and performance diagnostics. *Mathematical Medicine and Biology*, 21:347–368, 2004.
- [34] S. Shaw, M.K. Warby, J.R. Whiteman, C. Dawson, and M.F. Wheeler. Numerical techniques for the treatment of quasistatic viscoelastic stress problems in linear isotropic solids. *Computer Methods in Applied Mechanics and Engineering*, 118:211–237, 1994.
- [35] S. Shaw and J.R. Whiteman. A posteriori error estimates for space-time finite element approximation of quasistatic hereditary linear viscoelasticity problems. *Computer Methods in Applied Mechanics and Engineering*, 193:5551–5572, 2004.
- [36] Simon Shaw. *Finite Element and Discrete Time Method for Continuum Problems with Memory and Applications to Viscoelasticity*. PhD thesis, Department of Mathematics and Statistics, Brunel University, November 1993.
- [37] L.Z. Shuck and S.H. Advani. Rheological response of human brain tissue in shear. *Journal of Basic Engineering*, pages 905–911, December 1972.
- [38] L.Z. Shuck, R.R. Haynes, and J.L. Fogle. Determination of viscoelastic properties of human brain tissue. *The American Society of Mechanical Engineers*, 12:1–7, 1970.
- [39] A. Simillie, I. Sobey, and Z. Zolnar. A hydro-elastic model of hydrocephalus. *Journal of Fluid Mechanics*, 539:417–443, 2005.
- [40] S. Sivaloganathan, M. Stastna, G. Tenti, and J.M. Drake. Biomechanics of the brain: a theoretical and numerical study of Biot’s equations of consolidation theory with deformation-dependent permeability. *International Journal of Non-Linear Mechanics*, 40:1149–1159, 2005.
- [41] S. Sivaloganathan, M. Stastna, G. Tenti, and J.M. Drake. A viscoelastic approach to the modelling of hydrocephalus. *Applied Mathematics and Computation*, 163:1097–1107, 2005.

- [42] S. Sivaloganathan, M. Stastna, G. Tenti, and J.M. Drake. A viscoelastic model of the brain parenchyma with pulsatile ventricular pressure. *Applied Mathematics and Computation*, 165:687–698, 2005.
- [43] S. Sivaloganathan, G. Tenti, and J.M. Drake. Mathematical pressure volume models of the cerebrospinal fluid. *Applied Mathematics and Computation*, 94:243–266, 1998.
- [44] M. Stastna, G. Tenti, S. Sivaloganathan, and J.M. Drake. Brain biomechanics: Consolidation theory of hydrocephalus. variable permeability and transient effect. *Canadian Applied Mathematics Quarterly*, 7:111–124, 1999.
- [45] Zeike Taylor and Karol Millier. Reassessment of brain elasticity for analysis of biomechanisms of hydrocephalus. *Journal of Biomechanics*, 37, 2004.
- [46] G. Tenti, S. Sivaloganathan, and James M. Drake. Brain biomechanics: steady-state consolidation theory of hydrocephalus. *Can. Appl. Math. Q.*, 7, 1999.
- [47] S.P. Timoskenko and J.N. Goodier. *Theory of Elasticity*. McGraw-Hill Book Company, 1970.
- [48] Joseph J. West. Application of the level set method to hydrocephalus: Simulating the motion of the ventricles. Master’s thesis, University of Waterloo, 2004.
- [49] O.C. Zienkiewicz. *The Finite Element Method*. McGraw-Hill Book Company Limited, 1977.